DOCTORAL THESIS

ON THE ROLE OF ZERO MODES AND SPACING DISTRIBUTIONS IN RANDOM MATRIX THEORY AND ITS APPLICATIONS

Author:
Adam Mielke

Supervisor:
Prof. Dr. Gernot Akemann

Second Supervisor:
Dr. Mario Kieburg

Submited:
15 October 2019

FACULTY OF PHYSICS
BIELEFELD UNIVERSITY

Abstract

I consider the applications of random matrix ensembles in statistical physics. Of special interest are topology and systems that transition between two states modelled with two-matrix models. I first look at the transition between the symmetry class chiral Gaussian orthogonal ensemble and the ensemble of antisymmetric Hermitian random matrices, where topology is preserved during the transition in the form of either one exact eigenvalue at the origin or none. This ensemble shares symmetry properties with topological superconductors in the gapless phase. On a technical level, this ensemble is a Pfaffian point process and may be solved with skew-orthogonal polynomials, which I show how to obtain.

I secondly analyse the weak breaking of topology in a general setting, where the second matrix is viewed as a perturbation. I show that the spectrum of the perturbed topological modes decouples from the bulk to first order. They also spread out as a finite-size Gaussian ensemble of size $\nu \times \nu$, where ν is the number of former zero modes, through a mechanism reminiscent of the central limit theorem.

I finally consider the transition between integrability and chaos in dissipative open quantum systems through the nearest neighbour spacing distribution. I compare to the analytical result for Poisson and Ginibre variables, which are conjectured to correspond to integrable and chaotic respectively. I also compare the intermediate case with numerically generated Coulomb gasses at inverse temperature $\beta \in (0, 2)$ and find good agreement. The comparison is only valid for uniform spectra, which means that for non-uniform cases, a change of variables must be made. This process is known as unfolding, and I show it may be achieved by approximating the empirical spectrum as a sum of Gaussians.

Statement of Authorship

I am familiar with the doctoral regulations of the Department of Physics at Bielefeld University from 10 January 2012. This thesis has been composed by myself and describes my own work, unless otherwise stated in the text. All references have been quoted and all sources of information have been acknowledged. It has not been accepted as part of any previous application for an academic degree.

Bielefeld, 15 October 2019

Adam Mielke

Publications

The following publications should be considered part of the dissertation:

[AKMV] G. Akemann, M. Kieburg, A. Mielke, and P. Vidal, *Preserving Topology while Breaking Chirality: From Chiral Orthogonal to Anti-symmetric Hermitian Ensemble*, J. Stat. Mech., 023102 (2019) [arXiv:1806.10977 [math-ph]].

[KMS] M. Kieburg, A. Mielke, and K. Splittorff, *Universal Broadening of Zero Modes: A General Framework and Identification,* Phys. Rev. E **99**, 052112 (2019) [arXiv:1902.01733 [cond-mat.stat-mech]].

[AKMP] G. Akemann, M. Kieburg, A. Mielke, and T. Prosen, *Universal Signature from Integrability to Chaos in Open Quantum Systems*, (2019) [arXiv:1910.03520 [cond-mat.stat-mech]].

Acknowledgements

I would first of all like to thank Gernot Akemann and Mario Kieburg for many interesting discussions and for professional advice as well as personal. Thank you both for including me in your research group from the beginning and for introducing me to both the people and the problems of random matrix theory.

One of those people is Jacobus Verbaarschot, whose hospitality I enjoyed during my stay at Stony Brook University in October 2017. Thank you for inviting me to your office for discussions and to your home for barbecue. Stony Brook University also deserves my gratitude for welcoming me there and "Bielefeld Graduate School in Theoretical Sciences Mobility Grant" for funding the stay.

The work in this thesis has been supported by the German research council DFG through International Research Training Group 2235 Bielefeld-Seoul "Searching for the regular in the irregular: Analysis of singular and random systems."

The people of the IRTG, in particular my fellow PhD-students, also deserve a mention along with the other friends I have made here in Bielefeld. They have been a much needed help and hindrance in my work with cards, quizzes, and encouragement.

I would like to thank my co-authors Gernot Akemann, Mario Kieburg, Kim Splittorff, Tomaž Prosen, and Pedro Vidal for all our collaborations as well as Tim Würfel for feedback on the thesis manuscript.

Last but not least to my friends and family back home for being patient with both tales of my work, stories from abroad, and my absence.

Adam Mielke
Bielefeld University
15 October 2019

Contents

1 Introduction: Random Matrix Theory in Physics **1**

2 Mathematical and Physical Framework **5**
2.1 Joint Probability Density of the Eigenvalues 5
2.2 Orthogonal- and Skew-Orthogonal Polynomials 8
2.3 Symmetry Classes 17
2.4 Exact Zero Modes and Topology 18
2.5 Two-Matrix Models and Symmetry Transitions 19
2.6 Solid State Physics 20

3 Transition Between chGOE and GAOE **25**
3.1 Symmetry Transition and Main Results 26
3.2 Joint Probability Density of the Eigenvalues 30
3.3 Skew-Orthogonal Polynomials 34
3.4 Limits $a \to 0, 1, \infty$ 42
3.5 Spectral Density and Distribution of Smallest Eigenvalue 50
3.6 Limit of Large Matrix Size 52
3.7 Conclusion 57

4 Universal Broadening of Zero Modes **59**
4.1 Estimate of Scales with Perturbation Theory 60
4.2 Conditions on Operators and Decoupling 63
4.3 Central Limit Theorem for Matrices 66
4.4 Scaling and Application 70
4.5 Conclusion 74

5 Universal Spacing Distributions in 2D **75**
5.1 Spacing Distribution of Eigenvalues 76
5.2 Unfolding of the Spectrum 81
5.3 Comparison to Data 83
5.4 Conclusion 88

6 Concluding Remarks and Outlook **91**

Appendix A Technical Calculations for Chapter 3 **93**

Bibliography **102**

Chapter 1

Introduction: Random Matrix Theory in Physics

The field of random matrix theory (RMT) is concerned with the study of eigenvalues of matrices with random elements. If the elements of the matrix are random variables, the eigenvalues are random variables as well. But even if the entries are independent, the eigenvalues will be highly dependent on each other, and their distribution therefore gives insight into the behaviour of correlated random variables. While there are other questions (such as eigenvector distributions), this is by far the most considered and the one that I have focused on.

Historically speaking, RMT started in mathematical statistics with Wishart in 1928 [1], but the application in physics is generally attributed to Wigner [2] in relation to neutron resonances in heavy nuclei. In general, because linear operators may be written as matrices, one may analyse the statistical properties of an operator spectrum and obtain insight in systems where exact calculation of the equations of motion is impossible. This is exactly what Wigner took advantage of. The identifying aspect applied was the spacing between eigenvalues and the distribution of the spacings is today known as the Wigner surmise. The "surmise" was that the exact spacing distribution for 2×2 Hermitian matrices would describe larger matrix sizes as well. This turned out not to be the case, though it is still a good approximation.

The spacing statistics provide understanding of chaotic quantum systems as well [3, 4]. The distinguishing feature is that integrable systems follow Poisson statistics (corresponding to uncorrelated variables) and chaotic systems follow the Wigner surmise. Exactly the behaviour of the spacing distribution has been compared to different real-world data and is a powerful tool for distinguishing correlated and uncorrelated variables, see for instance a comparison of the Wigner surmise to times between buses in Cuernavaca (Mexico) [5]. The aforementioned difference between chaotic and integrable systems has also been measured [6, 7]. For more historical context and general introduction to RMT, see also [8, 9].

The goal of modern RMT in physics is to apply universality results to make general statements about operators. (By universal I mean determined by the global symmetries alone.) The fulcrum here is that if one can show that a property is universal, any aspect of it can be calculated in any model that has the required symmetries. The advantage of a random matrix model here is that they are usually comparably easy to calculate analytically. (And often very simple numerically.) An often-considered example of a universal property is the small eigenvalues close to the origin, known as the microscopic spectrum [10]. Because both energy and virtuality (eigenvalues of Hamiltonian and Dirac operators respectively) in general are related

to inverse length scales (the intuition here is the de Broglie-relation), and because the microscopic eigenvalues are of the order of the inverse system size, they hold information about long-range properties such as symmetry breaking [11]. It is perhaps therefore not surprising that they are determined by global symmetries alone. These global symmetries of Hermitian matrices have been classified by Altland and Zirnbauer [12] and comprise ten classes. I here want to highlight that some of these ensembles have the possibility of eigenvalues exactly at the origin, which becomes important, as they are related to the topology of the system. The microscopic spectrum becomes even more relevant in this light. For an intuition of this connection, take again the relation to the inverse length scale, which makes the modes exactly at the origin pertain to global properties. This can also be shown rigorously with the Atiyah-Singer index theorem [13]. Apart from these ten Hermitian classes, matrix ensembles that transition between them have also been considered as two-matrix models, see for instance [14, 15].

Notable among modern RMT-applications in physics is the so-called ϵ-regime of effective field theory, relevant for Quantum Chromodynamics (QCD) [16, 17, 18]. This regime considers the effect of the potential term of the Lagrangian on its own. That is, one introduces a counting where the dynamics decouple from the potential term and exactly gives access to the microscopic spectrum, which as mentioned is important for the global symmetries, in QCD the spontaneous breaking of chiral symmetry [11]. The Goldstone fields that arise from this break correspond to the pions, explaining why pions are lighter than one would expect. (The kaon, the lightest hadron after the pion, is about 3.6 times as heavy as the pion [19].) See also [20, 21] for an introduction to effective field theory and chiral perturbation theory.

The connection between QCD and RMT was introduced in a number of papers for different cases [22, 23, 24, 25] and is based on three ensembles with either real, complex, or quaternion entries. All have chiral symmetry, which means that the matrix anticommutes with a unitary operator that squares to $\mathbb{1}$, here γ_5. The relation between chiral perturbation theory and RMT was later established in [26]. I refer to it for the full derivation, but to see the connection one calculates the σ-model (or chiral Lagrangian) of the random matrix model, which for all symmetry classes (also non-chiral) has the form

$$S(U) \;=\; N\ \mathrm{Tr}\big(U + U^{-1}\big)\,, \tag{1.1}$$

where N is the matrix size and U is a field that depends on the symmetry of the matrix model. This is compared to action from effective field theory in the ϵ-regime

$$S(U) \;=\; mV\Sigma_0\ \mathrm{Tr}\big(U + U^{-1}\big)\,, \tag{1.2}$$

where m is the quark mass assuming equal mass, V is the volume of the system, and Σ_0 is a constant that cannot be determined by the symmetries alone. (For chiral perturbation theory, Σ_0 is the order parameter of the spontaneous chiral symmetry break [11].) The counting scheme of the ϵ-regime zooms in on the low-energy spectrum and makes the kinetic term of the Lagrangian decouple, which gives the structure (1.2). The exact nature of the Goldstone field U will depend on the symmetry class. Comparing Equations (1.1) and (1.2) also gives the relation $V \sim N$, which is important for identifying matrix models with real-world Hamiltonians and Dirac operators.

Within this framework, the aforementioned ensembles that transition between symmetry classes also become relevant when modelling finite lattice effects in numerical lattice simulations. This is known as Wilson theory [27], and it models the way chiral symmetry is broken

by simulations on a lattice. In RMT, this is modelled through a random two-matrix model

$$\not{D} = \begin{pmatrix} 0 & W \\ W^\dagger & 0 \end{pmatrix} + a \begin{pmatrix} A & 0 \\ 0 & B \end{pmatrix} , \tag{1.3}$$

where W are generic matrices with either real, complex, or quaternion matrix entries, and A, B are either symmetric, Hermitian, or self-dual matrices, respectively. The chiral symmetry of the Dirac operator is contained in the first matrix which anticommutes with γ_5 ($= \mathrm{diag}(\mathbb{1}, -\mathbb{1})$ in chiral basis), and has the possibility of exact topological zero modes. The second matrix models the breaking arising from the finite lattice spacing. Notably, the two sectors A and B are independent. This will not always be the case for other models I consider, see for instance Chapter 4. Again, because the microscopic spectrum is universal, its behaviour may be calculated in RMT as well as effective field theory, see [28, 29, 30, 31]. The symmetry breaking by the second matrix is treated as a perturbation, which means that a is small and, because perturbation breaks the symmetry that gave rise to the topological modes at the origin, these modes spread out. The scaling with the volume of these former zero modes turned out to be significant; the one found in [28, 29] helped explain the unusual scaling observed in [32].

Apart from QCD, relating random matrix models to physical operators has become relevant in condensed matter physics in more recent years, particularly for topological superconductors. See for instance [33], see also [34] for a review. My starting point here will be the Kitaev model [35] which gives a basic understanding of the formation of exact zero modes in a fermion chain. These modes are often called Majorana zero modes, because they mimic Majorana fermions in the sense that creation and annihilation is the same action. However, these should not be confused, as the solid state zero modes are states rather than particles. (For a Majorana particle all states would have this property rather than just the zero modes.) It should be noted that the Kitaev model represents an idealised, spinless system, which so far has not been observed in nature [36, 37, 38, 39]. Instead, a more complicated experimental setup is needed to realise the Majorana modes, and the goal for RMT is therefore either to construct more realistic matrix models of the topological superconductors or to make general statements about the behaviour of topological modes.

See also [9] for a number of other applications such as finance, information theory, and number theory.

In this thesis I present results on two of the topics described above. Firstly, I consider the statistical behaviour of Hamiltonians with eigenvalues exactly at the origin. This is related to topological superconductors and the behaviour of topology under different circumstances. Secondly, I look into spacing distributions for non-Hermitian matrices and compare these to data. The structure of the thesis is as follows. Each of the projects corresponding to my publications [AKMV], [KMS], and [AKMP] have their own chapter, namely Chapters 3, 4, and 5 respectively. Chapter 5 is also partially based on work done with Rebecca Werdehausen and Oliver Krüger as part of the former's bachelor project [40].

Chapter 2: I introduce the relevant mathematics and physics. I endeavour to give a introduction to random matrix theory and related concepts meant for readers unfamiliar with these, firstly the subject in general, and secondly the specific branch that I have investigated. This will include how to find the distribution of eigenvalues from a matrix model and derive the density correlation functions, the classification of Hermitian matrices and the transition between them, and the solid state perspective on eigenvalues at the origin.

Chapter 3: I consider an ensemble that describes the transition between two symmetry classes, the chiral orthogonal ensemble and the ensemble of antisymmetric Hermitian matrices. Noteworthy is that they both have a possible topological zero mode, and the application in mind is exactly the topological superconductors mentioned above where such a symmetry transition has been conjectured. The focus is on understanding the density correlation functions for this ensemble. I also consider the distribution of the smallest eigenvalue to understand its behaviour during the transition.

Chapter 4: The study of eigenvalues at the origin may also be treated in a more general framework, where the two-matrix ensemble models a perturbation of the zero modes. Here I show how the spectrum of the perturbed modes decouples from the bulk and that it is distributed according to a Gaussian ensemble of finite size $\nu \times \nu$, where ν is the number of broadened zero modes. I also clarify the conditions under which this happens and how the results hold for all ten Altland-Zirnbauer classes. The former zero modes of the ensemble also exhibit a particular scaling with the volume of the system, which allows identification of them compared to bulk modes. This is the same scaling that was observed in Wilson theory.

Chapter 5: I consider the spacing distribution of eigenvalues in the complex plane. I compare this to the spectrum of a Liouville operator to be able to distinguish integrable and chaotic open quantum systems. The 2D case is more complicated than for real eigenvalues, partially because there is no Wigner surmise here, and partially because universality of spacings only holds for uniform distributions. This is true for the real line as well, but the change of coordinates that transforms a given dataset into a uniform distribution is less clear in two dimensions. I also compare the spacing to biological data in the form of buzzard nests in the local forest around Bielefeld to get a sense of territorial behaviour.

Chapter 6: Finally I collect the results with a few concluding remarks and give an outlook with a discussion of open problems.

Appendix A: The more technical calculations from Chapter 3 are left for the appendices.

Each chapter also has a separate conclusion to allow them to be read on their own.

Chapter 2

Mathematical and Physical Framework

Let me start by going through the tools I will be applying and the systems I will consider. This will include standard methods used in random matrix theory and introductions to the physical concepts needed.

First, I show how to change variables from the entries of matrices to their eigenvalues, which leads to the joint probability density function (jpdf) of the eigenvalues. This gives a sense of how the eigenvalues interact with each other. I then introduce orthogonal and skew-orthogonal polynomials and show how they may be used to solve matrix models. These are standard techniques that can be found in [8, 9]. I then introduce the symmetry classes of Hermitian matrices that make up the basis of comparison to physical systems. They are then extended to two-matrix models that transition between different symmetry classes. These models form the main starting point of Chapters 3 and 4. Finally, I show some basic analysis of the Kitaev model and how to model this with random matrices.

2.1 Joint Probability Density of the Eigenvalues

Start with the $\frac{N(N+1)}{2}$ independent entries x_{jk} of an $N \times N$ Hermitian matrix X. If these are taken as identically distributed, centred complex Gaussian (as I will in the following unless otherwise indicated), one may write the joint distribution of these variables as

$$P\left(\{x_{jk}\}_{\substack{j=1\ldots N \\ k=1\ldots j}}|\sigma\right) = \left(2\pi\sigma^2\right)^{-\frac{N(N+1)}{4}} \prod_{j\geq k} e^{-\frac{|x_{jk}|^2}{\sigma^2}}, \tag{2.1}$$

where σ is the width of the Gaussian. It may be rewritten in terms of the full matrix X

$$P\left(X|\sigma\right) = \left(2\pi\sigma^2\right)^{-\frac{N(N+1)}{4}} \prod_{j\geq k} e^{-\frac{1}{\sigma^2}\operatorname{Tr}\left(XX^\dagger\right)}. \tag{2.2}$$

This structure (or a similar one) is the starting point of most random matrix models. The choice of width $\frac{\beta}{2\sigma^2}$, with $\beta = 1, 2, 4$ for real, complex, and quaternion variables respectively, is common convention. This particular ensemble for $\beta = 2$ is called the Gaussian unitary ensemble (GUE), see Section 2.3. From here the idea is to make a decomposition and change variables to the eigenvalues. Consider therefore

$$X = U\Lambda U^\dagger \tag{2.3}$$

where $\Lambda = \mathrm{diag}(\lambda_1, ..., \lambda_N)$ is a diagonal matrix containing the eigenvalues of X and $U \in U(N)/U(1)^N$. The pair (Λ, U) may be seen as the matrix equivalent of the modulus and argument of X. For other ensembles other decompositions may prove more useful. For instance in Chapter 3 the decomposition has the structure

$$\Lambda \quad = \quad \mathrm{diag}\left(\lambda_1 i\tau_2, \ldots, \lambda_{N/2} i\tau_2\right) \ , \tag{2.4}$$

and for products of random matrices, a chain of unitary matrices is used. I will not go into further details regarding the distribution of eigenvalues for products, instead I refer to [41].

The transformation yields a Jacobian, which ends up determining the local behaviour of the eigenvalues, see the following subsection.

2.1.1 The Vandermonde Determinant

The focus of this subsection is to calculate the Jacobian for the change of variables between matrix entries and eigenvalues. See for instance also [8, 42].

Consider the differential

$$dX \quad = \quad dU\Lambda U^\dagger + Ud\Lambda U^\dagger + U\Lambda dU^\dagger \ . \tag{2.5}$$

Define

$$\delta U \quad \equiv \quad U^\dagger dU \ , \tag{2.6}$$

and note that

$$\begin{aligned} & 0 = d(\mathbb{1}) = d(U^\dagger U) = U^\dagger dU + dU^\dagger U \\ \Rightarrow \quad & (\delta U)^\dagger = -\delta U \ . \end{aligned} \tag{2.7}$$

This means (2.5) can be rewritten as

$$dX \quad = \quad U\left(d\Lambda + [\delta U, \Lambda]\right) U^\dagger \ . \tag{2.8}$$

From here the goal is the find the metric g of dX in Equation (2.5) and write the Jacobian as $\sqrt{\det(g)}$, which may be done by considering

$$\mathrm{Tr}\, dX^2 \quad = \quad \mathrm{Tr}\left(d\Lambda^2 + 2\delta U\Lambda\delta U\Lambda - 2\Lambda^2\delta U^2\right) \ , \tag{2.9}$$

where I have used that the diagonal matrices commute and that the trace is cyclic. So in terms of the variables λ_j and δU_{jk}

$$\mathrm{Tr}\, dX^2 \quad = \quad \sum_{j=1}^{N} {\lambda_j}^2 + 2 \sum_{N \geq j > k \geq 1} \left(\lambda_j - \lambda_k\right)^2 |\delta U_{jk}|^2 \ , \tag{2.10}$$

where I have again used the anti-hermiticity of δU. These are now ordered to obtain the metric

$$g \quad = \quad \mathrm{diag}\left(\mathbb{1}_N, 2(\lambda_1 - \lambda_2)^2, 2(\lambda_1 - \lambda_2)^2, 2(\lambda_1 - \lambda_3)^2, 2(\lambda_1 - \lambda_3)^2, \ldots\right) \ , \tag{2.11}$$

which leads directly to

$$\sqrt{\det(g)} \quad = \quad 2^{\frac{N(N-1)}{2}} \prod_{j>k} (\lambda_j - \lambda_k)^2 \ . \tag{2.12}$$

Real and imaginary parts of δU each contribute once in the last part of (2.11). In general, the exponent of $(\lambda_j - \lambda_k)$ in (2.12) is determined by the number of degrees of freedom in the matrix entries, namely $\beta = 1, 2, 4$ (1 for real, 2 for complex, and 4 for quaternion as mentioned above).

The product of differences in (2.12) is called the Vandermonde determinant

$$\Delta_N(\{\lambda\}) = \prod_{1 \le a < b \le N} (\lambda_b - \lambda_a) = \det \left[\lambda_j^{k-1} \right]_{j,k=1\ldots,N} . \tag{2.13}$$

Using (2.12), the jpdf of eigenvalues for the Gaussian unitary ensemble becomes [8, 9]

$$P_N(\lambda_1, \ldots, \lambda_N) \quad \propto \quad \prod_{j=1}^{N} e^{-\lambda_j^2/\sigma^2} \Delta_N(\{\lambda\})^2 . \tag{2.14}$$

Note how it vanishes for equal arguments, which makes it unlikely that two eigenvalues are close to each other. This is the origin of the so-called level repulsion. It is straightforward to show that the nearest neighbour spacing distribution of a 2×2 Hermitian matrix is

$$p_\beta(s) \quad = \quad 2 \frac{\Gamma\left(\frac{\beta+2}{2}\right)^{\beta+1}}{\Gamma\left(\frac{\beta+1}{2}\right)^{\beta+2}} s^\beta \exp\left\{ - \left(\frac{\Gamma\left(\frac{\beta+2}{2}\right)}{\Gamma\left(\frac{1+\beta}{2}\right)} s \right)^2 \right\} , \tag{2.15}$$

where $\beta = 1, 2, 4$ for real, complex, and quaternion entries respectively and the mean has been normalised to 1. This is known as the Wigner surmise, and is a good approximation for the spacing distribution of nearest neighbours for $N > 2$ as well [8].

Level repulsion has seen application in many areas such as the aforementioned neutron resonance of heavy nuclei [8], quantum chaos [3, 4, 6, 43], and spacings of random variables in general, see for instance [5] and also Chapter 5 which is dedicated to extending spacing laws to the complex plane.

The normalisation of the jpdf (2.14) can be found through the Selberg integral

$$\begin{aligned} & \prod_{i=1}^{N} \int_0^\infty dx_i x_i^\kappa \, |\Delta_N(\{x\})|^\beta e^{-\frac{\beta}{2}\sum_{j=1}^N x_j} \qquad (2.16) \\ = \quad & \left(\frac{2}{\beta}\right)^{N(\kappa+1)+\frac{\beta}{2}N(N-1)} \prod_{j=0}^{N-1} \frac{\Gamma\left(1+\frac{\beta}{2}(j+1)\right)\Gamma\left(1+\kappa+\frac{\beta}{2}j\right)}{\Gamma\left(1+\frac{\beta}{2}\right)} , \end{aligned}$$

see e.g. [8, Chapter 17].

From here the challenge is to integrate out the variables in (2.14) to obtain the k-point correlation functions

$$P_k^N(\lambda_1, \ldots, \lambda_k) \quad = \quad \frac{N!}{(N-k)!} \int_a^b P_N(\lambda_1, \ldots, \lambda_N) d\lambda_{N-k+1} , \tag{2.17}$$

where I have made it slightly more general by considering eigenvalues on $[a, b]$ rather than $(-\infty, \infty)$. This is the objective of the next section.

2.2 Orthogonal- and Skew-Orthogonal Polynomials

For the sake of the work in this thesis, orthogonal- and skew-orthogonal polynomials are a tool for expanding the Vandermonde in a way that makes it possible to integrate the variables in (2.17) out. The kind of polynomials needed depends on the exponent β of the Vandermonde in the jpdf. For $\beta = 2$ the orthogonal polynomials (OP) are used, whereas $\beta = 1$ requires skew-orthogonal polynomials (sOP) [8, 9]. Both are each defined through an inner product:

- Orthogonal polynomials ($\beta = 2$)

$$\langle p_j | p_k \rangle = \int_a^b p_j(x) p_k(x) w(x) dx = h_j \delta_{jk} \tag{2.18}$$

- Skew-orthogonal polynomials ($\beta = 1$)

$$\langle p_j | q_k \rangle = \int_a^b p_j(x) q_k(y) w(x,y) dx dy = h_j \delta_{jk}, \quad \text{where } w(x,y) = -w(y,x) \tag{2.19}$$

The skew-orthogonal pairs $p_j(x)$ and $q_j(x)$ are usually pairs of even and odd polynomials [25], but note that the skew-orthogonal polynomials considered in Chapter 3 do not have this structure. There two skew-orthogonal products are also defined, depending on the matrix dimension.

2.2.1 Orthogonal Polynomials

This subsection partially follows [44]. Start with the Vandermonde determinant

$$\Delta_N(\{\lambda\}) \quad = \quad \det_{j,k=1\ldots,N} \left[\lambda_j^{k-1} \right] . \tag{2.20}$$

By addition of rows, this can be rewritten in terms of an arbitrary set of monic polynomials $C_k(\lambda_j)$

$$\Delta_N(\{\lambda\}) \quad = \quad \det_{j,k=1\ldots,N} (C_k(\lambda_j)) . \tag{2.21}$$

Take now the squared Vandermonde of Equation (2.14) and combine the determinants. For generality, I introduce another set of monic polynomials $D_k(\lambda_j)$ and write

$$\Delta_N(\{\lambda\})\Delta_N(\{\lambda\}) \quad = \quad \det_{j,k=1\ldots,N} \left(\sum_{l=0}^{N-1} C_l(\lambda_j) D_l(\lambda_k) \right) . \tag{2.22}$$

The sum in the determinant comes from the matrix product of $C_k(\lambda_j)$ and $D_k(\lambda_j)$. By choosing both these polynomials as orthogonal with respect to a weight $w(\lambda)$ determined by the jpdf, the integrals in (2.17) can be performed. I denote the monic set of orthogonal polynomials by $p_k(\lambda_j)$, and in other words set $C_k(\lambda_j) = D_k(\lambda_j) = p_k(\lambda_j)$. For GUE the choice $w(\lambda) = e^{-\lambda^2}$ on the interval $[-\infty, \infty]$ is made, which corresponds to the Hermite polynomials. However, I want to emphasise that the structure presented here holds for every ensemble with exponent 2 in the Vandermonde.

The jpdf is often written as

$$P_N(\lambda_1, \ldots, \lambda_N) \quad \propto \quad \det_{j,k=1\ldots,N} \left(K_N(\lambda_j, \lambda_k)\right) \ , \tag{2.23}$$

where

$$K(\lambda_j, \lambda_k) \quad = \quad \sum_{l=0}^{N-1} \frac{\sqrt{w(\lambda_j)} p_l(\lambda_j) \sqrt{w(\lambda_k)} p_l(\lambda_k)}{h_l} \tag{2.24}$$

is called the kernel.[1] The structure comes directly from (2.22) and pulling the weight $w(\lambda)$ into the determinant. Note that I have included the normalisation constants h_j from (2.18). This gives the kernel the property

$$\int_a^b K_N(x,z) K_N(z,y) dz \quad = \quad K_N(x,y) \tag{2.25}$$

and allows the $N-k$ integrals in the k-point correlation (2.17) functions to be performed [9]

$$\begin{aligned} P_k\left(\lambda_1, \ldots, \lambda_k\right) \quad &= \quad \frac{N!}{(N-k)!} \int_a^b \det_{j,k=1\ldots,N} \left(K_N(\lambda_j, \lambda_k)\right) dx_1 \ldots dx_{N-k} \\ &= \quad \det_{j,k=1\ldots,k} \left(K_N(\lambda_j, \lambda_k)\right) \ . \end{aligned} \tag{2.26}$$

The determinant structure of the correlation functions gives rise to the name determinantal point process (DPP), see for instance [9].

The special case of the 1-point correlation function, also known as the spectral density and denoted by $\rho(\lambda)$, is

$$\rho_N(\lambda) \quad = \quad \sum_{j=0}^{N-1} w(\lambda) p_j(\lambda)^2 \ . \tag{2.27}$$

This will be of particular interest for the ensembles considered in this thesis. The spectral density of the GUE is [8]

$$\begin{aligned} \rho^N_{\mathrm{GUE}}(\lambda) \quad &= \quad \frac{1}{2\sigma} \sum_{j=0}^{N-1} \varphi_j \left(\frac{\lambda}{\sigma}\right)^2 \ , \\ \varphi_j(\lambda) \quad &= \quad \frac{1}{\sqrt{2^j j! \sqrt{\pi}}} e^{-\lambda^2/2} H_j(\lambda) \ , \end{aligned} \tag{2.28}$$

where σ is the width of the Gaussian entries in the original matrix, see (2.1). (Being able to choose this becomes relevant in Chapter 4.)

[1] There are two conventions for defining the kernel, with or without the weight function. I will include the weight function in this thesis.

Recurrence Relations and Christoffel-Darboux

The kernel may be simplified with the Christoffel-Darboux relation. Derivation of this will also help show some of the properties of orthogonal polynomials. I start with the three-step recurrence relation

$$xp_j(x) = p_{j+1}(x) + \alpha_j^j p_j(x) + \alpha_j^{j-1} p_{j-1}(x), \tag{2.29}$$

where

$$\alpha_j^k = h_j^{-1} \int_a^b w(x) x \, p_j(x) p_k(x) dx \, . \tag{2.30}$$

This can be realised by expanding $xp_j(x)$ in terms of the orthogonal polynomials (because they form a complete set)

$$xp_j(x) = \sum_{k=0}^{j+1} \alpha_j^k p_k(x) \, , \tag{2.31}$$

where α_j^k is the same as above. See also [45]. Note that, because of orthogonality, $\alpha_j^k = 0$ for $j < k - 1$. Note also that $\alpha_j^{j-1} = h_j/h_{j-1}$. This follows from the fact that $p_j(x)$ is orthogonal to any polynomial of degree less than j and that the polynomials are monic. So, inside the integral, only the x^j part of $xp_{j-1}(x)$ is relevant and it gives the same coefficient as would $p_j(x)$. For the next part, it is slightly simpler to consider orthonormal polynomials, denoted by $\hat{p}_j(x)$, which are obtained by dividing by $\sqrt{h_j}$ on either side

$$x\hat{p}_j(x) = c_j \hat{p}_{j+1}(x) + \alpha_j^j \hat{p}_j(x) + c_{j-1}\hat{p}_{j-1}(x) \quad , \quad c_j = \sqrt{\frac{h_{j+1}}{h_j}} \, . \tag{2.32}$$

This recursion relation may be used to derive the Christoffel-Darboux formula. Take the following sum of orthonormal polynomials and apply the recursion relation to it

$$\begin{aligned}
(x-y) \sum_{j=0}^{N-1} \hat{p}_j(x)\hat{p}_j(y) &= \sum_{j=0}^{N-1} \Big[\hat{p}_j(y) \left(c_j \hat{p}_{j+1}(x) + \alpha_j^j \hat{p}_j(x) + c_{j-1}\hat{p}_{j-1}(x) \right) \\
&\quad - \hat{p}_j(x) \left(c_j \hat{p}_{j+1}(y) + \alpha_j^j \hat{p}_j(y) + c_{j-1}\hat{p}_{j-1}(y) \right) \Big] \\
&= \sum_{j=0}^{N-1} \Big[\hat{p}_j(y) \left(c_j \hat{p}_{j+1}(x) + c_{j-1}\hat{p}_{j-1}(x) \right) \\
&\quad - \hat{p}_j(x) \left(c_j \hat{p}_{j+1}(y) + c_{j-1}\hat{p}_{j-1}(y) \right) \Big] \, .
\end{aligned} \tag{2.33}$$

The $\hat{p}_{-1}$-terms are 0 by definition, and all but the $\hat{p}_N\hat{p}_{N-1}$-terms are cancelled by the next term in the sum. Divide by $x - y$ (for $x \neq y$) to obtain the final version of the Christoffel-Darboux formula

$$\sum_{j=0}^{N-1} \hat{p}_j(x)\hat{p}_j(y) = c_{N-1} \frac{\hat{p}_N(x)\hat{p}_{N-1}(y) - \hat{p}_{N-1}(x)\hat{p}_N(y)}{x-y} \, . \tag{2.34}$$

Note that this is exactly (2.24). The special case $x = y$ can be found with l'Hopital's rule

$$\sum_{j=0}^{N-1} \hat{p}_j(x)\hat{p}_j(x) = c_{N-1}\left(\left(\frac{d}{dx}\hat{p}_N(x)\right)\hat{p}_{N-1}(x) - \left(\frac{d}{dx}\hat{p}_{N-1}(x)\right)\hat{p}_N(x)\right) , \quad (2.35)$$

which is applicable to the spectral density.

Calculating Orthogonal Polynomials

So far I have simply assumed the existence of the orthogonal polynomials, but this is not necessary. In general, they may be written with Gram-Schmidt orthogonalisation as

$$p_k(x) = \det\begin{pmatrix} \langle e_0|e_0\rangle & \langle e_0|e_1\rangle & \dots & \langle e_0|e_{k-1}\rangle & 1 \\ \langle e_1|e_0\rangle & \langle e_1|e_1\rangle & \dots & \langle e_1|e_{k-1}\rangle & x \\ \vdots & \vdots & \ddots & \vdots & \vdots \\ \langle e_k|e_0\rangle & \langle e_k|e_1\rangle & \dots & \langle e_k|e_{k-1}\rangle & x^k \end{pmatrix} , \quad (2.36)$$

where $e_a = x^a$ and $\langle\cdot|\cdot\rangle$ is the product from (2.18). The product with any lower-order polynomial will vanish because of equal columns. In practice, this is not a viable method to find the polynomials, so let me now show how this is done. Start from the Heine identity [46, 47]

$$p_j(x) = \left\langle \prod_{k=1}^{j}(x-\lambda_k)\right\rangle_j , \quad (2.37)$$

where the average is over the matrix ensemble of size $j = N$. This can be proven as follows. Write out the expectational value

$$\left\langle \prod_{k=1}^{j}(x-\lambda_k)\right\rangle_j = \frac{1}{Z_j}\int_0^\infty dx\, w(x) \prod_{k=1}^{j}(x-\lambda_j)\Delta_j(\{\lambda\})^2 , \quad (2.38)$$

where Z_j is the partition function

$$\begin{aligned} Z_N &= \int_a^b w(x)\Delta_N(\{x\})^2 dx_1 \dots dx_N \\ &= N! \prod_{k=1}^{N} h_{k-1} . \end{aligned} \quad (2.39)$$

Note that

$$\begin{aligned} \prod_{k=1}^{j}(x-\lambda_k)\Delta_j(\{\lambda\}) &= \Delta_{j+1}\left(\{\lambda\}, x=\lambda_{j+1}\right) \\ &= \det_{1\le k,l\le j+1}(p_{k-1}(x_l)). \end{aligned} \quad (2.40)$$

Pulling in the extra product into one of the Vandermonde determinant and inserting from (2.14) leads to

$$\begin{aligned} \left\langle \prod_{k=1}^{j}(x-\lambda_k)\right\rangle_j &= \frac{1}{Z_j}\sum_{\substack{\sigma\in S_j \\ \sigma'\in S_{j+1}}} (-1)^{\sigma+\sigma'} \prod_{k=1}^{j}\int_0^\infty w(\lambda_k) p_{\sigma(k)-1}(\lambda_k) p_{\sigma'(k)-1}(\lambda_k) p_{\sigma'(j+1)-1}(x) d\lambda_k \\ &= p_j(x). \end{aligned} \quad (2.41)$$

For each term in the determinant the orthogonality leaves only $p_j(x)$. The rest of the factors cancel. The kernel may be obtained in similar fashion

$$\begin{aligned}\left\langle \prod_{j=1}^{N}(x-\lambda_j)(y-\lambda_j)\right\rangle_N &= \frac{1}{Z_N}\sum_{\sigma,\sigma'\in S_{N+1}}(-1)^{\sigma+\sigma'}\prod_{j=1}^{N}\int_0^\infty w(\lambda_j)p_{\sigma(j)-1}(\lambda_j)p_{\sigma'(j)-1}(\lambda_j)\\ &\quad\times p_{\sigma(L+1)-1}(x)p_{\sigma'(N+1)-1}(y)\,d\lambda_j\\ &= \frac{1}{Z_N}\sum_{k=0}^{N}N!\prod_{j=1}^{N+1}h_{j-1}\frac{p_k(x)p_k(y)}{h_k}\\ &= h_N\frac{p_{N+1}(x)p_N(y)-p_N(x)p_{N+1}(y)}{x-y}\\ &= h_N K_{N+1}(x,y). \end{aligned} \tag{2.42}$$

Note that the orthogonality here reduces the sum over configurations to a simple sum over the final terms. With this, all ensembles with $\beta = 2$ may in principle be solved. The difficulty lies in writing (2.37) in a closed form. As an example, let me show the derivation of (2.28). Start with the set of polynomials from (2.37) and rewrite it in terms of the original matrix X from (2.2)

$$\begin{aligned} p_j(x) &= \left\langle \prod_{k=1}^{j}(x-\lambda_k)\right\rangle_j\\ &= \langle \det(x\mathbb{1}_j - X)\rangle_j\\ &\propto \int [dX]\det(x\mathbb{1}_j - X)\exp\left[-\frac{1}{\sigma^2}\operatorname{Tr}X^2\right], \end{aligned} \tag{2.43}$$

where the measure $[dX]$ is over the independent entries of the matrix X. I express the determinant as a Grassmann integral over a vector ψ of anticommuting variables, see [9, 48, 49] for an introduction to supermathematics. This yields

$$p_j(x) \propto \int [dX][d\psi]\exp\left[-\frac{1}{\sigma^2}\operatorname{Tr}X^2 - \operatorname{Tr}(x\mathbb{1}_j - X)\,\psi\psi^\dagger\right]. \tag{2.44}$$

I have collected the Grassmann variables using the cyclic property of the trace. The sign comes from anticommuting them. Performing the integral over X gives

$$\begin{aligned} p_j(x) &\propto \int [dX][d\psi]\exp\left[-\frac{1}{\sigma^2}\operatorname{Tr}X^2 - \operatorname{Tr}(x\mathbb{1}_j - X)\,\psi\psi^\dagger\right]\\ &\propto \int [d\psi]\exp\left[\frac{\sigma^2}{4}\operatorname{Tr}\psi\psi^\dagger\psi\psi^\dagger - x\operatorname{Tr}\psi\psi^\dagger\right] \end{aligned} \tag{2.45}$$

Using bosonisation [50, 51, 52], I rewrite the integrals over the Grassmann variables as a contour integral $\psi^\dagger\psi \to \frac{2}{\sigma}ie^{i\theta}$ and obtain

$$p_j(x) \propto \int_0^{2\pi}\frac{d\theta}{2\pi}e^{-ij\theta}\exp\left[-e^{2i\theta} + \frac{2x}{\sigma}e^{i\theta}\right], \tag{2.46}$$

which is the contour integral representation of the Hermite polynomials. Adding the weight from (2.14), normalising, and inserting in (2.24) leads to (2.28).

Another example of a determinantal point process that will become relevant later is the set of antisymmetric Hermitian matrices (GAOE). With the matrix size $N = 2n + \nu$, $\nu \in \{0, 1\}$ to distinguish between even and odd size, it has the density [8]

$$\rho^{N,\nu}_{\mathrm{GAOE}}(\lambda) = \sum_{j=0}^{n-1} \frac{1}{\sqrt{\pi} 2^{2j+\nu-3/2}(2j+\nu)!} e^{-2\lambda^2} H_{2j+\nu}\left(\sqrt{2}\,\lambda\right)^2 , \tag{2.47}$$

where $H_j(x)$ are the Hermite polynomials. I will go into more detail about the different ensembles and symmetry classes in Section 2.3.

2.2.2 Skew-Orthogonal Polynomials

An important part of the orthogonal polynomial machinery is the structure (2.22), where the product of two Vandermonde determinants allows a matching of two polynomials of the same order, which leads to (2.25). For $\beta = 1$ skew-orthogonal polynomials are used instead, where the idea is to match consecutive orders within the same set of polynomials (usually even and odd powers). One also has to distinguish between even or odd matrix size of the ensemble.

In this section I introduce the polynomials in the form they are needed for Chapter 3. Here the ensemble builds a Pfaffian-point process, which means that the k-point correlation functions can be expressed in terms of three kernels I^ν_n, S^ν_n and D^ν_n, which depend on the corresponding skew-orthogonal polynomials and their integral transforms,

$$R^\nu_k(\lambda_1, \ldots, \lambda_k) = \mathrm{Pf}\left[\begin{pmatrix} I^\nu_n(\lambda_i, \lambda_j) & S^\nu_n(\lambda_i, \lambda_j) \\ -S^\nu_n(\lambda_i, \lambda_j) & D^\nu_n(\lambda_i, \lambda_j) \end{pmatrix}\right]_{i,j=1,\ldots,k} , \tag{2.48}$$

where the Pfaffian is defined as

$$(\mathrm{Pf}(M))^2 = \det(M) \tag{2.49}$$

for an antisymmetric, $N \times N$ matrix M with N even. Alternatively, given the pairs

$$\xi = \{(j_1, k_1), (j_2, k_2), \ldots, (j_{N/2}, k_{N/2})\} \tag{2.50}$$

with $j_i < k_i$ and $j_1 < j_2 < \cdots < j_{N/2}$, and given the corresponding permutation

$$\pi_\xi = \begin{bmatrix} 1 & 2 & 3 & 4 & \ldots & N-1 & N \\ j_1 & k_1 & j_2 & k_2 & \ldots & j_{N/2} & k_{N/2} \end{bmatrix} , \tag{2.51}$$

the Pfaffian may also be defined as

$$\mathrm{Pf}(M) = \sum_\xi \mathrm{sign}(\pi_\xi) M_{j_1,k_1} M_{j_2,k_2} \ldots M_{j_{N/2},k_{N/2}} . \tag{2.52}$$

The inner bracket of (2.48) reflects the fact that I consider a 2×2 block matrix kernel in the Pfaffian determinant. I will elucidate this structure below, which also depends on the matrix dimension. As an example I will consider the chiral orthogonal ensemble (chGOE) given by

$$X = \begin{pmatrix} 0 & iW \\ -iW^T & 0 \end{pmatrix} , \tag{2.53}$$

where W is an $n \times (n+\nu)$ real matrix without further symmetries. Note that it is n even or odd that has to be distinguished rather than $N = 2n + \nu$. The eigenvalues also come in $\pm$ pairs, which makes the argument of the Vandermonde squared $\Delta_n(\{\lambda^2\})$.

Skew-Orthogonal Polynomials for Even Dimension

For even matrix dimension $n = 2m$, $m \in \mathbf{N}$ the inner product is

$$\langle f_1, f_2\rangle_e = -\langle f_2, f_1\rangle_e = \int_0^\infty dx \int_0^\infty dy\, f_1(x) f_2(y) G_\nu(x,y), \tag{2.54}$$

where the subscript "e" denotes the even case. The two-point weight function is denoted by $G_\nu(x,y)$, which comes from the jpdf, which has the structure

$$P_n^{(\nu)}(\lambda_1, \ldots, \lambda_n) = C_{n,\nu}\, \Delta_n\left(\{\lambda^2\}\right) \mathrm{Pf}\left[G_\nu(\lambda_j, \lambda_k)\right]_{j,k=1,\ldots,n} . \tag{2.55}$$

Because I need different weight functions for the even and odd cases, I denote these $G_\nu(x,y)$ and $H_\nu(x,y)$ respectively. This notation is chosen to align with Chapter 3, which follows [AKMV].

The orthogonality conditions are

$$\langle p_{2j}^{(\nu)}, p_{2k}^{(\nu)}\rangle_e = \langle q_{2j}^{(\nu)}, q_{2k}^{(\nu)}\rangle_e = 0 \quad \text{and} \quad \langle p_{2j}^{(\nu)}, q_{2k}^{(\nu)}\rangle_e = h_{2j}^{(\nu)}\delta_{jk}, \quad k,l = 0, \ldots, m-1. \tag{2.56}$$

The three kernels that determine the k-point correlation functions (2.17) can be expressed in terms of these quantities as [8, 9, 53]

$$S_{2m}^{\nu}(x,y) = \sum_{j=0}^{m-1} \frac{p_{2j}^{(\nu)}(x)\bar{q}_{2j}^{(\nu)}(y) - q_{2j}^{(\nu)}(x)\bar{p}_{2j}^{(\nu)}(y)}{h_{2j}^{(\nu)}} , \tag{2.57}$$

$$D_{2m}^{\nu}(x,y) = \sum_{j=0}^{m-1} \frac{\bar{q}_{2j}^{(\nu)}(x)\bar{p}_{2j}^{(\nu)}(y) - \bar{p}_{2j}^{(\nu)}(x)\bar{q}_{2j}^{(\nu)}(y)}{h_{2j}^{(\nu)}} + G_\nu(x,y) , \tag{2.58}$$

$$I_{2m}^{\nu}(x,y) = \sum_{j=0}^{m-1} \frac{q_{2j}^{(\nu)}(x)p_{2j}^{(\nu)}(y) - p_{2j}^{(\nu)}(x)q_{2j}^{(\nu)}(y)}{h_{2j}^{(\nu)}} . \tag{2.59}$$

Here I have introduced the following integral transforms of the polynomials:

$$\bar{p}_{2j}^{(\nu)}(x) = \int_0^\infty dy\, p_{2j}^{(\nu)}(y) G_\nu(x,y) \quad \text{and} \quad \bar{q}_{2j}^{(\nu)}(x) = \int_0^\infty dy\, q_{2j}^{(\nu)}(y) G_\nu(x,y) . \tag{2.60}$$

The spectral density is given by (2.48) for $k = 1$,

$$R_1^{\nu}(\lambda) = S_{2m}^{\nu}(\lambda,\lambda) = \sum_{j=0}^{m-1} \frac{p_{2j}^{(\nu)}(\lambda)\bar{q}_{2j}^{(\nu)}(\lambda) - q_{2j}^{(\nu)}(\lambda)\bar{p}_{2j}^{(\nu)}(\lambda)}{h_{2j}^{(\nu)}} . \tag{2.61}$$

As an example, consider the chGOE (2.53) where $G_\nu(x,y) = (xy)^\nu e^{-2(x^2+y^2)}\mathrm{sign}(x-y)$ and the polynomials for even j are [25]

$$p_j^{(\nu)}(x) = \frac{j!}{(-4)^j} L_j^{(\nu)}\left(4x^2\right) , \tag{2.62}$$

$$q_j^{(\nu)}(x) = \frac{j!}{(-4)^j} \Big[(j+1)L_{j+1}^{(\nu)}\left(4x^2\right) - c_j^{(\nu)} L_j^{(\nu)}\left(4x^2\right) - (j+\nu)L_{j-1}^{(\nu)}\left(4x^2\right) . \tag{2.63}$$

The second line has been rewritten with the following identities for generalised Laguerre polynomials [54],

$$L_j^{(\nu-1)}(z) = L_j^{(\nu)}(z) - L_{j-1}^{(\nu)}(z) \quad \text{and} \quad L_{j-1}^{(\nu)}(z) = (j+\nu)L_{j-1}^{(\nu)}(z) - jL_j^{(\nu)}(z)\,. \tag{2.64}$$

The special case of the spectral density is

$$\begin{aligned} R_1^\nu(\lambda) &= \sum_{j=0}^{m-1} \frac{2^{2\nu+2}(2j)!}{(2j+\nu)!} \int_0^\infty du (\lambda u)^\nu e^{-2u^2-2\lambda^2} \mathrm{sign}(\lambda-u) \\ &\times \left[L_{2j}^{(\nu)}\left(4\lambda^2\right) \left((2j+1) L_{2j+1}^{(\nu)}\left(4u^2\right) - (2j+\nu) \left(L_{2j}^{(\nu)}\left(4u^2\right) + L_{2j-1}^{(\nu)}\left(4u^2\right) \right) \right) - (\lambda \leftrightarrow u) \right]\,. \end{aligned} \tag{2.65}$$

The chiral orthogonal ensemble will function as a limiting case of the ensemble considered in Chapter 3.

Skew-Orthogonal Polynomials for Odd Dimension

For odd dimension $n = 2m-1$ with $m \in \mathbf{N}$ the Pfaffian determinant in the jpdf has one extra row and column containing a one-point weight function $g_\nu(x)$

$$P_n^{(\nu)}(\lambda_1, \ldots, \lambda_n) = C_{n,\nu}\, \Delta_n\left(\{\lambda^2\}\right) \mathrm{Pf} \left[\begin{array}{cc} G_\nu(\lambda_j, \lambda_k) & g_\nu(\lambda_j) \\ -g_\nu(\lambda_k) & 0 \end{array} \right]_{j,k=1,\ldots,n}\,. \tag{2.66}$$

This can also be obtained from (2.55) for even $n = 2m$ by sending one of its singular values, say λ_{2m}, to infinity, following the ideas of [55]. This procedure leads to the relation $\lim_{y\gg 1} G_\nu(x,y) = g_\nu(x) y^\nu g_0(y)$. For chGOE $g_\nu(x) = x^\nu e^{-2x^2}$.

A standard approach to Pfaffian point processes with odd dimension n is to modify all polynomials from the case of even n to obtain a skew-orthogonality relation for the polynomials with respect to the one-point weight. I use the ideas presented in [31, 56] instead and modify the skew-symmetric product while keeping the same polynomials $p_j^{(\nu)}(x)$ and $q_j^{(\nu)}(x)$. For odd $n = 2m-1$, the skew-symmetric product, denoted by the subscript "o", is chosen to be

$$\langle f_1, f_2\rangle_o = -\langle f_2, f_1\rangle_o = \int_0^\infty dx \int_0^\infty dy\, f_1(x) f_2(y) H_\nu(x,y) \tag{2.67}$$

with the weight

$$H_\nu(x,y) = G_\nu(x,y) - \frac{g_\nu(x)}{\bar{g}_\nu} \int_0^\infty dx' G_\nu(x',y) - \frac{g_\nu(y)}{\bar{g}_\nu} \int_0^\infty dy' G_\nu(x,y') \tag{2.68}$$

and the constant

$$\bar{g}_\nu = \int_0^\infty dx\, g_\nu(x)\,. \tag{2.69}$$

The jpdf (2.66) does not change under replacing $G_\nu(x,y)$ by $H_\nu(x,y)$. The switch simply corresponds to adding multiples of the last row and column to the other rows and columns under

which the Pfaffian is invariant. Note that $H_\nu(x,y)$ is also antisymmetric. The redefinition (2.67) of the skew-product immediately implies that

$$\langle p^{(\nu)}_{2j-1}, 1\rangle_o \;=\; \langle q^{(\nu)}_{2j-1}, 1\rangle_o = 0, \qquad \text{for } j = 1, 2, \ldots \tag{2.70}$$

This means that any polynomial is skew-orthogonal to the monomial of zeroth order. The remaining sOP starting from degree 1 in x^2 satisfy

$$\langle p^{(\nu)}_{2j-1}, p^{(\nu)}_{2k-1}\rangle_o = \langle q^{(\nu)}_{2j-1}, q^{(\nu)}_{2k-1}\rangle_o = 0 \quad \text{and} \quad \langle p^{(\nu)}_{2j-1}, q^{(\nu)}_{2k-1}\rangle_o = h^{(\nu)}_{2j-1}\delta_{jk}\,, \tag{2.71}$$

for $j,k = 1,\ldots,m$, with respect to the new skew-symmetric product (2.67). The following relations are also needed

$$\int_0^\infty dx\, p^{(\nu)}_{2j-1}(x) g_\nu(x) = \int_0^\infty dx\, q^{(\nu)}_{2j-1}(x) g_\nu(x) = 0\,, \tag{2.72}$$

where $j,k = 1,\ldots,m$. The kernels of the k-point correlation function (2.48) take a slightly different form[2]

$$S^\nu_{2m-1}(x,y) \;=\; \sum_{j=1}^{m-1} \frac{p^{(\nu)}_{2j-1}(x)\tilde{q}^{(\nu)}_{2j-1}(y) - q^{(\nu)}_{2j-1}(x)\tilde{p}^{(\nu)}_{2j-1}(y)}{h^{(\nu)}_{2j-1}} + \frac{g_\nu(x)}{\bar{g}_\nu}\,, \tag{2.73}$$

$$D^\nu_{2m-1}(x,y) \;=\; \sum_{j=1}^{m-1} \frac{\tilde{q}^{(\nu)}_{2j-1}(x)\tilde{p}^{(\nu)}_{2j-1}(y) - \tilde{p}^{(\nu)}_{2j-1}(x)\tilde{q}^{(\nu)}_{2j-1}(y)}{h^{(\nu)}_{2j-1}} + H_\nu(x,y)\,, \tag{2.74}$$

$$I^\nu_{2m-1}(x,y) \;=\; \sum_{j=1}^{m-1} \frac{q^{(\nu)}_{2j-1}(x)p^{(\nu)}_{2j-1}(y) - p^{(\nu)}_{2j-1}(x)q^{(\nu)}_{2j-1}(y)}{h^{(\nu)}_{2j-1}}\,. \tag{2.75}$$

Here the transformed polynomials are integrated with respect to the new two-point weight (2.68)

$$\tilde{p}^{(\nu)}_{2j-1}(x) = \int_0^\infty dy\, p^{(\nu)}_{2j-1}(y) H_\nu(x,y) \quad \text{and} \quad \tilde{q}^{(\nu)}_{2j-1}(x) = \int_0^\infty dy\, q^{(\nu)}_{2j-1}(y) H_\nu(x,y), \tag{2.76}$$

for $j = 1,2,\ldots$ Due to the additional row in the Pfaffian, the spectral density now reads

$$R^\nu_1(\lambda) = S^\nu_{2m-1}(\lambda,\lambda) = \sum_{j=1}^{m-1} \frac{p^{(\nu)}_{2j-1}(\lambda)\tilde{q}^{(\nu)}_{2j-1}(\lambda) - q^{(\nu)}_{2j-1}(\lambda)\tilde{p}^{(\nu)}_{2j-1}(\lambda)}{h^{(\nu)}_{2j-1}} + \frac{g_\nu(\lambda)}{\bar{g}_\nu}\,. \tag{2.77}$$

The new term $g_\nu(\lambda)/\bar{g}_\nu$, compared to the density (2.61), comes from this particularity for odd $n = 2m-1$. It can be interpreted as the distribution of the smallest singular value of the random matrix X as it is the only term left for $m = 1$. Adding more singular values, represented as new peaks, arise only on the right-hand side of the maximum of this distribution. The new terms in the sum (2.77) also contribute corrections to the individual distribution of the smallest eigenvalue due to the level repulsion of the other singular values. The identification of the term $g_\nu(\lambda)/\bar{g}_\nu$ with the smallest eigenvalue is therefore not exact, but a good approximation.

This concludes the introduction of the general tools needed to solve the matrix models in the thesis. Additional chapter-specific techniques will be introduced in the respective chapters.

From here I will look more closely at the models I will consider. This includes the classification of symmetry classes and how to extend the classification scheme to transition ensembles.

[2] I use the same names for the three kernels and the normalisation constants, though this is a slight abuse of notation. Only their subscript indicates even or odd n.

RMT	Cartan Class	$\mathcal{H}_N$	Matrix Structure
GUE	A	$\mathrm{Herm}(N)$	$H = H^\dagger \in \mathbf{C}^{N\times N}$
GOE	AI	$\mathrm{Sym}(N)$	$H = H^T = H^* \in \mathbf{R}^{N\times N}$
GSE	AII	$\mathrm{Self}(N)$	$H = \tau_2 H^T \tau_2 = \tau_2 H^* \tau_2 \in \mathbf{C}^{N\times N},\ N \in 2\mathbf{N}$
GAOE	B|D	$\mathrm{ASym}(N)$	$H = -H^T = -H^* \in i\mathbf{R}^{N\times N}$
GASE	C	$\mathrm{ASelf}(N)$	$H = -\tau_2 H^T \tau_2 = -\tau_2 H^* \tau_2 \in \mathbf{C}^{N\times N},\ N \in 2\mathbf{N}$
chGUE	AIII	$\mathrm{Mat}_{\mathbf{C}}(n+\nu, n)$	$H = \begin{bmatrix} 0 & W \\ W^\dagger & 0 \end{bmatrix},\ W \in \mathbf{C}^{(n+\nu)\times n}$
chGOE	B|DI	$\mathrm{Mat}_{\mathbf{R}}(n+\nu, n)$	$H = \begin{bmatrix} 0 & W \\ W^\dagger & 0 \end{bmatrix},\ W = W^* \in \mathbf{R}^{(n+\nu)\times n}$
chGSE	CII	$\mathrm{Mat}_{\mathbf{H}}(n+\nu, n)$	$H = \begin{bmatrix} 0 & W \\ W^\dagger & 0 \end{bmatrix},\ W = \tau_2 W^* \tau_2 \in \mathbf{C}^{(n+\nu)\times n},\ n, \nu \in 2\mathbf{N}$
GBOE	CI	$\mathrm{Sym}_{\mathbf{C}}(N/2)$	$H = \begin{bmatrix} 0 & W \\ W^\dagger & 0 \end{bmatrix},\ W = W^T \in \mathbf{C}^{N/2\times N/2},\ N \in 2\mathbf{N}$
GBSE	DIII	$\mathrm{ASym}_{\mathbf{C}}(N/2)$	$H = \begin{bmatrix} 0 & W \\ W^\dagger & 0 \end{bmatrix},\ W = -W^T \in \mathbf{C}^{N/2\times N/2},\ N \in 2\mathbf{N}$

Table 2.1: The ten symmetry classes given in terms of the acronym of the Gaussian random matrix ensemble (first column, notation follows [68]) and the symbol from the Cartan classification scheme (second column, see [12, 57, 59]). The third column is the matrix space of the class [12, 57, 59], and the fourth column shows the structure of it in matrix form. The matrix τ_2 denotes the second Pauli matrix. The first five rows are the non-chiral classes, the next three are the classical chiral ensembles where $N = 2n + \nu$. The last two rows are the two Boguliubov–de Gennes classes. For the symplectic cases (third, fifth and eighth row) the dimensions N, ν, n all have to be even. This table is printed in [KMS] and continued in Tables 2.2 and 2.3.

2.3 Symmetry Classes

There are ten symmetry classes of Hermitian operators in total, which have been classified by Altland and Zirnbauer [12, 57]. Five of the ten classes exhibit a chiral symmetry and the other five do not. In this section I review this classification. Substantial further treatment may be found in the literature, see for instance [8, 9, 57, 58, 59, 60, 61] for symmetry classifications in RMT and [12, 24, 58, 62, 63, 64, 65, 66, 67, 68] for the classification of these symmetries in physical systems. Some of the considerations in this section are made in anticipation of the calculations made in Chapter 4. I therefore include the needed groups here to keep the discussion in one place.

In Chapter 5 I will also consider non-Hermitian matrices. The classification of these is not yet clear and several schemes with different number of classes exist [60].

2.3.1 Properties of the Classes

Let me briefly go through some properties of the different classes that will be relevant for future use, especially the number of exact zero modes, which I denote by ν. Where confusion

can arise, I denote the broadened zero modes of the unperturbed ensemble of Chapter 4 by $\widetilde{\nu}$. These discussions are summarised in Tables 2.1, 2.2, and 2.3.

Non-Chiral Classes

The non-chiral symmetries may be described through the three number fields of real ($\mathbf{R}$), complex ($\mathbf{C}$), and quaternion ($\mathbf{H}$) numbers. These three fields each have a corresponding group: The orthogonal matrices $\mathrm{O}(N)$, the unitary matrices $\mathrm{U}(N)$, and the unitary symplectic matrices $\mathrm{USp}(N)$ with N even. They are also the maximal compact subgroups of the general linear groups $\mathcal{G} = \mathrm{Gl}_{\mathbf{R}}(N), \mathrm{Gl}_{\mathbf{C}}(N), \mathrm{Gl}_{\mathbf{H}}(N)$, respectively.

There are two Hermitian subsets invariant under $\mathrm{O}(N)$ which are the real symmetric matrices $\mathcal{H} = \mathrm{Sym}(N)$ and the imaginary antisymmetric matrices $\mathcal{H} = \mathrm{ASym}(N)$. The same holds true for the quaternion case where it is the self-dual Hermitian matrices $\mathcal{H} = \mathrm{Self}(N)$ and the anti-self-dual Hermitian matrices $\mathcal{H} = \mathrm{ASelf}(N)$. For the complex case only the Hermitian matrices $\mathcal{H} = \mathrm{Herm}(N)$ are invariant under $\mathrm{U}(N)$.

For the calculations in Chapter 4, I will need the projection of U to its last $\widetilde{\nu}$ rows. That is, not the whole group $\mathcal{K} = \mathrm{O}(N), \mathrm{U}(N), \mathrm{USp}(N)$ but the corresponding Stiefel manifolds $\mathcal{K}_{\widetilde{\nu}} = \mathrm{O}(N)/\mathrm{O}(N-\widetilde{\nu}), \mathrm{U}(N)/\mathrm{U}(N-\widetilde{\nu}), \mathrm{USp}(N)/\mathrm{USp}(N-\widetilde{\nu})$. The last case also requires $\widetilde{\nu}$ even. The space $\mathcal{K}_{\widetilde{\nu}}$ can be embedded into $\widetilde{\nu} \times N$ matrices which are given by the matrix spaces $\mathcal{G}_{\widetilde{\nu}} = \mathrm{Mat}_{\mathbf{R}}(\widetilde{\nu}, N), \mathrm{Mat}_{\mathbf{C}}(\widetilde{\nu}, N), \mathrm{Mat}_{\mathbf{H}}(\widetilde{\nu}, N)$.

Chiral Classes

There are three standard chiral symmetry classes [24], where

$$H = \begin{pmatrix} 0 & W \\ W^\dagger & 0 \end{pmatrix} \tag{2.78}$$

is a real ($W \in \mathrm{Mat}_{\mathbf{R}}(n+\nu, n)$), complex ($W \in \mathrm{Mat}_{\mathbf{C}}(n+\nu, n)$), or a quaternion ($W \in \mathrm{Mat}_{\mathbf{H}}(n+\nu, n)$ with ν and n even) matrix with $N = 2n + \nu$. See also the structure in (1.3).

The remaining two symmetry classes are the Bogoliubov–de Gennes type where W is either complex symmetric $\mathrm{Sym}_{\mathbf{C}}(n + \nu = n = N/2)$ or complex antisymmetric $\mathrm{ASym}_{\mathbf{C}}(n + \nu = n = N/2)$. In both cases this structure is invariant under transformations of the unitary group $\mathcal{K} = \mathrm{U}(N/2)$, but the unitary matrix $U = \mathrm{diag}(V_1, V_2)$ has the condition $V_1 = V_2^*$.

The Stiefel manifolds are now $\mathcal{K}_{\widetilde{\nu}} = \mathrm{O}(n+\widetilde{\nu})/\mathrm{O}(n+\widetilde{\nu}-(n'+\nu')) \times \mathrm{O}(n)/\mathrm{O}(n-n'), \mathrm{U}(n+\widetilde{\nu})/\mathrm{U}(n+\widetilde{\nu}-(n'+\nu')) \times \mathrm{U}(n)/\mathrm{U}(n-n'), \mathrm{USp}(n+\widetilde{\nu})/\mathrm{USp}(n+\widetilde{\nu}-(n'+\nu')) \times \mathrm{USp}(n)/\mathrm{USp}(n-n')$ for the three classical chiral ensembles with $2n' + \nu' = \widetilde{\nu}$. As for the non-chiral ensembles, the embedding in a flat vector space is needed which here is $\mathcal{G}_{\widetilde{\nu}} = \mathrm{Mat}_{\mathbf{R}}(n' + \nu', n + \widetilde{\nu}) \oplus \mathrm{Mat}_{\mathbf{R}}(n', n), \mathrm{Mat}_{\mathbf{C}}(n' + \nu', n + \widetilde{\nu}) \oplus \mathrm{Mat}_{\mathbf{C}}(n', n), \mathrm{Mat}_{\mathbf{H}}(n' + \nu', n + \widetilde{\nu}) \oplus \mathrm{Mat}_{\mathbf{H}}(n', n)$. For the two Boguliubov–de Gennes classes the two spaces are $\mathcal{K}_{\widetilde{\nu}} = \mathrm{U}(N/2)/\mathrm{U}((N-\widetilde{\nu})/2)$ and $\mathcal{G}_{\widetilde{\nu}} = \mathrm{Mat}_{\mathbf{C}}((N-\widetilde{\nu})/2, N/2)$. Let me again emphasise that N and $\widetilde{\nu}$ are even here as well.

2.4 Exact Zero Modes and Topology

As stated above, several of the classes have eigenvalues exactly at the origin. These are of particular importance, as they are related to the topology of the underlying system through the Atiyah-Singer index theorem [13]. This means that a study of the exact zero modes by

RMT	$\mathcal{K}_{\widetilde{\nu}}$	$\mathcal{G}_{\widetilde{\nu}}$
GUE	$\frac{\mathrm{U}(N)}{\mathrm{U}(N-\widetilde{\nu})}$	$\mathrm{Mat}_{\mathbf{C}}(\widetilde{\nu}, N)$
GOE	$\frac{\mathrm{O}(N)}{\mathrm{O}(N-\widetilde{\nu})}$	$\mathrm{Mat}_{\mathbf{R}}(\widetilde{\nu}, N)$
GSE	$\frac{\mathrm{USp}(N)}{\mathrm{USp}(N-\widetilde{\nu})}$	$\mathrm{Mat}_{\mathbf{H}}(\widetilde{\nu}, N)$
GAOE	$\frac{\mathrm{O}(N)}{\mathrm{O}(N-\widetilde{\nu})}$	$\mathrm{Mat}_{\mathbf{R}}(\widetilde{\nu}, N)$
GASE	$\frac{\mathrm{USp}(N)}{\mathrm{USp}(N-\widetilde{\nu})}$	$\mathrm{Mat}_{\mathbf{H}}(\widetilde{\nu}, N)$
chGUE	$\frac{\mathrm{U}(n+\widetilde{\nu})}{\mathrm{U}(n+\widetilde{\nu}-(n'+\nu'))} \times \frac{\mathrm{U}(n)}{\mathrm{U}(n-n')}$	$\mathrm{Mat}_{\mathbf{C}}(n'+\nu', n+\widetilde{\nu}) \oplus \mathrm{Mat}_{\mathbf{C}}(n', n)$
chGOE	$\frac{\mathrm{O}(n+\widetilde{\nu})}{\mathrm{O}(n+\widetilde{\nu}-(n'+\nu'))} \times \frac{\mathrm{O}(n)}{\mathrm{O}(n-n')}$	$\mathrm{Mat}_{\mathbf{R}}(n'+\nu', n+\widetilde{\nu}) \oplus \mathrm{Mat}_{\mathbf{R}}(n', n)$
chGSE	$\frac{\mathrm{USp}(n+\widetilde{\nu})}{\mathrm{USp}(n+\widetilde{\nu}-(n'+\nu'))} \times \frac{\mathrm{USp}(n)}{\mathrm{USp}(n-n')}$	$\mathrm{Mat}_{\mathbf{H}}(n'+\nu', n+\widetilde{\nu}) \oplus \mathrm{Mat}_{\mathbf{H}}(n', n)$
GBOE	$\frac{\mathrm{U}(N/2)}{\mathrm{U}((N-\widetilde{\nu})/2)}$	$\mathrm{Mat}_{\mathbf{C}}(\widetilde{\nu}/2, N/2)$
GBSE	$\frac{\mathrm{U}(N/2)}{\mathrm{U}((N-\widetilde{\nu})/2)}$	$\mathrm{Mat}_{\mathbf{C}}(\widetilde{\nu}/2, N/2)$

Table 2.2: Continuation of Table 2.1. The order of the rows is the same. For the chiral classes $2n'+\nu' = \widetilde{\nu}$, where n', ν' are the matrix size and zero modes of the perturbed zero modes and $\widetilde{\nu}$ is the number of zero modes in the unperturbed ensemble, all in Chapter 4. The first column again shows the acronym of the ensembles [68]. The second column is the corresponding Stiefel manifold $\mathcal{K}_{\widetilde{\nu}}$, which here simply is the projection of the diagonalising unitary matrix U to its last $\widetilde{\nu}$. The third one shows the matrix space $\mathcal{G}_{\widetilde{\nu}}$, to which $\mathcal{K}_{\widetilde{\nu}}$ may be extended. These quantities are relevant for Chapter 4. This table is also printed in [KMS] and continued in Table 2.3.

extension is also a study of the underlying topology. The intuitive explanation comes from eigenvalues of Hamiltonians typically being related to the inverse length scales. This means that an eigenvalue exactly at the origin is related to properties on the scale of the whole system size. Topological zero modes see application in high energy physics [69, 70] as well as in solid state systems [71, 72]. For the latter, see also Section 2.6.

Being closely related to symmetries of the system makes the zero modes very susceptible to perturbations that break the symmetries behind them. I investigate such perturbations more closely in Chapter 4. Here the bulk is left unaffected to first order in perturbation theory, whereas the zero modes are spread out immediately.

2.5 Two-Matrix Models and Symmetry Transitions

Apart from the pure symmetry classes considered in the previous section, it has proven necessary to extend to multi-matrix models, see for instance [14, 15, 30, 56, 73, 74, 75, 76, 77, 78]. These models allow investigation of ensembles that transition between two or more symmetry

RMT	$\mathcal{P}_{\widetilde{\nu}}$	γ	Zero Modes, ν
GUE	$\mathrm{Herm}(\widetilde{\nu})$	1	0
GOE	$\mathrm{Sym}(\widetilde{\nu})$	$1/2$	0
GSE	$\mathrm{Self}(\widetilde{\nu})$	$1/2$	0
GAOE	$\mathrm{Sym}(\widetilde{\nu})$	$1/2$	$0, 1$
GASE	$\mathrm{Self}(\widetilde{\nu})$	$1/2$	0
chGUE	$\mathrm{Herm}(n' + \widetilde{\nu}') \oplus \mathrm{Herm}(n')$	1	$\mathbf{N}_0$
chGOE	$\mathrm{Sym}(n' + \widetilde{\nu}') \oplus \mathrm{Sym}(n')$	$1/2$	$\mathbf{N}_0$
chGSE	$\mathrm{Self}(n' + \widetilde{\nu}') \oplus \mathrm{Self}(n')$	$1/2$	$2\mathbf{N}_0$
GBOE	$\mathrm{Herm}(\widetilde{\nu}/2)$	$1/2$	0
GBSE	$\mathrm{Herm}(\widetilde{\nu}/2)$	$1/2$	$2\mathbf{N}_0$

Table 2.3: Continuation of Tables 2.1 and 2.2, where the order of the rows is the same, and first column again shows the acronym of the ensembles [68]. The $2n' + \nu' = \widetilde{\nu}$ for the chiral classes. The Hermitian matrix spaces $\mathcal{P}_{\widetilde{\nu}}$ given in the second column may be employed to rewrite the Haar measures as Gaussian integrals. This is relevant for Chapter 4, and $\widetilde{\nu}$ denotes the number of zero modes in the unperturbed ensemble in that chapter (to distinguish it from the number of zero modes of the matrix ensembles in this table). Also needed is the parameter γ in the third column. It is essentially the exponent of the determinant that can be obtained by a multivariate Gaussian integral. The final column shows the amount of possible zero modes. The first three columns of this table are also printed in [KMS].

classes. The two-matrix models I consider are of the form

$$M \;=\; A + aB\,. \tag{2.79}$$

Here A and B belong to different classes, and picking $a \in [0, \infty[$ allows each of the matrices to dominate in turn. $M = A$ for $a = 0$, the two matrices are on equal footing for $a = 1$, and $M = B$ for $a \to \infty$ (after rescaling). The ensembles I consider in Chapters 3 and 4 are both of this kind and illustrate the slightly different interpretations of (2.79). In Chapter 3 I consider the full transition between two symmetry classes. The goal is understand the behaviour of a specific ensemble for every value of a, and the structure of both jpdf and k-point correlation functions is therefore studied in detail. This is in contrast to the ensembles in Chapter 4, where a is considered as a perturbation. Here one can see how an ensemble behaves when its symmetry is weakly broken. The specific mechanism under scrutiny in Chapter 4 is the breaking of symmetries that give rise to zero modes.

Typically, A and B are in different symmetric spaces, but it is not necessary to restrict them to one of the ensembles outlined in Section 2.3. In general any substructure is allowed, and as I will show in Chapter 4, it is in some cases not necessary to average over the spectrum.

2.6 Solid State Physics

In this section I move away from random matrix theory to give a short introduction to the topics in solid state physics that will be relevant in the later chapters.

This section is based on unpublished work done with Jacobus Verbaarschot during my stay at Stony Brook.

2.6.1 Kitaev Chain

Consider a simple model that shows how Majorana zero modes appear in a chain of Fermions, introduced by Kitaev in [35] and followed elsewhere, such as [36]. While quite far from a realistic system, it still encaptures some of the essential features. The model is

$$H = -\mu \sum_{x=1}^{N} c_x^\dagger c_x - \sum_{x=1}^{N} (t c_x^\dagger c_{x+1} + |\Delta| e^{i\phi} c_x c_{x+1} + h.c.) \tag{2.80}$$

for $\mu = 0$ and $t = |\Delta|$ it reduces to

$$H = -it \sum_{x=1}^{N-1} \gamma_{B,x} \gamma_{A,x+1} \, , \tag{2.81}$$

where

$$c_x = \frac{1}{2} e^{-i\phi/2} (\gamma_{B,x} + i\gamma_{A,x}) \, . \tag{2.82}$$

The Majorana operators γ obey the Euclidean Clifford algebra $\{\gamma_{\alpha,x}, \gamma_{\alpha',x'}\} = 2\delta_{\alpha\alpha'}\delta_{xx'}$, so they may be represented as odd- and even-dimensional γ-matrices.

The operator $d_{end} = (\gamma_{A,1} + i\gamma_{B,N})$ corresponds to the non-local end fermion, meaning a fermion consisting of the Majorana operators at either end.

Each of the terms in the Hamiltonian commute with each other, so they may be diagonalised simultaneously. Each term squares to $-\mathbb{1}$, so each eigenvalues must be $\pm i$ and the eigenvalues of H is just the sum of these. It is never possible to create a zero for an odd number of terms (N even). For odd N note that each product of two consecutive γ-matrices have to be uniformly different. This makes it a combinatorial problem, and thus the amount of zeroes is $2\binom{N}{N/2}$. The end fermion shows that the states are degenerate as $[d_{end}, H] = 0$, and as this is a creation/annihilation operator, one may create an extra state with zero energy. This is the Majorana state.

I look again at the original model in (2.80) and express it in the basis $H = \bar{\Psi}\mathcal{H}\Psi$, where

$$\Psi = \begin{pmatrix} c_1 \\ \vdots \\ c_N \\ c_1^\dagger \\ \vdots \\ c_N^\dagger \end{pmatrix} \quad , \quad \bar{\Psi} = \begin{pmatrix} c_1^\dagger \\ \vdots \\ c_N^\dagger \\ c_1 \\ \vdots \\ c_N \end{pmatrix}^T \quad , \tag{2.83}$$

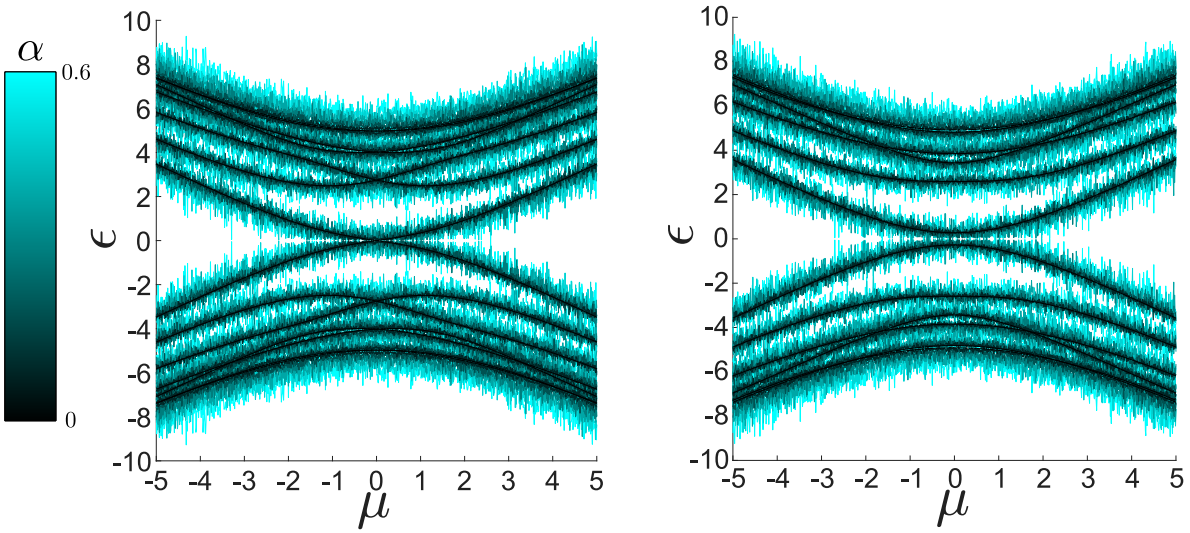

Figure 2.1: The spectral flow of the Kitaev chain with the disorder of Equation (2.87). That is, the eigenvalues ϵ of the matrix in Equation (2.84) are plotted as a function of the chemical μ with the parameters $\Delta = 2.66, t = 1$. The parameter α sets the strength of the disorder, which broadens the single levels to a band. **Left:** $N = 7$ odd. The zero modes may be seen as the crossing lines at the origin. **Right:** $N = 6$ even. In this case the smallest eigenvalues do not cross, because there is no zero mode present.

which makes the single particle Hamiltonian

$$\mathcal{H} = \begin{pmatrix} -\mu & -t & 0 & 0 & 0 & -\Delta & 0 & 0 \\ -t & \ddots & \ddots & 0 & \Delta & \ddots & \ddots & 0 \\ 0 & \ddots & \ddots & -t & 0 & \ddots & \ddots & -\Delta \\ 0 & 0 & -t & -\mu & 0 & 0 & \Delta & 0 \\ 0 & \Delta & 0 & 0 & \mu & t & 0 & 0 \\ -\Delta & \ddots & \ddots & 0 & t & \ddots & \ddots & 0 \\ 0 & \ddots & \ddots & \Delta & 0 & \ddots & \ddots & t \\ 0 & 0 & -\Delta & 0 & 0 & 0 & t & \mu \end{pmatrix} . \tag{2.84}$$

This may be rewritten with row and column operations as

$$\mathcal{H} = \begin{pmatrix} 0 & 0 & 0 & 0 & \mu & t+\Delta & 0 & 0 \\ 0 & 0 & 0 & 0 & t-\Delta & \ddots & \ddots & 0 \\ 0 & 0 & 0 & 0 & 0 & \ddots & \ddots & t+\Delta \\ 0 & 0 & 0 & 0 & 0 & 0 & t-\Delta & \mu \\ \mu & t-\Delta & 0 & 0 & 0 & 0 & 0 & 0 \\ t+\Delta & \ddots & \ddots & 0 & 0 & 0 & 0 & 0 \\ 0 & \ddots & \ddots & t-\Delta & 0 & 0 & 0 & 0 \\ 0 & 0 & t+\Delta & \mu & 0 & 0 & 0 & 0 \end{pmatrix} , \tag{2.85}$$

which also reveals the chiral structure of the Hamiltonian. Both blocks (here named W and W^T) have a zero mode for $\mu = 0$. Consider the N-dimensional matrix $D = \mathrm{diag}(1, -1, 1, -1, \dots)$. For $\mu = 0$ we have $DWD = -W$, which means $\det(W) = (-1)^N \det(DWD) = (-1)^N \det(W)$. The two zero modes therefore appear for odd N.

For the dependency on the chemical potential μ, see Figure 2.1, where I also add disorder of the form

$$\mathcal{H} + \alpha \mathcal{H}_{rand}, \tag{2.86}$$

where $\mathcal{H}_{rand}$ is a real symmetric matrix with the structure

$$\mathcal{H}_{rand} = \begin{pmatrix} S & 0 \\ 0 & -S \end{pmatrix} \quad , \quad S = S^T \, . \tag{2.87}$$

The topologically protected zero modes are seen as the modes crossing at the origin. The noise is added to see the spread of each eigenvalue. The behaviour of the zero mode in case $\mu = 0$ and N odd with added noise is treated in Chapter 4. The noise has this substructure because the symmetry

$$\begin{pmatrix} 0 & 1 \\ 1 & 0 \end{pmatrix} \mathcal{H}_{rand} \begin{pmatrix} 0 & 1 \\ 1 & 0 \end{pmatrix} \quad = \quad -\mathcal{H}_{rand}, \tag{2.88}$$

is needed, as it corresponds to the algebra of the creation-/annihilation-operators.

Note that the matrix in Equation (2.84) correspond to the single-particle Hamiltonian, as opposed to the full many-body version. This would be possible in terms of γ-matrices. This concludes the introduction of the framework in which I will work.

Chapter 3

Transition Between the Chiral Orthogonal and the Antisymmetric Hermitian Ensemble

In this chapter I look at a transition ensemble where topology is preserved. That is, the number of generic eigenvalues at the origin does not change during the transition. Chiral symmetry is, however, broken. One realisation of the corresponding random matrix may be written as

$$J = i \begin{pmatrix} aA & \widetilde{W} \\ -\widetilde{W}^T & aB \end{pmatrix}, \tag{3.1}$$

where A and B are two real antisymmetric matrices of sizes $n \times n$ and $(n+\nu) \times (n+\nu)$, respectively, $\widetilde{W}$ is an $n \times (n+\nu)$ real matrix with $\nu = 0, 1$, and a is a positive real coupling constant. The topology depends on whether A and B are even- or odd-dimensional. This is a more concrete example of a random two-matrix model of the form (2.79), namely the transition between the ensemble of chiral orthogonal matrices and the one of antisymmetric matrices.

The motivation behind studying such a transition comes from topological insulators. I have already discussed the classification of these in Section 2.3, but for reference see [35, 63, 64, 65, 66] or [34, 38, 67] for reviews. Chiral symmetry appears there due to a combination of time-reversal and particle-hole symmetry, see for instance [34]. Furthermore, with the presence of disorder Majorana modes in quasi one-dimensional quantum wires with spin-orbit coupling, the relevant symmetry class is the ensemble of antisymmetric hermitian matrices [79]. It was subsequently suggested in [39] to study the transition between GAOE and chGOE. The transition ensemble (3.1) is one possible choice, and other transitions have been suggested for the corresponding Bogoliubov–de Gennes Hamiltonian, including the chGUE. I will not repeat the arguments for the respective symmetry transitions here, but refer to [36, 37].

A Gaussian weight is chosen for simplicity, but it is expected that the model (3.1) will capture the statistical properties of the topological insulators in the limit of large matrices where universality of the spectrum is typically found, based only on the global symmetries.

Especially the regime $a \gg 1$ for n odd and $\nu = 0$ may be relevant for the topological insulators. Here the zero modes of the antisymmetric matrices A and B, present for $a = \infty$, can be identified as a pair of Majorana zero modes at either end of a quantum wire [35, 37, 39, 79]. When closing the spectral gap with a magnetic field and neglecting higher order corrections,

the Hamilton splits into a direct sum of two antisymmetric matrices. This is mirrored by (3.1), which for $a = \infty$ the Hamiltonian J splits into A and B. They are chosen independent to make the model analytically viable. They are therefore not the same as in the physical situation, but the important features should be preserved. The matrices $\widetilde{W}$ then act as a perturbation of the zero modes and model impurities, thermal fluctuations, or inaccuracies in the experimental setup. This regime will also be treated in Chapter 4 for small $1/a$.

The model (3.1) may have an arbitrary amount of zero modes for $a = 0$ if extended to $\nu \in \mathbf{N}_0$ such that the random matrix $\widetilde{W}$ becomes of size $n \times (n + \nu)$ [25]. Here I restrict myself to $\nu = 0, 1$.

This chapter is based on the work in [AKMV].

3.1 Symmetry Transition and Main Results

As this chapter is rather technical, I start by reviewing the main results before going into the details. I will show how this ensemble is of the type described in Section 2.5 and how the random matrix theory machinery may be used to solve it.

3.1.1 Random Two-Matrix Model

I will be working with the transition ensemble in a form that differs slightly from (3.1), but as shall be seen, they are equivalent. The random two-matrix ensemble is of the form

$$J \;=\; Y + X\,, \tag{3.2}$$

where the matrices are drawn from the normalised distribution

$$P(Y,X) \;=\; \left(\frac{\pi a^2}{2}\right)^{-N(N-1)/4} \left(\frac{\pi(1-a^2)}{2}\right)^{-n(n+\nu)/2} \exp\left[-\frac{1}{a^2}\mathrm{Tr}\, Y^2 - \frac{1}{1-a^2}\mathrm{Tr}\, X^2\right]. \tag{3.3}$$

Here $a \in (0,1)$ is a real parameter and $N = 2n + \nu$ is the size of J. The first matrix Y is an $N \times N$ antisymmetric Hermitian matrix, which means that it can be written as

$$Y \;=\; iH\,, \tag{3.4}$$

where $H = -H^T$ is real antisymmetric. The second matrix X is a chiral antisymmetric Hermitian matrix of the same dimension as Y,

$$X \;=\; \begin{pmatrix} 0 & iW \\ -iW^T & 0 \end{pmatrix}, \tag{3.5}$$

where W is an $n \times (n + \nu)$ real matrix without further symmetries. The parameter $\nu = 0, 1$ takes two values and indicates whether the total matrix dimension N is even ($\nu = 0$) or odd ($\nu = 1$). For this reason ν counts the number of exact zero eigenvalues of the matrix J, independently of the transition parameter a. I therefore call ν the preserved topology. The two random matrices are equipped with flat Lebesgue measures for all independent matrix elements, $[dY] = \prod_{i=1}^{N}\prod_{i<j=2}^{N} dH_{i,j}$ and $[dX] = \prod_{i=1}^{n}\prod_{j=1}^{n+\nu} dW_{i,j}$ on the real numbers. This is equivalent to the above stated normalisation in (3.3), i.e.,

$$\int [dX][dY] P(Y,X) \;=\; 1\,. \tag{3.6}$$

Note that the limits $a \to 0$ and $a \to 1$ yield the two classical ensembles between which a interpolates.

3.1.2 Pfaffian Point Process

The first main result is the general structure of spectral statistics of the eigenvalues of (3.2). The jpdf of of the eigenvalues $(\pm\lambda_1, \ldots, \pm\lambda_n)$, with $\lambda_j \geq 0$ the singular values of the random matrix J distributed according to (3.3), is given by a product of the Vandermonde determinant and a Pfaffian

$$P_n^{(\nu)}(\lambda_1, \ldots, \lambda_n) = C_{n,\nu}\, \Delta_n\left(\{\lambda^2\}\right) \begin{cases} \mathrm{Pf}\left[\ G_\nu(\lambda_j, \lambda_k)\ \right]_{j,k=1,\ldots,n} , & \text{for } n = 2m\,, \\ \mathrm{Pf}\begin{bmatrix} G_\nu(\lambda_j, \lambda_k) & g_\nu(\lambda_j) \\ -g_\nu(\lambda_k) & 0 \end{bmatrix}_{j,k=1,\ldots,n}, & \text{for } n = 2m+1. \end{cases} \tag{3.7}$$

As can be seen, the specific form depends on n and ν.

The antisymmetric two-point weight function $G_\nu(x, y) = -G_\nu(y, x)$ is explicitly given by (see Appendix A.1)

$$\begin{aligned} G_\nu(x,y) &= \frac{\pi a^2(1-a^2)}{8}(xy)^\nu e^{-2(x^2+y^2)} \Bigg(\mathrm{erf}\left[\gamma(y-x)\right] \mathrm{erf}\left[\gamma(x+y)\right] \\ &\quad -\delta_{\nu,1}\frac{2}{\sqrt{\pi}} \int_{\sqrt{2}\gamma x}^{\sqrt{2}\gamma y} du\ \mathrm{erf}\left[\sqrt{2}\gamma(x+y) - u\right] e^{-u^2} \Bigg) \end{aligned} \tag{3.8}$$

with $\gamma = \sqrt{(1-a^2)/a^2}$, and the one-point weight function can be written as

$$g_\nu(y) = \sqrt{\frac{\pi a^2(1-a^2)}{8}}\, \exp\left[-2y^2\right] \left(y\, \mathrm{erf}\left[\sqrt{2}\gamma y\right]\right)^\nu \tag{3.9}$$

with

$$\bar{g}_\nu = \int_0^\infty dx\, g_\nu(x) = \sqrt{\frac{\pi^3 a^2}{32}} \left(\frac{1-a^2}{2\pi}\right)^{(\nu+1)/2} . \tag{3.10}$$

The integral $\int_0^\infty dx' G_\nu(x', y)$ needed in the skew-symmetric product for odd n is computed in Appendix A.1.

The normalisation constant reads

$$C_{n,\nu} = \frac{2^{\frac{n}{2}(3+n+\nu)}}{a^n(1-a^2)^{\frac{n}{2}(n+\nu)}} \prod_{j=0}^{n-1} \frac{1}{\Gamma\left(\frac{j+3}{2}\right)\Gamma\left(\frac{j+\nu+1}{2}\right)} , \tag{3.11}$$

such that the jpdf (3.7) is normalised to unity,

$$\prod_{j=1}^{n} \int_0^\infty d\lambda_j\ P_n^\nu(\lambda_1, \ldots, \lambda_n) = 1\,. \tag{3.12}$$

The k-point correlation functions are given as in (2.17) and can be expressed in terms of three kernels I_n^ν, S_n^ν and D_n^ν, which depend on the corresponding skew-orthogonal polynomials and their integral transforms, see (2.48).

The explicit expressions for the three kernels are different for even and odd n and are given below. The corresponding skew-orthogonal polynomials also depend on the matrix dimension, though both n even and odd share the Heine-like formulas, extending (2.37),

$$\begin{aligned} p_j^{(\nu)}(x) &= x^{-\nu} \left\langle \det(x\mathbf{1}_{2j+\nu} - J) \right\rangle_{j,\nu} , \\ q_j^{(\nu)}(x) &= x^{-\nu} \left\langle \det(x\mathbf{1}_{2j+\nu} - J) \left(x^2 + \frac{1}{2} \text{Tr } J^2 + c_j^{(\nu)}(a) \right) \right\rangle_{j,\nu} . \end{aligned} \tag{3.13}$$

Here $\langle \dots \rangle$ indicates the average over the matrix J with the dimensions $(n, \nu) \to (j, \nu)$. This is shown in Appendix A.2. The constants $c_j^{(\nu)}(a)$ are arbitrary as the polynomials are not uniquely defined by 3.13. In Section 3.3 I show that these polynomials have the representation

$$\begin{aligned} p_j^{(\nu)}(x) &= x^{-\nu} \frac{4}{\pi\sqrt{1-a^4}} \int_{-\infty}^{\infty} dy \int_{-\infty}^{\infty} d\lambda \, e^{-\frac{4}{1+a^2}y^2 - \frac{4}{1-a^2}\lambda^2} (iy + \lambda + x)^j (iy - \lambda + x)^{j+\nu} , \\ q_j^{(\nu)}(x) &= x^{-\nu} \left[x^2 - \frac{1}{16}\partial_x^2 + \frac{a^4-1}{2}\partial_{a^2} + \tilde{c}_j^{(\nu)}(a) \right] \left(x^\nu p_j^{(\nu)}(x) \right) . \end{aligned} \tag{3.14}$$

The constants $\tilde{c}_j^{(\nu)}(a)$ differ from $c_j^{(\nu)}(a)$ by a shift. This representation of the polynomials $p_j^{(\nu)}(x)$ is only valid for $0 \le a < 1$ because of the integrand. Other representations are available in Section 3.3 that extend to $a \ge 1$. The normalisation constants of the these polynomials are

$$h_j^{(\nu)} = \frac{\pi a^2 (1-a^2)^{2j+2+\nu}}{2^{4j+2\nu+7}} j!(j+\nu)! , \tag{3.15}$$

see (2.19).

I would like to emphasise that $p_j^{(\nu)}(x)$ and $q_j^{(\nu)}(x)$ are monic polynomials of degree j and $j+1$ in x^2 respectively. The index is therefore not the degree in x. For the classical ensembles that are given by Pfaffian point processes, the sOP given by (3.13) come in pairs of even and odd, see e.g. chGOE in Section 2.2. The polynomials $p_j^{(\nu)}(x)$ and $q_j^{(\nu)}(x)$ play a slightly different role here. For $n = 2m$ even, only the polynomials $p_{2k}^{(\nu)}(x)$ of even degree $2k$ in x^2 and the polynomials $q_{2k}^{(\nu)}(x)$ of odd degree $2k+1$ in x^2, for $k = 0, 1, 2, \dots$ are needed. For $n = 2m+1$ odd, only the polynomials $p_{2k-1}^{(\nu)}(x)$ of odd degree $2k-1$ in x^2 and the polynomials $q_{2k-1}^{(\nu)}(x)$ of even degree $2k$ in x^2, for $k = 1, 2, \dots$, are of use.

These polynomials are inserted in the kernels described in Section 2.2.2. See Figure 3.1 for plots of the density for even n and Figure 3.2 for odd n.

3.1.3 Equivalence with a Three-Matrix Model

While the form (3.2-3.5) will be more useful for later calculations in this chapter, let me as a final note show the connection to (2.79) by showing it can be written as

$$J = i \begin{pmatrix} aA & \widetilde{W} \\ -\widetilde{W}^T & aB \end{pmatrix} , \tag{3.16}$$

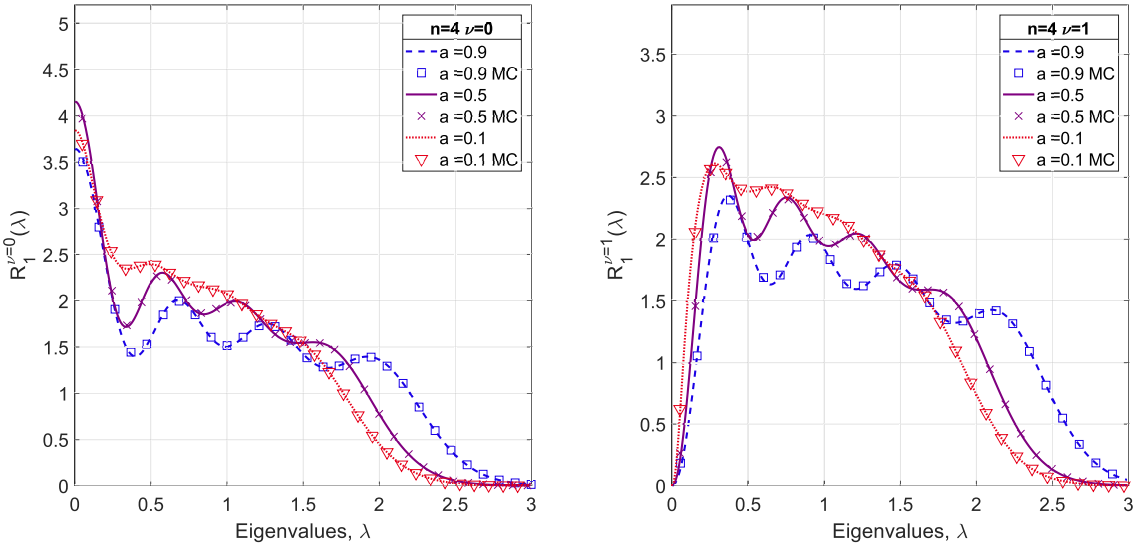

Figure 3.1: The spectral density $R_1^\nu(\lambda)$ taken from the analytical result (2.61) (solid curves) with polynomials from (3.14) compared to Monte-Carlo (MC) simulations (symbols) for $n = 4$ even with $\nu = 0$ (left) and $\nu = 1$ (right) at three different values of $a = 0.1$ (triangles), 0.5 (crosses), and 0.9 (squares). The ensemble size is 10^6 and the bin size approximately 0.1. This figure has also been published in [AKMV].

where the three individual matrices are distributed according to the normalised density

$$P(A, B, \widetilde{W}) = \left(\frac{\pi}{2}\right)^{-N(N-1)/4} \exp\left[\mathrm{Tr}\, AA^T + \mathrm{Tr}\, BB^T - 2\mathrm{Tr}\, \widetilde{W}\widetilde{W}^T\right] . \tag{3.17}$$

The anti-symmetric matrix $Y = iH$ is spelt out in block form

$$Y \;=\; i\begin{pmatrix} \widetilde{A} & V \\ -V^T & \widetilde{B} \end{pmatrix} \;\Rightarrow\; J = Y + X = i\begin{pmatrix} \tilde{A} & V+W \\ -V^T - W^T & \widetilde{B} \end{pmatrix}. \tag{3.18}$$

The matrices $\widetilde{A}$ and $\widetilde{B}$ are real antisymmetric of dimensions n and $n+\nu$, respectively, and V and W are real rectangular $n \times (n+\nu)$ matrices. The probability density reads

$$P(Y, X) = \left(\frac{\pi a^2}{2}\right)^{-\frac{N(N-1)}{4}} \left(\frac{\pi(1-a^2)}{2}\right)^{-\frac{n(n+\nu)}{2}} e^{\frac{1}{a^2}(\mathrm{Tr}\,\widetilde{A}^2 + \mathrm{Tr}\,\widetilde{B}^2) - \frac{2}{a^2}\mathrm{Tr}\, VV^T - \frac{2}{1-a^2}\mathrm{Tr}\, WW^T} . \tag{3.19}$$

One can identify

$$J \;=\; i\begin{pmatrix} \tilde{A} & V+W \\ -V^T - W^T & \widetilde{B} \end{pmatrix} = i\begin{pmatrix} aA & \widetilde{W} \\ -\widetilde{W}^T & aB \end{pmatrix} , \tag{3.20}$$

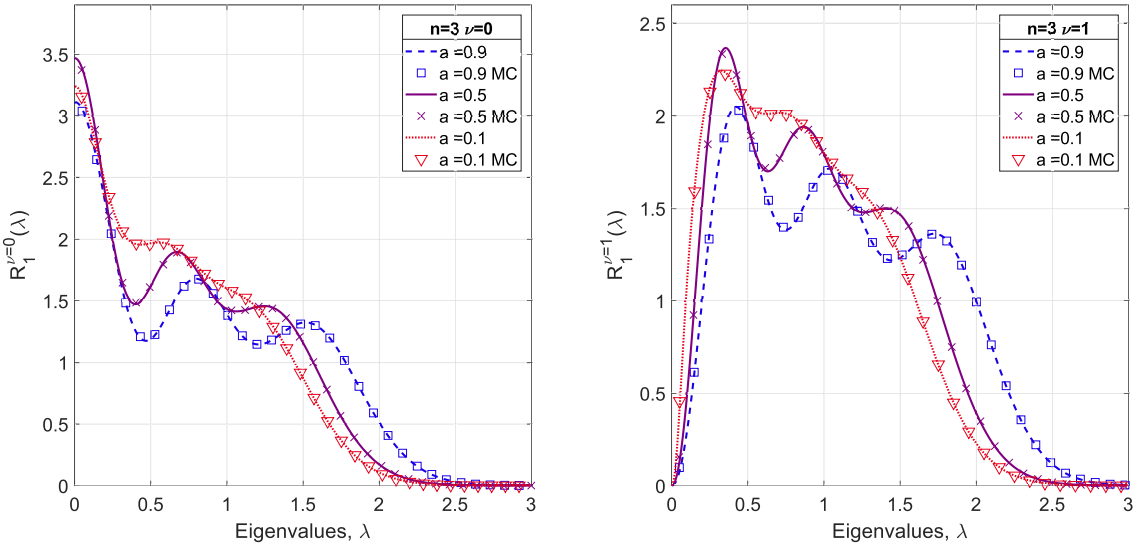

Figure 3.2: The spectral density $R_1^\nu(\lambda)$ taken from the analytical result (2.77) (solid curves) with polynomials from (3.14) compared to Monte-Carlo (MC) simulations (symbols) for $n = 3$ even with $\nu = 0$ (left) and $\nu = 1$ (right) at three different values of $a = 0.1$ (triangles), 0.5 (crosses), and 0.9 (squares). The ensemble size is 10^6 and the bin size approximately 0.1. This figure has also been published in [AKMV].

and relate the two densities by

$$
\begin{aligned}
P(A,B,\widetilde{W}) &= \int \delta(A-\widetilde{A}/a)\delta(B-\widetilde{B}/a)\delta(\widetilde{W}-V-W)P(Y,X)[d\widetilde{A}][d\widetilde{B}][dV][dW] \qquad (3.21)\\
&= \left(\frac{\pi a^2}{2}\right)^{-\frac{N(N-1)}{4}} \left(\frac{\pi(1-a^2)}{2}\right)^{-\frac{n(n+\nu)}{2}} a^{\frac{n(n-1)}{2}+\frac{(n+\nu)(n+\nu-1)}{2}}\\
&\quad \times \int e^{\mathrm{Tr}\,A^2+\mathrm{Tr}\,B^2-\frac{2}{a^2}\mathrm{Tr}\,VV^T-\frac{2}{1-a^2}\mathrm{Tr}\,(\widetilde{W}-V)(\widetilde{W}-V)^T}[dV]\\
&= \left(\frac{\pi a^2}{2}\right)^{-\frac{N(N-1)}{4}} \left(\frac{\pi(1-a^2)}{2}\right)^{-\frac{n(n+\nu)}{2}} a^{\frac{n(n-1)}{2}+\frac{(n+\nu)(n+\nu-1)}{2}} \left(\frac{\pi a^2(1-a^2)}{2}\right)^{\frac{n(n+\nu)}{2}}\\
&\quad \times e^{\mathrm{Tr}\,A^2+\mathrm{Tr}\,B^2-2\mathrm{Tr}\,\widetilde{W}\widetilde{W}^T}.
\end{aligned}
$$

After evaluating the δ-functions, the integral over V is shifted by $a^2\widetilde{W}$, which decouples the matrix $\widetilde{W}$. The Gaussian integral over V is finally done, leading to the last line. (3.17) is obtained by simplifying the constant.

This concludes the statement of the main results, and I will now go into the details of each.

3.2 Joint Probability Density of the Eigenvalues

The first step is to show the structure of the jpdf, that is, the results (3.7-3.11). For most of the derivation, the four cases n, ν even and odd will be treated simultaneously. I will indicate when they differ.

The starting point is (3.3) and, with a change of variables $Y \to J = Y + X$ while keeping the matrix X unchanged, the pdf reads

$$\begin{aligned} P(J,X) &= \left(\frac{2}{\pi a^2}\right)^{(2n+\nu)(2n+\nu-1)/4} \left(\frac{2}{\pi(1-a^2)}\right)^{n(n+\nu)/2} \\ &\quad \times \exp\left[-\frac{1}{a^2}\mathrm{Tr}\, J^2 - \frac{1}{a^2(1-a^2)}\mathrm{Tr}\, X^2 + \frac{2}{a^2}\mathrm{Tr}\, JX\right] . \end{aligned} \tag{3.22}$$

The Jacobian is unity. The next steps are as follows. First I block-diagonalise the matrices J and X. These transformations are standard and have well-known Jacobians. Next I integrate out the angular degrees of freedom, which is more complicated because the term $\mathrm{Tr}\, JX$ retains the group integrals. Fortunately these may be rewritten as the Harish-Chandra integral, which is a known integral. Finally, I perform the integral over the eigenvalues of X to find the jpdf of the eigenvalues of J.

The antisymmetric imaginary matrix J can be brought to block-diagonal form

$$J = i\mathcal{O}\Lambda_\lambda\mathcal{O}^T , \tag{3.23}$$

where

$$\Lambda_\lambda = \begin{cases} \mathrm{diag}\,(\lambda_1 i\tau_2, \ldots, \lambda_n i\tau_2) , & \text{for } N = 2n \ (\nu = 0) , \\ \mathrm{diag}\,(\lambda_1 i\tau_2, \ldots, \lambda_n i\tau_2, 0) , & \text{for } N = 2n+1 \ (\nu = 1) , \end{cases} \tag{3.24}$$

and $\mathcal{O}$ is orthogonal. This follows from Cartan's Theorem. The matrices J and Λ_λ are both of size $N \times N$, and Λ_λ contains the eigenvalues pairs $\pm\lambda_{j=1,\ldots,n}$ of J, written with the second Pauli matrix τ_2. Each of the blocks are invariant under the orthogonal group, and therefore $\mathcal{O} \in O(N)/O(2)^n$. The subscript of Λ indicates which set of eigenvalues are considered. The same notation is used below for X.

The Jacobian for (3.23) is known [80]. In terms of the Vandermonde (2.13) and the normalised Haar measure on the orthogonal group $[d\mathcal{O}]$

$$[dJ] = \frac{2^n \pi^{n(n+\nu-\frac{1}{2})}}{n! \prod_{j=0}^{n-1} \Gamma(j+1)\Gamma\left(j+\nu+\frac{1}{2}\right)} [d\mathcal{O}] \prod_{j=1}^{n} d\lambda_j \lambda_j^{2\nu}\, \Delta_n(\{\lambda^2\})^2 , \tag{3.25}$$

with $\int [d\mathcal{O}] = 1$. The constant is equal to the quotient of the integrals before and after

$$\frac{\int [dJ] \exp\left[-\mathrm{Tr}\, J^2\right]}{\prod_{k=1}^{n} \int_0^\infty d\lambda_k \lambda_k^{2\nu} \Delta_n(\{\lambda^2\})^2 \exp\left[-2\sum_{j=1}^{n} \lambda_j^2\right]} = \frac{(\pi/2)^{\frac{(2n+\nu)(2n+\nu-1)}{4}}\, 2^{n(n+\nu+\frac{1}{2})}}{\prod_{j=0}^{n-1} \Gamma(j+2)\Gamma\left(j+\nu+\frac{1}{2}\right)} . \tag{3.26}$$

The constant a has been set to 1 for the calculation of the norm. The exponent comes from

$$\mathrm{Tr}\, J^2 = 2\sum_{j=1}^{n} \lambda_j^2 \tag{3.27}$$

and J having $N(N-1)/2$ independent real matrix elements. The denominator comes from a Selberg integral (2.16) for $\beta > 0$ and $\kappa > -1$. The eigenvalues pairs $\pm x_{j=1,\ldots,n}$ of X (3.5), the singular values of W, are treated the same way. Using the singular value composition

$W = P\mathrm{diag}(x_1,\ldots,x_n)Q^T$, where $P,Q \in O(n)$ for $\nu = 0$, and $P \in O(n)$ and $Q^TQ = \mathbb{1}_n$ with Q of size $(n+1)\times n$ for $\nu = 1$, one finds

$$X = i\begin{pmatrix} P & 0 \\ 0 & Q \end{pmatrix}\begin{pmatrix} 0 & \mathrm{diag}(x_1,\ldots,x_n) \\ -\mathrm{diag}(x_1,\ldots,x_n) & 0 \end{pmatrix}\begin{pmatrix} P^T & 0 \\ 0 & Q^T \end{pmatrix}. \quad (3.28)$$

I denote this the same way, because a permutation of rows and columns leads to a representation similar to (3.23),

$$X = i\widetilde{\mathcal{O}}\Lambda_x\widetilde{\mathcal{O}}^T \quad (3.29)$$

with the notation (3.24) for Λ_x. The matrix $\widetilde{\mathcal{O}}$ is also orthogonal, i.e., $\widetilde{\mathcal{O}} \in O(2n+\nu)$, though with some substructure. However, this substructure will be irrelevant in later calculations.

The Jacobian is also known for this transformation [25] (and a different one than for the diagonalisation of J)

$$[dX] = \frac{\pi^{\frac{n}{2}(n+\nu+1)}}{\prod_{j=0}^{n-1}\Gamma\left(\frac{j+3}{2}\right)\Gamma\left(\frac{j+\nu+1}{2}\right)}[d\widetilde{\mathcal{O}}]\prod_{j=1}^{n} dx_j x_j^\nu \,|\Delta_n(\{x^2\})|\,. \quad (3.30)$$

As before, I denote the normalised Haar measure on the corresponding coset by $[d\widetilde{\mathcal{O}}]$.

Gathering all constants, the jpdf reads

$$\begin{aligned} & P_n^{(\nu)}(\lambda_1,\ldots,\lambda_n) \quad (3.31)\\ = & \left(\frac{2}{\pi a^2}\right)^{n(n+\nu-\frac{1}{2})}\left(\frac{2}{\pi(1-a^2)}\right)^{\frac{n(n+\nu)}{2}}\frac{2^n\pi^{\frac{3n}{2}(n+\nu)}}{n!\prod_{j=0}^{n-1}\Gamma(j+1)\Gamma\left(j+\nu+\frac{1}{2}\right)\Gamma\left(\frac{j+3}{2}\right)\Gamma\left(\frac{j+\nu+1}{2}\right)} \\ & \times\int[d\widetilde{\mathcal{O}}][d\mathcal{O}]\prod_{j=1}^{n}\left(\int_0^\infty dx_j x_j^\nu\lambda_j^{2\nu}\right)|\Delta_n(\{x^2\})|\Delta_n(\{\lambda^2\})^2 \\ & \times\exp\left[-\frac{2}{a^2}\sum_{j=1}^{n}\lambda_j^2 - \frac{2}{a^2(1-a^2)}\sum_{j=1}^{n}x_j^2 - \frac{2}{a^2}\,\mathrm{Tr}\;\mathcal{O}\Lambda_\lambda\mathcal{O}^T\widetilde{\mathcal{O}}\Lambda_x\widetilde{\mathcal{O}}^T\right]. \end{aligned}$$

The smaller group $\widetilde{\mathcal{O}}$ may be absorbed into the larger one $\mathcal{O}$ in the coupling term due to the invariance of the Haar measure. The integral over $\widetilde{\mathcal{O}}$ is then unity by construction, and the remaining integral over $\mathcal{O}$ is the Harish-Chandra integral [81] over the orthogonal group

$$\int[d\mathcal{O}]\exp\left[-\frac{2}{a^2}\,\mathrm{Tr}\;\mathcal{O}\Lambda_\lambda\mathcal{O}^T\Lambda_x\right] = \left(\prod_{j=0}^{n-1}(2j+\nu)!\left(\frac{a^2}{4}\right)^{2j+\nu}\right)\frac{\det\left[f_\nu(x_i\lambda_j)\right]_{i,j=1}^n}{\Delta_n(\{x^2\})\Delta_n(\{\lambda^2\})\prod_{k=1}^n(x_k\lambda_k)^\nu}\,, \quad (3.32)$$

where

$$f_\nu(x) = \begin{cases} \cosh\left[\frac{4}{a^2}x\right]\,, & \text{for } \nu = 0\,, \\ \sinh\left[\frac{4}{a^2}x\right]\,, & \text{for } \nu = 1\,. \end{cases} \quad (3.33)$$

The details of its derivation may be found in [82]. The normalisation of (3.32) is determined by setting the integral to unity for $\lambda_1, \ldots, \lambda_n = 0$. The jpdf becomes

$$\begin{aligned} & P_n^{(\nu)}(\lambda_1, \ldots, \lambda_n) \\ = \; & \frac{\pi^{\frac{n}{2}} 2^{\frac{n}{2}(5-n-\nu)}}{a^n (1-a^2)^{\frac{n}{2}(n+\nu)}} \frac{1}{n!} \prod_{j=0}^{n-1} \frac{\Gamma(2j+\nu+1)}{\Gamma(j+1)\Gamma\left(j+\nu+\frac{1}{2}\right)\Gamma\left(\frac{j+3}{2}\right)\Gamma\left(\frac{j+\nu+1}{2}\right)} \\ & \times \prod_{j=1}^{n} \left(\lambda_j^{\nu} e^{-\frac{2}{a^2}\lambda_j^2} \int_0^{\infty} dx_j e^{-\frac{2}{a^2(1-a^2)}x_j^2} \right) \frac{|\Delta_n(\{x^2\})|}{\Delta_n(\{x^2\})} \Delta_n(\{\lambda^2\}) \det\left[f_\nu(x_k\lambda_l)\right]_{k,l=1}^n \, . \end{aligned} \tag{3.34}$$

The remaining integrals over x may be brought to a standard form because of the sign of the Vandermonde determinant $\Delta_n(\{x^2\})$. This is how the Pfaffian point process-structure appears, see [83]. The sign of the Vandermonde may be rewritten [84]

$$\begin{aligned} \frac{|\Delta_n(\{x^2\})|}{\Delta_n(\{x^2\})} &= \prod_{i<j}^{n} \mathrm{sign}(x_j^2 - x_i^2) = \prod_{i<j}^{n} \mathrm{sign}(x_j - x_i) \\ &= \begin{cases} \mathrm{Pf}\left[\mathrm{sign}(x_j - x_i)\right]_{i,j=1}^n \, , & \text{for } \; n = 2m \, , \\ \mathrm{Pf}\left[\begin{array}{c|c} \mathrm{sign}(x_j - x_i) & \vec{1} \\ \hline -\vec{1}^T & 0 \end{array}\right]_{i,j=1}^n \, , & \text{for } \; n = 2m-1 \, , \end{cases} \end{aligned} \tag{3.35}$$

where $\vec{1}$ is a column vector of length n with each entry equal to 1. Exactly because of (3.35), I have to distinguish between even and odd n. After the application the de Brujin integral [84, Section 4]

$$\int dx_1 \ldots dx_n \frac{|\Delta_n(\{x^2\})|}{\Delta_n(\{x^2\})} \det[\varphi_i(x_j)]_{i,j=1}^n = \begin{cases} \mathrm{Pf}\left[a_{i,j}\right]_{i,j=1}^n \, , & \text{for } \; n = 2m \, , \\ \mathrm{Pf}\left[\begin{array}{c|c} a_{i,j} & b_i \\ \hline -b_j & 0 \end{array}\right]_{i,j=1}^n \, , & \text{for } \; n = 2m+1 \, , \end{cases} \tag{3.36}$$

with

$$a_{i,j} = \int_0^{\infty} dx \int_0^{\infty} dy \; \mathrm{sign}(y-x)\varphi_i(x)\varphi_j(y) \quad \text{and} \quad b_j = \int_0^{\infty} dx \; \varphi_i(x) \tag{3.37}$$

the weights $\lambda_j^{\nu} e^{-\frac{2}{a^2}\lambda_j^2}$ in (3.34) can be pulled into the rows and columns of the Pfaffian determinant to yield the final result of this subsection

$$P_n^{(\nu)}(\lambda_1, \ldots, \lambda_n) = C_{n,\nu} \, \Delta_n(\{\lambda^2\}) \begin{cases} \mathrm{Pf}\left[G_\nu(\lambda_i, \lambda_j)\right]_{i,j=1}^n \, , & \text{for } \; n = 2m \, , \\ \mathrm{Pf}\left[\begin{array}{c|c} G_\nu(\lambda_i, \lambda_j) & g_\nu(\lambda_i) \\ \hline -g_\nu(\lambda_j) & 0 \end{array}\right]_{i,j=1}^n \, , & \text{for } \; n = 2m+1 \, , \end{cases} \tag{3.38}$$

with

$$\begin{aligned} G_\nu(\lambda,u) &= (\lambda u)^\nu e^{-\frac{2}{a^2}(\lambda^2+u^2)} \int_0^\infty dx \int_0^\infty dy\, \mathrm{sign}(y-x) \\ &\quad \times e^{-\frac{2}{a^2(1-a^2)}(x^2+y^2)} f_\nu(x\lambda) f_\nu(yu)\,, \end{aligned} \tag{3.39}$$

$$g_\nu(\lambda) = \lambda^\nu e^{-\frac{2}{a^2}\lambda^2} \int_0^\infty dx\, e^{-\frac{2}{a^2(1-a^2)}x^2} f_\nu(x\lambda)\,, \tag{3.40}$$

$$C_{n,\nu} = \frac{2^{\frac{n}{2}(3+n+\nu)}}{a^n(1-a^2)^{\frac{n}{2}(n+\nu)}} \prod_{j=0}^{n-1} \frac{1}{\Gamma\left(\frac{j+3}{2}\right)\Gamma\left(\frac{j+\nu+1}{2}\right)}\,. \tag{3.41}$$

As the integrand is antisymmetric under interchange of integration variables x and y, the weight function is antisymmetric $G_\nu(\lambda,u) = -G_\nu(u,\lambda)$. Note also that both $G_\nu(\lambda,u)$ and $g_\nu(\lambda)$ are even functions in their arguments λ and u, separately. This is of course related to the fact that J has eigenvalues in pairs around the origin.

As a consistency check, I show that the joint density (3.7) with $n = 2m+1$ odd can be obtained from $n = 2m+2$ even by sending $\lambda_{2m+2} \to \infty$, following the ideas of [55]

$$P^{(\nu)}_{2m+2}(\lambda_1,\ldots,\lambda_{2m+2}) \overset{\lambda_{2m+2}\gg 1}{\approx} \eta^{(\nu)}_{2m+2}(\lambda_{2m+2}) P^{(\nu)}_{2m+1}(\lambda_1,\ldots,\lambda_{2m+1})\,. \tag{3.42}$$

The function $\eta^{(\nu)}_{2m+2}(\lambda_{2m+2})$ combines the leading power λ^{2m}_{2m+2} of the Vandermonde determinant $\Delta_{2m+2}(\{\lambda^2\})$ with a factor coming from the asymptotic limit of the two-point weight function $G_\nu(\lambda_j,\lambda_{2m+2})$.

For $\nu = 0$, Equation (3.8) can be approximated by

$$G_0(s,z) \overset{z\gg 1}{\approx} \frac{\pi a^2(1-a^2)}{8}\, e^{-2(s^2+z^2)} = g_0(s) g_0(z)\,, \tag{3.43}$$

where $g_0(z)$ comes from (3.9) at $\nu = 0$. This comes from the asymptotic expansion $\mathrm{erf}(\lambda) \sim 1 - e^{-\lambda^2}/(\lambda^2\sqrt{\pi})$ for $\lambda \gg 1$. Pulling out $g_0(z)$ from the Pfaffian (3.7) for $n = 2m+2$ (and keeping $g_0(s)$ inside), $\eta^{(0)}_{2m+2}(z) = z^{2m} g_0(z)$ can be identified.

The same asymptotics can be used for $\nu = 1$ to let the error function in the integral of (3.8) go to unity

$$\begin{aligned} G_1(s,z) &\overset{z\gg 1}{\approx} \frac{\pi a^2(1-a^2)}{8}\, sz\, e^{-2(s^2+z^2)} \left\{ 1 - \left(\mathrm{erf}\left[z\sqrt{\frac{(1-a^2)}{a^2}} \right] - \mathrm{erf}\left[s\sqrt{\frac{(1-a^2)}{a^2}} \right] \right) \right\} \\ &\overset{z\gg 1}{\approx} \frac{\pi a^2(1-a^2)}{8}\, sz\, e^{-2(s^2+z^2)}\, \mathrm{erf}\left[s\sqrt{\frac{(1-a^2)}{a^2}} \right] = z g_0(z) g_1(s)\,. \end{aligned} \tag{3.44}$$

Again $g_0(z)$ can be pulled out of the weight function in the Pfaffian (3.7) for $n = 2m+2$ with $\eta^{(1)}_{2m+2}(z) = z^{2m+1} g_0(z)$. This leads to the weight function for $n = 2m+1$ with $g_1(s)$ from (3.9). This shows that it is possible to write the case for $n = 2m+1$ odd as a limit of the case $n = 2m+2$ even.

3.3 Skew-Orthogonal Polynomials

In this section I derive the results (3.14) alongside other representations of the skew-orthogonal polynomials. Combined with the normalisation constants, which will be derived in Section

3.3.3, these will determine the kernels and by extension the k-point correlation functions in the respective cases of even or odd n. My starting point is the Heine-like formulas [44, 56, 85] that I briefly rederive in Appendix A.2

$$\begin{aligned} p_j^{(\nu)}(x) &= x^{-\nu}\langle \det(x\mathbb{1}_{2j+\nu} - J)\rangle_{j,\nu}, \\ q_j^{(\nu)}(x) &= x^{-\nu}\left\langle \det(x\mathbb{1}_{2j+\nu} - J)\left(x^2 + \frac{1}{2}\operatorname{Tr}\left[J^2\right] + c_j^{(\nu)}(a)\right)\right\rangle_{j,\nu}. \end{aligned} \tag{3.45}$$

The first articles on transition ensembles [14, 15] do not give a method of calculating the polynomials. The approach we used in [AKMV] is the following. Define a generating function from which both expectation values (3.45) follow. I do this in Subsection 3.3.1. The generating function is computed by first integrating out the matrix X. I then rewrite the determinant over J inside the expectation value as a Grassmann integral, which allows the remaining Gaussian integrals over J to be performed. With bosonisation, the resulting expression can be mapped to a double contour integral. This is the method I used in Section 2.2.1 to calculate the polynomials of GUE. In this form, the polynomials $q_j^{(\nu)}(x)$ follow directly by applying a differential operator in x and a to the polynomials $p_j^{(\nu)}(x)$. In Section 3.3.2, I present other representations of the sOP. These are the Gaussian integrals quoted in (3.14), as well as versions in terms of classical Hermite or Laguerre polynomials.

3.3.1 Derivation of Contour Integral Representations

Let me start by introducing the following function

$$\begin{aligned} Q_j^{(\nu)}(x;s) &= D_{j,\nu}(a)\int [dJ][dX]\det(x\mathbb{1}_{2j+\nu} - J) \\ &\quad \times \exp\left[-\frac{s}{a^2}\operatorname{Tr}\left[J^2\right] - \frac{1}{a^2(1-a^2)}\operatorname{Tr}\left[X^2\right] + \frac{2}{a^2}\operatorname{Tr}\left[JX\right]\right], \end{aligned} \tag{3.46}$$

where the integrals over the matrices J and X are of size $2j+\nu$. An extra parameter s has been added in front of the term $\operatorname{Tr}\left[J^2\right]$ compared to the density (3.22). The constant is

$$D_{j,\nu}(a) = \left(\frac{2}{\pi a^2}\right)^{(2j+\nu)(2j+\nu-1)/4}\left(\frac{2}{\pi(1-a^2)}\right)^{j(j+\nu)/2} \tag{3.47}$$

and depends on j, ν and a, but not on s. The generating function (3.46) can be used to find the averages (3.45)

$$x^\nu p_j^{(\nu)}(x) = Q_j^{(\nu)}(x;s=1) \quad \text{and} \quad x^\nu q_j^{(\nu)}(x) = \left(x^2 - \frac{a^2}{2}\frac{\partial}{\partial s} + c_j^{(\nu)}(a)\right)Q_j^{(\nu)}(x;s)\Big|_{s=1}. \tag{3.48}$$

The following parametrisation in terms of block matrices is used

$$J = i\begin{pmatrix} A & V \\ -V^T & B \end{pmatrix} \quad \text{and} \quad X = i\begin{pmatrix} 0 & W \\ -W^T & 0 \end{pmatrix}, \tag{3.49}$$

as in Section 3.2, with A and B real antisymmetric matrices of dimensions j and $j+\nu$, and V as well as W of dimensions $j \times (j+\nu)$, respectively. I insert this in the generating function

$$\begin{aligned} Q_j^{(\nu)}(x;s) &= D_{j,\nu}(a) \int [dA][dB][dV][dW] \det \begin{bmatrix} x\mathbb{1}_j - iA & -iV \\ iV^T & x\mathbb{1}_{j+\nu} - iB \end{bmatrix} e^{-\frac{s}{a^2}\left(2\mathrm{Tr}\, VV^T - \mathrm{Tr}\, A^2 - \mathrm{Tr}\, B^2\right)} \\ &\quad \times e^{-\frac{2}{a^2(1-a^2)}\mathrm{Tr}\, WW^T + \frac{2}{a^2}\mathrm{Tr}[WV^T + VW^T]} \\ &= D_{j,\nu}(a) \left(\frac{\pi a^2(1-a^2)}{2}\right)^{\frac{n(n+\nu)}{2}} \int [dA][dB][dV] \det \begin{bmatrix} x\mathbb{1}_j - iA & -iV \\ iV^T & x\mathbb{1}_{j+\nu} - iB \end{bmatrix} \\ &\quad \times e^{\frac{s}{a^2}(\mathrm{Tr}\, A^2 + \mathrm{Tr}\, B^2) - \frac{2(s-1+a^2)}{a^2}\mathrm{Tr}\, VV^T} . \end{aligned} \tag{3.50}$$

In the second step the integral over W has been performed, which yields an s-independent constant. I will ignore s-independent normalisation in the following. The normalisation of the polynomials $p_j^{(\nu)}(x)$ and $q_j^{(\nu)}(x)$ is fixed by making them monic.

To deal with the determinant, I express it as a Grassmann integral over two complex anti-commuting vectors ψ_L and ψ_R of dimensions j and $j+\nu$, respectively, as done in Section 2.2.1.

The product of differentials over all independent Grassmann variables $(\psi_L)_l$, $(\psi_L^*)_l$, $(\psi_R)_k$, $(\psi_R^*)_k$ is denoted by $[d\psi]$, and I obtain

$$\begin{aligned} Q_j^{(\nu)}(x,s) &\propto \int [dA][dB][dV][d\psi] \exp\left[\frac{s}{a^2}\left(\mathrm{Tr}\ A^2 + \mathrm{Tr}\ B^2\right) - \frac{2(a^2+s-1)}{a^2}\,\mathrm{Tr}\ VV^T\right] \\ &\quad \times \exp\left[x(\psi_L^\dagger\psi_L + \psi_R^\dagger\psi_R) + i\,\mathrm{Tr}\ A\psi_L\psi_L^\dagger + i\,\mathrm{Tr}\ B\psi_R\psi_R^\dagger - i\,\mathrm{Tr}\Big[V^T\psi_L\psi_R^\dagger - V\psi_R\psi_L^\dagger\Big]\right] . \end{aligned} \tag{3.51}$$

The trace is projective, which means the antisymmetry of A and B is imposed on the terms $\psi_L^\dagger\psi_L$ and $\psi_R^\dagger\psi_R$, which therefore can be antisymmetrised as well. I there take into account that the Grassmann variables anti-commute. I now gather all independent Grassmann variables in the $j \times 2$ and $(j+\nu) \times 2$ dimensional matrices $\phi_L = (\psi_L, \psi_L^*)$ and $\phi_R = (\psi_R, \psi_R^*)$ and rewrite the above equation using the Pauli matrices σ_1 and σ_2,

$$\begin{aligned} Q_j^{(\nu)}(x,s) &\propto \int [dA][dB][dV][d\psi] \exp\left[\frac{s}{a^2}\left(\mathrm{Tr}\ A^2 + \mathrm{Tr}\ B^2\right) - \frac{2(a^2+s-1)}{a^2}\,\mathrm{Tr}\ VV^T\right] \\ &\quad \times \exp\left[\frac{x}{2}\,\mathrm{Tr}\ i\sigma_2(\phi_L^T\phi_L + \phi_R^T\phi_R) + \frac{i}{2}\,\mathrm{Tr}\ A\phi_L\sigma_1\phi_L^T + \frac{i}{2}\,\mathrm{Tr}\ B\phi_R\sigma_1\phi_R^T\right] \\ &\quad \times \exp\left[\frac{i}{2}\,\mathrm{Tr}\ V\phi_R\sigma_1\phi_L^T - \frac{i}{2}\,\mathrm{Tr}\ V^T\phi_L\sigma_1\phi_R^T\right] \\ &\propto \left(\frac{\pi a^2}{s}\right)^{\frac{n(n+\nu-1)}{2}} \left(\frac{\pi a^2}{2(s+a^2-1)}\right)^{\frac{n(n+\nu)}{2}} \\ &\quad \times \int [d\psi] \exp\left[-\frac{a^2}{16s^2}\,\mathrm{Tr}\left(\sigma_1\phi_L^T\phi_L\right)^2 - \frac{a^2}{16s^2}\,\mathrm{Tr}\left(\sigma_1\phi_R^T\phi_R\right)^2\right] \\ &\quad \times \exp\left[\frac{x}{2}\,\mathrm{Tr}\ i\sigma_2(\phi_L^T\phi_L + \phi_R^T\phi_R) - \frac{a^2}{8(a^2+s-1)}\,\mathrm{Tr}\ \sigma_1\phi_L^T\phi_L\sigma_1\phi_R^T\phi_R\right] . \end{aligned} \tag{3.52}$$

The Gaussian matrices A, B and V have been integrated out, which gives an extra s-dependent normalisation factor. This makes no difference for the polynomial $p_j^{(\nu)}(x)$, because the monic

normalisation cancels out any factor in front. But for $q_j^{(\nu)}(x)$, the differentiation with respect to s also acts on this s-dependent prefactor as well as on the integrand, see Equation (3.48). However, the term from differentiation of the prefactor is proportional to the polynomial $p_j^{(\nu)}(x)$, so it just contributes to the constant $c_j^{(\nu)}(a)$ in (3.45). This shift is denoted by making a shift $c_j^{(\nu)}(a) \to \tilde{c}_j^{(\nu)}(a)$. The previous constant is arbitrary, so the precise value of this shift is irrelevant. This modification allows me to drop the s-dependent prefactors in (3.52) as well.

To perform the Grassmann integrals, I rewrite them as contour integrals with bosonisation [50, 51, 52]. The crucial observation is that the right-hand side of (3.52) only depends on the combinations $\phi_L^T\phi_L$ and $\phi_R^T\phi_R$, and that these two matrices are two-dimensional and antisymmetric with the only non-zero entries being two nilpotent scalar variables which can be represented by $\mathrm{Tr}\ \sigma_2\phi_L^T\phi_L$ and $\mathrm{Tr}\ \sigma_2\phi_R^T\phi_R$. Taylor expanding the function in these two variables, the Grassmann integrals removes all but the highest order, because it involves the product of all Grassmann variables. This term may also be written as a contour integral over two phases. One can therefore replace $\phi_L^T\phi_L \to ie^{i\varphi_L}\sigma_2$ and $\phi_R^T\phi_R \to ie^{i\varphi_R}\sigma_2$ with $\varphi_L, \varphi_R \in [0, 2\pi]$, which picks out the j'th and $(j+\nu)$'th power of these phases, respectively. This identification is exactly the bosonisation trick [50, 51, 52], and leaves the result for the generating function

$$\begin{aligned} Q_j^{(\nu)}(x,s) \;\propto\; & \int_0^{2\pi}\frac{d\varphi_L}{2\pi}e^{-ij\varphi_L}\int_0^{2\pi}\frac{d\varphi_R}{2\pi}e^{-i(j+\nu)\varphi_R}\exp\left[-\frac{a^2}{8s}(e^{2i\varphi_L}+e^{2i\varphi_R})\right] \\ & \times\exp\left[-x(e^{i\varphi_L}+e^{i\varphi_R})-\frac{a^2}{4(a^2+s-1)}e^{i(\varphi_L+\varphi_R)}\right]. \end{aligned} \tag{3.53}$$

The polynomials are then obtained via (3.48) by setting $s=1$ for the polynomials $p_j^{(\nu)}(x)$,

$$\begin{aligned} p_j^{(\nu)}(x) \;=\; & \frac{j!(j+\nu)!}{(-x)^\nu}\int_0^{2\pi}\frac{d\varphi_L}{2\pi}e^{-ij\varphi_L}\int_0^{2\pi}\frac{d\varphi_R}{2\pi}e^{-i(j+\nu)\varphi_R} \\ & \times\exp\left[-\frac{a^2}{8}(e^{2i\varphi_L}+e^{2i\varphi_R})-x(e^{i\varphi_L}+e^{i\varphi_R})-\frac{1}{4}e^{i(\varphi_L+\varphi_R)}\right], \end{aligned} \tag{3.54}$$

where the normalisation and $x^{-\nu}$ have already been added. The normalisation is determined by expanding the two x-dependent exponential factors $-xe^{i\varphi_L}$ and $-xe^{i\varphi_R}$ in two Taylor series. The highest contributing powers in x^2 are j and $j+\nu$, respectively. The rest contributes only unity for the highest order, and the Taylor coefficients cancel the factorials in (3.54). The polynomials are therefore

$$p_j^{(\nu)}(x) = x^{2j} + O(x^{2j-1}). \tag{3.55}$$

For the polynomial $q_j^{(\nu)}(x)$ one has to differentiate (3.53) and set $s=1$ which yields

$$\begin{aligned} q_j^{(\nu)}(x) \;=\; & \frac{j!(j+\nu)!}{(-x)^\nu}\int_0^{2\pi}\frac{d\varphi_L}{2\pi}e^{-ij\varphi_L}\int_0^{2\pi}\frac{d\varphi_R}{2\pi}e^{-i(j+\nu)\varphi_R} \\ & \times\exp\left[-\frac{a^2}{8}(e^{2i\varphi_L}+e^{2i\varphi_R})-x(e^{i\varphi_L}+e^{i\varphi_R})-\frac{1}{4}e^{i(\varphi_L+\varphi_R)}\right] \\ & \times\left(x^2-\frac{a^4}{16}(e^{2i\varphi_L}+e^{2i\varphi_R})-\frac{1}{8}e^{i(\varphi_L+\varphi_R)}+\tilde{c}_j^{(\nu)}(a)\right), \end{aligned} \tag{3.56}$$

where the constant $\tilde{c}_j^{(\nu)}(a)$ is modified as explained above.

The relation between $p_j^{(\nu)}(x)$ and $q_j^{(\nu)}(x)$ from (3.14) is more clear in this form. The polynomials $q_j^{(\nu)}(x)$ may be generated with differential operator in x and a from $p_j^{(\nu)}(x)$, and not with respect to an auxiliary variable like s, i.e.,

$$q_j^{(\nu)}(x) = x^{-\nu}\left(x^2 - \frac{1}{16}\partial_x^2 + \frac{a^4-1}{2}\partial_{a^2} + \tilde{c}_j^{(\nu)}(a)\right)\left(x^\nu p_j^{(\nu)}(x)\right) . \tag{3.57}$$

The normalisation of (3.56) is also clear from (3.57) and (3.55) as only the multiplication by x^2 contributes to the highest power. Equations (3.54), (3.56) and the relation (3.57) are the main results of this subsection.

3.3.2 Equivalent Representations of sOP

There are other ways of representing the polynomials (3.54) and (3.56) that give a sense of how they relate to known polynomials, and are also useful for taking limits. In this subsection, I derive 3 equivalent representations: The Gaussian integrals given in (3.14) as well as sums or integrals over classical Hermite or Laguerre polynomials.

Representation as Gaussian Integrals

Applying two Hubbard-Stratonovich transformations to linearise the angular dependence in the exponent of (3.54), the polynomials are

$$\begin{aligned} p_j^{(\nu)}(x) &= \frac{j!(j+\nu)!}{(-x)^\nu}\frac{4}{\pi\sqrt{1-a^4}}\int_{-\infty}^{\infty}dy\int_{-\infty}^{\infty}d\lambda\int_0^{2\pi}\frac{d\varphi_L}{2\pi}e^{-ij\varphi_L}\int_0^{2\pi}\frac{d\varphi_R}{2\pi}e^{-i(j+\nu)\varphi_R} \\ &\quad\times\exp\left[-\frac{4}{1+a^2}y^2 - \frac{4}{1-a^2}\lambda^2 - (iy+\lambda+x)e^{i\varphi_L} - (iy-\lambda+x)e^{i\varphi_R}\right] . \end{aligned} \tag{3.58}$$

The angular integrals are now possible to do

$$p_j^{(\nu)}(x) = x^{-\nu}\frac{4}{\pi\sqrt{1-a^4}}\int_{-\infty}^{\infty}dy\int_{-\infty}^{\infty}d\lambda\, e^{-\frac{4}{1+a^2}y^2-\frac{4}{1-a^2}\lambda^2}(iy+\lambda+x)^j(iy-\lambda+x)^{j+\nu} . \tag{3.59}$$

This is the form stated in (3.14). The normalisation is checked by looking at the limit for large x. For $q_j^{(\nu)}(x)$ the relation (3.57) is used

$$\begin{aligned} q_j^{(\nu)}(x) &= x^{-\nu}\frac{4}{\pi\sqrt{1-a^4}}\int_{-\infty}^{\infty}dy_1dy_2\, e^{-\frac{4}{1+a^2}{y_1}^2-\frac{4}{1-a^2}{y_2}^2}(iy_1+y_2+x)^j(iy_1-y_2+x)^{j+\nu} \\ &\quad\times\left(4x^2 - \frac{(j+\nu-1)(j+\nu)}{4(x+iy_1-y_2)^2} - \frac{(j-1)j}{4(x+iy_1+y_2)^2} - \frac{j(j+\nu)}{2(iy_1+y_2+x)(iy_1-y_2+x)}\right. \\ &\quad\left.-2\frac{a^6-4{y_1}^2+4{y_2}^2-4a^4({y_1}^2+{y_2}^2)+a^2(8{y_1}^2+8{y_2}^2-1)}{a^4-1}\right) . \end{aligned} \tag{3.60}$$

This form is useful for taking limits, see Section 3.6.

Representation as Hermite Polynomials

Taylor expanding the term coupling the two angles in the second line of (3.54), the two angular integrals decouple. They are represented as complex contour integrals, integrating counter-clockwise around the origin.

$$\begin{aligned} p_j^{(\nu)}(x) &= \frac{j!(j+\nu)!}{(-x)^\nu}\sum_{k=0}^{\infty}\frac{1}{(-4)^k k!}\oint\frac{dz_L}{2\pi i}\frac{1}{z_L^{j-k+1}}\oint\frac{dz_R}{2\pi i}\frac{1}{z_R^{j+\nu-k+1}}e^{-\frac{a^2}{8}({z_L}^2+{z_R}^2)-x(z_L+z_R)} \\ &= \left(\frac{a^2}{8}\right)^{j+\nu/2}x^{-\nu}\sum_{k=0}^{j}\frac{j!(j+\nu)!}{k!(j-k)!(j-k+\nu)!}\left(-\frac{2}{a^2}\right)^k H_{j-k}\left(\sqrt{\frac{2}{a^2}}x\right)H_{j-k+\nu}\left(\sqrt{\frac{2}{a^2}}x\right)\,. \end{aligned} \tag{3.61}$$

The sum terminates at $k=j$ because the poles at the origin disappear for higher k. Identifying the contour representation of the Hermite polynomials and cancelling some signs for $\nu=1$, the second step is achieved. The polynomials $q_j^{(\nu)}(x)$ are found through the relation (3.57) as before.

Representation as Laguerre Polynomials

Starting from the Gaussian representation (3.59)

$$\begin{aligned} p_j^{(\nu)}(x) &= \frac{4x^{-\nu}}{\pi\sqrt{1-a^4}}\int_{-\infty}^{\infty}dy\,e^{-\frac{4}{1+a^2}y^2}\int_{-\infty}^{\infty}d\lambda\,e^{-\frac{4}{1-a^2}\lambda^2}((iy+x)^2-\lambda^2)^j(iy+x-\lambda)^\nu \\ &= \frac{4x^{-\nu}}{\pi\sqrt{1-a^4}}\int_{-\infty}^{\infty}dy\int_{-\infty}^{\infty}d\lambda\,e^{-\frac{4}{1+a^2}y^2-\frac{4}{1-a^2}\lambda^2}\sum_{k=0}^{j}\binom{j}{k}(iy+x)^{2(j-k)+\nu}(i\lambda)^{2k} \\ &= \frac{2x^{-\nu}}{\sqrt{\pi}\sqrt{1-a^2}}\int_{-\infty}^{\infty}d\lambda\,e^{-\frac{4}{1-a^2}\lambda^2}\sum_{k=0}^{j}\binom{j}{k}\left(\frac{\sqrt{1+a^2}}{4}\right)^{2j-2k+\nu} \\ &\quad\times H_{2(j-k)+\nu}\left(\frac{2x}{\sqrt{1+a^2}}\right)(i\lambda)^{2k}\,. \end{aligned} \tag{3.62}$$

The parity of the integrand in λ allows the term $(iy+x-\lambda)^\nu$ in the first line to be replaced by $(iy+x)^\nu$. In the second line the binomials expansion and the integral representation of the Hermite polynomials orthogonal with respect to $\exp\left[-x^2\right]$

$$H_n(x) = \frac{2^n}{\sqrt{\pi}}\int_{-\infty}^{\infty}dt(it+x)^n e^{-t^2} \tag{3.63}$$

have been used. The following identity is also needed

$$\begin{aligned} (2i)^{2n}n!\int_{-\infty}^{\infty}dy\,e^{-(y-\lambda)^2}L_n(x^2+y^2) &= \int_{-\infty}^{\infty}dy\,e^{-(y-\lambda)^2}\sum_{m=0}^{n}\binom{n}{m}H_{2(n-m)}(x)H_{2m}(y) \\ &= \sqrt{\pi}\sum_{m=0}^{n}\binom{n}{m}(2\lambda)^{2m}H_{2(n-m)}(x)\,, \end{aligned} \tag{3.64}$$

where the first line is given in [86, Eq. 18.18.40] and the second line follows from [54, Sec. 7.374]. Inserting this into (3.62) at $\nu = 0$ yields

$$\begin{aligned} p_j^{(0)}(x) &= \frac{(-1)^j j!(1+a^2)^j}{2^{2j-1}\pi\sqrt{1-a^2}} \int_{-\infty}^{\infty} dy \int_{-\infty}^{\infty} d\lambda\, L_j\left(\frac{4x^2}{1+a^2}+y^2\right) e^{-\left(y-\frac{2i\lambda}{\sqrt{1+a^2}}\right)^2 - \frac{4}{1-a^2}\lambda^2} \\ &= \frac{j!(1+a^2)^{j+1/2}}{(-4)^j\sqrt{2\pi}a} \int_{-\infty}^{\infty} dy\, L_j\left(\frac{4x^2}{1+a^2}+y^2\right) e^{-\frac{1+a^2}{2a^2}y^2}\,. \end{aligned} \tag{3.65}$$

The last line is obtained by completing the square in λ and integrating it out.

For $\nu = 1$, a slightly modified version of the identity (3.64) is needed. Apply the well-known relations for Hermite and Laguerre polynomials for $k > 0$

$$\frac{\partial H_k(x)}{\partial x} = 2kH_{k-1}(x) \quad \text{and} \quad \frac{\partial L_k^{(0)}(x)}{\partial x} = -L_{k-1}^{(1)}(x), \tag{3.66}$$

to (3.64) by differentiating with respect to x and shifting $n-1 \to n$ to obtain

$$2x(2i)^{2n} n! \int_{-\infty}^{\infty} dy\, e^{-(y-\lambda)^2} L_n^{(1)}(x^2+y^2) = \sqrt{\pi} \sum_{m=0}^{n} \binom{n}{m} (2\lambda)^{2m} H_{2(n-m)+1}(x)\,. \tag{3.67}$$

This can be inserted into (3.62) to obtain the following representation of polynomials for $\nu = 1$,

$$p_j^{(1)}(x) = \frac{(-1)^j j!(1+a^2)^j}{2^{2j-1}\pi\sqrt{1-a^2}} \int_{-\infty}^{\infty} dy \int_{-\infty}^{\infty} d\lambda\, L_j^{(1)}\left(\frac{4x^2}{1+a^2}+y^2\right) e^{-\left(y-\frac{2i\lambda}{\sqrt{1+a^2}}\right)^2 - \frac{4}{1-a^2}\lambda^2} \tag{3.68}$$

So the two cases of ν may be unified and, after integrating over λ, it reads

$$p_j^{(\nu)}(x) = \frac{j!(1+a^2)^{j+1/2}}{(-4)^j\sqrt{2\pi}a} \int_{-\infty}^{\infty} dy\, L_j^{(\nu)}\left(\frac{4x^2}{1+a^2}+y^2\right) e^{-\frac{1+a^2}{2a^2}y^2}\,. \tag{3.69}$$

Using the leading order coefficient of the generalised Laguerre polynomial, given by $L_j^{(\alpha)}(x) = \frac{(-x)^j}{j!} + O(x^{j-1})$, it is easily shown that the normalisation is monic for both values of $\nu = 0, 1$.

The polynomials $q_j^{(\nu)}(x)$ are again given by the relation (3.57), but as I will need the explicit form later, I state it here

$$\begin{aligned} q_j^{(\nu)}(x) &= \frac{j!(1+a^2)^{j+1/2}}{(-4)^j\sqrt{2\pi}a} \int_{-\infty}^{\infty} dy\, e^{-\frac{1+a^2}{2a^2}y^2} \left\{ \frac{-4x^2}{(1+a^2)^2} L_{j-2}^{(\nu+2)}\left(\frac{4x^2}{1+a^2}+y^2\right) \right. \\ &+ \frac{1}{2(1+a^2)}\left(2\nu - 1 - 4(1-a^2)x^2\right) L_{j-1}^{(\nu+1)}\left(\frac{4x^2}{1+a^2}+y^2\right) \\ &\left. + \left[x^2 - \frac{(1-a^2)}{4a^2}(2ja^2-1) - \frac{(1-a^4)}{4a^4}y^2 + \tilde{c}_j^{(\nu)}(a)\right] L_j^{(\nu)}\left(\frac{4x^2}{1+a^2}+y^2\right)\right\}\,. \end{aligned} \tag{3.70}$$

Laguerre polynomials with negative subscript are formally set to 0. The expression may be simplified slightly by absorbing the term $(1-a^2)(2ja^2-1)/4a^2$ in the constant $\tilde{c}_j^{(\nu)}(a)$.

3.3.3 Determination of the Normalisation

Now that the various representations of the skew-orthogonal polynomials have been established, I turn my attention to the normalisation constants $h_j^{(\nu)}$. These are needed for the three kernels (2.57) and (2.73).

Direct evaluation of the constants through evaluating the integrals in (2.54) and (2.67) turns out to be unrealistic, and I therefore use a different method. Because the normalised jpdf can be written as a product of the polynomial normalisation constants, I can simply compare it to the known normalisation of the jpdf (3.11). This is a well-known feature of the jpdf [8].

Even Dimension $n = 2m$

For even $n = 2m$ the product is

$$\begin{aligned} C_{2m,\nu}^{-1} &= \int_0^\infty d\lambda_1 \ldots \int_0^\infty d\lambda_{2m} \Delta_{2m} \left(\{\lambda^2\}\right) \mathrm{Pf}\left[\, G_\nu(\lambda_j, \lambda_k) \,\right]_{j,k=1,\ldots,2m} \\ &= (2m)! \prod_{k=0}^{m-1} h_{2k}^{(\nu)} \,. \end{aligned} \tag{3.71}$$

This is inverted

$$\begin{aligned} h_{2m}^{(\nu)} &= \frac{(2m)!}{(2m+2)!} \frac{C_{2m,\nu}}{C_{2m+2,\nu}} \\ &= \frac{a^2(1-a^2)^{4m+2+\nu}}{(2m+2)(2m+1)2^{4m+5+\nu}} \Gamma\left(\frac{2m+3}{2}\right) \Gamma\left(\frac{2m+\nu+1}{2}\right) \Gamma\left(\frac{2m+4}{2}\right) \Gamma\left(\frac{2m+\nu+2}{2}\right) \\ &= \frac{\pi a^2(1-a^2)^{4m+2+\nu}}{2^{8m+2\nu+7}} (2m)!(2m+\nu)! \,. \end{aligned} \tag{3.72}$$

In the first step (3.11) has been inserted, and in the second step the Γ-functions have been rewritten.

Odd Dimension $n = 2m + 1$

For odd $n = 2m$ there is an additional contribution to the product from the integral over the extra row and column denoted by $\bar{g}_\nu$ in (3.10)

$$\begin{aligned} C_{2m+1,\nu}^{-1} &= \int_0^\infty d\lambda_1 \ldots \int_0^\infty d\lambda_{2m+1} \Delta_{2m+1} \left(\{\lambda^2\}\right) \mathrm{Pf} \left[\begin{array}{c|c} H_\nu(\lambda_j, \lambda_k) & g_\nu(\lambda_j) \\ \hline -g_\nu(\lambda_k) & 0 \end{array}\right]_{j,k=1,\ldots,2m+1} \\ &= (2m+1)!\, \bar{g}_\nu \prod_{k=1}^{m} h_{2k-1}^{(\nu)} \end{aligned} \tag{3.73}$$

Because $\bar{g}_\nu$ is independent of m, it is cancelled in the ratio $C_{2m+1,\nu}/C_{2m+3,\nu}$.

$$h_{2m+1}^{(\nu)} = \frac{(2m+1)!}{(2m+3)!} \frac{C_{2m+1,\nu}}{C_{2m+3,\nu}} = \frac{\pi a^2(1-a^2)^{4m+4+\nu}}{2^{8m+2\nu+11}} (2m+1)!(2m+\nu+1)! \,. \tag{3.74}$$

The procedure is the same calculation as for $n = 2m$. The normalisation constants may now be written in the following unified form for even and odd index j alike,

$$h_j^{(\nu)} = \frac{\pi a^2(1-a^2)^{2j+2+\nu}}{2^{4j+2\nu+7}} j!(j+\nu)! \,. \tag{3.75}$$

This is the final piece needed for the correlation functions of this transition ensemble. The remainder of this chapter will be dedicated to showing that the limits of a do indeed give the corresponding limiting ensembles and analysis of the smallest eigenvalue.

3.4 Limits $a \to 0, 1, \infty$

Let me briefly address this ensemble in the limits of a. As stated above, the limit $a \to 0$ should lead to the chiral orthogonal ensemble and $a \to 1$ to the antisymmetric hermitian ensemble. This is clear on a matrix level using the relation

$$\lim_{\epsilon\to 0} \sqrt{\frac{2}{\pi\epsilon^2}}\, e^{-\frac{2}{\epsilon^2}x^2} \quad = \quad \delta(x)\,, \tag{3.76}$$

for $a \to 0$, the limit

$$\begin{aligned}\lim_{a\to 0}\int [dY]P(Y,X) &= \lim_{a\to 0}\prod_{i<k}^{N}\int_{-\infty}^{\infty} dH_{i,k}\left(\frac{\pi a^2}{2}\right)^{\frac{1}{2}} e^{-\frac{2}{a^2}H_{i,k}^2}\left(\frac{\pi(1-a^2)}{2}\right)^{-n(n+\nu)/2} e^{-\frac{1}{1-a^2}\mathrm{Tr}\,X^2}\\ &= \left(\frac{\pi}{2}\right)^{-n(n+\nu)/2}\exp\left[-\mathrm{Tr}\,X^2\right], \end{aligned}\tag{3.77}$$

is obtained. The same may be done for $a \to 1$. The limit $a \to \infty$ also leads to the direct sum of two GAOE's, which is better seen where when rescaling the spectrum in Equation (3.16), as (3.3) is not defined for $a \geq 1$.

Note that while the transition ensemble is a Pfaffian point process, one of the limiting ensembles (antisymmetric hermitian) is determinantal, similar to the classical interpolating ensembles [14, 15]. The limit $a \to \infty$ also yields two independent spectra, each of which are a determinantal. This limits the quantities that may be compared. In this section I verify the limits for the jpdf and the polynomials. For $a \to 1$ and $a \to \infty$, only the polynomials $p_j^{(\nu)}(x)$ are considered. For the GAOE the polynomials are orthogonal rather than skew-orthogonal. They should, however, agree as they are obtained from the same Heine-formula. The determinantal point processes, especially the $\beta = 2$ random matrix ensembles, may be written as a Pfaffian point processes in a non-trivial way and solved in terms of skew-orthogonal polynomials [87]. This has not been worked out in detail for GAOE, so I do not consider the limit for $q_j^{(\nu)}(x)$.

These limits act as a consistency check of the results in the previous sections.

3.4.1 Limiting JPDF

Consider the jpdf (3.7) and the weight function (3.8). For $a \to 0$ the variable $\gamma = \sqrt{(1-a^2)/a^2}$ diverges, which means the limit

$$\lim_{\gamma\to\infty}\mathrm{erf}(\gamma z) \quad = \quad \mathrm{sign}(z) \tag{3.78}$$

is needed. The constants $C_{n,\nu}$ in (3.11) provide sufficient powers of n and a to ensure convergence. The two-point weight function is

$$\lim_{a\to 0}\frac{G_\nu(x,y)}{a^2} = \frac{\pi}{8}(xy)^\nu e^{-2(x^2+y^2)}\mathrm{sign}(y^2-x^2) \tag{3.79}$$

for both cases of ν, as the second term in (3.8) vanishes as $a \exp\left[-4(\min\{x,y\})^2/a^2\right]$. The one-point weight function (3.9) is

$$\lim_{a\to 0} \frac{g_\nu(y)}{a} = \sqrt{\frac{\pi}{8}} y^\nu e^{-2y^2} \ , \tag{3.80}$$

where $\mathrm{sign}(y) = 1$ comes from $y > 0$. The identity [88]

$$\left\{ \begin{array}{ll} \mathrm{Pf}[\mathrm{sign}(\lambda_b^2 - \lambda_a^2)]_{a,b=1}^n \, , & n \ \text{even} \\ \mathrm{Pf}\left[\begin{array}{c|c} \mathrm{sign}(\lambda_b^2 - \lambda_a^2) & \vec{1} \\ \hline -\vec{1}^T & 0 \end{array} \right]_{a,b=1}^n , & n \ \text{odd} \end{array} \right\} \ = \ \mathrm{sign}(\Delta_n(\{\lambda^2\})) \tag{3.81}$$

may be used to find the limit

$$\begin{aligned} \lim_{a\to 0} P_n^{(\nu)}(\lambda_1, \ldots, \lambda_n) &= 2^{\frac{n}{2}(3+n+\nu)} \prod_{j=0}^{n-1} \frac{1}{\Gamma\left(\frac{j+3}{2}\right)\Gamma\left(\frac{j+\nu+1}{2}\right)} \left(\frac{\pi}{8}\right)^{\frac{n}{2}} \prod_{j=1}^n \lambda_j^\nu e^{-2\lambda_j^2} \, \Delta_n(\{\lambda^2\}) \mathrm{sign}(\Delta_n(\lambda^2)) \\ &= 2^{\frac{n}{2}(n+\nu)} \pi^{\frac{n}{2}} \prod_{j=0}^{n-1} \frac{1}{\Gamma\left(\frac{j+3}{2}\right)\Gamma\left(\frac{j+\nu+1}{2}\right)} \prod_{j=1}^n \lambda_j^\nu e^{-2\lambda_j^2} \, |\Delta_n(\{\lambda^2\})| \, , \end{aligned} \tag{3.82}$$

for both even and odd n. This is the expected limit, namely the jpdf of the chGOE (in terms of squared singular values) for $\nu = 0, 1$.

I omit the overall constants for $a \to 1$ because the jpdf is normalised, so appropriate factors of $1-a$ are provided by (3.11). The weight functions $G_\nu(x,y)$ and $g_\nu(x)$ are expanded in powers of $(1-a)$

$$G_\nu(x,y) \overset{a\approx 1}{\approx} (1-a)^{1+\nu} (xy)^{2\nu} e^{-2(x^2+y^2)} \sum_{k,l=0}^\infty c_{k,l}^{(\nu)} (1-a)^{k+l} x^{2k} y^{2l}, \tag{3.83}$$

$$g_\nu(x) \overset{a\approx 1}{\approx} (1-a)^{(1+\nu)/2} x^{2\nu} e^{-2x^2} \sum_{k=0}^\infty d_k^{(\nu)} (1-a)^k x^{2k} \, . \tag{3.84}$$

The expansion reflects the fact that the weight functions are even in x and y. The coefficients $c_{k,l}^{(\nu)} = -c_{l,k}^{(\nu)}$ are antisymmetric because $G_\nu(x,y) = -G_\nu(y,x)$.

I first consider $n = 2m$ even. The expansion of the Pfaffian is

$$\begin{aligned} \mathrm{Pf}[G_\nu(\lambda_k, \lambda_l)]_{k,l=1}^{2m} &= (1-a)^{(1+\nu)m} \mathrm{Pf}\left[\sum_{r,t=0}^\infty c_{r,t}^{(\nu)} (1-a)^{r+t} \lambda_k^{2r} \lambda_l^{2t} \right]_{k,l=1}^{2m} \prod_{j=1}^{2m} \lambda_j^{2\nu} e^{-2\lambda_j^2} \\ &\overset{a\approx 1}{\approx} (1-a)^{(1+\nu)m} \mathrm{Pf}\left[\sum_{r,t=0}^{2m-1} c_{r,t}^{(\nu)} (1-a)^{r+t} \lambda_k^{2r} \lambda_l^{2t} \right]_{k,l=1}^{2m} \prod_{j=1}^{2m} \lambda_j^{2\nu} e^{-2\lambda_j^2} \\ &= (1-a)^{(2m+\nu)m} \mathrm{Pf}\left[c_{r,t}^{(\nu)} \right]_{r,t=0}^{2m-1} \Delta_{2m}(\{\lambda^2\}) \prod_{j=1}^{2m} \lambda_j^{2\nu} e^{-2\lambda_j^2} \end{aligned} \tag{3.85}$$

to the lowest order in $(1-a)$. In the first line I have pulled out some factors, and then I have truncated the sum where the terms start to become higher order. The final line comes

from identifying the sum as a matrix product $B^T AB$, with $A = \{c_{r,t}^{(\nu)}\}_{r,t=0,\ldots,2m-1}$ and the Vandermonde matrix $B = \{(1-a)^t \lambda_l^{2t}\}_{\substack{t=0,\ldots,2m-1 \\ l=1,\ldots,2m}}$, and the identity $\mathrm{Pf}[B^T AB] = \mathrm{Pf}[A]\det[B]$.

The same is possible for $n = 2m'+1$

$$
\begin{aligned}
& \mathrm{Pf}\left[\begin{array}{cc} G_\nu(\lambda_k,\lambda_l) & g_\nu(\lambda_k) \\ -g_\nu(\lambda_l) & 0 \end{array}\right]_{k,l=1}^{2m'+1} \qquad (3.86)\\
\overset{a\approx 1}{\approx} \; & \mathrm{Pf}\left[\begin{array}{c|c} \sum_{r,t=0}^{2m'} c_{r,t}^{(\nu)} (1-a)^{r+t} \lambda_k^{2r} \lambda_l^{2t} & \sum_{r=0}^{2m'} d_r^{(\nu)} (1-a)^r \lambda_k^{2r} \\ \hline -\sum_{t=0}^{2m'} d_t^{(\nu)} (1-a)^t \lambda_l^{2t} & 0 \end{array}\right]_{r,t=1}^{2m'+1} \\
& \times (1-a)^{(1+\nu)(2m'+1)/2} \prod_{j=1}^{2m'+1} \lambda_j^{2\nu} e^{-2\lambda_j^2} \\
= \; & (1-a)^{(2m'+\nu)(2m'+1)/2} \mathrm{Pf}\left[\begin{array}{cc} c_{r,t}^{(\nu)} & d_r^{(\nu)} \\ -d_t^{(\nu)} & 0 \end{array}\right]_{r,t=0}^{2m'} \Delta_{2m'+1}(\{\lambda^2\}) \prod_{j=1}^{2m'+1} \lambda_j^{2\nu} e^{-2\lambda_j^2} ,
\end{aligned}
$$

except the matrix A is the matrix inside the Pfaffian in the last line and

$$
B = \mathrm{diag}\left(\{(1-a)^t \lambda_l^{2t}\}_{\substack{t=0,\ldots,2m' \\ l=1,\ldots,2m'+1}}, 1 \right) ,
$$

that is, a block diagonal matrix with a $(2m'+1)\times(2m'+1)$ block containing the Vandermonde matrix and a 1×1 block of unity.

These may be combined to yield

$$
\lim_{a\to 1} P_n^{(\nu)}(\lambda_1,\ldots,\lambda_n) \propto \prod_{j=1}^{n} \lambda_j^{2\nu} e^{-2\lambda_j^2} \, \Delta_n(\{\lambda^2\})^2 , \qquad (3.87)
$$

where the expansion of the Pfaffian provides the extra Vandermonde, and the normalisation constant (3.11) cancels all but the lowest order. This agrees with the jpdf of the GAOE for $N = 2n+\nu$, see [8, 68].

The final limit is $a\to\infty$. I first rewrite (3.8) and (3.9) for $a > 1$

$$
\begin{aligned}
G_\nu(x,y) = \; & \frac{\pi a^2(a^2-1)}{8} (xy)^\nu e^{-2(x^2+y^2)} \left(\mathrm{erfi}\left[\sqrt{\frac{a^2-1}{a^2}}(y-x)\right] \mathrm{erfi}\left[\sqrt{\frac{a^2-1}{a^2}}(x+y)\right] \right. \\
& \left. -\delta_{\nu,1} \frac{2}{\sqrt{\pi}} \int_{\sqrt{2(a^2-1)/a^2}x}^{\sqrt{2(a^2-1)/a^2}y} du \, \mathrm{erfi}\left[\sqrt{\frac{2(a^2-1)}{a^2}}(x+y) - u\right] e^{u^2} \right), \qquad (3.88)\\
g_\nu(y) = \; & i^{1+\nu} \sqrt{\frac{\pi a^2(a^2-1)}{8}} \exp\left[-2y^2\right] \left(y \, \mathrm{erfi}\left[\sqrt{\frac{2(a^2-1)}{a^2}} y\right] \right)^\nu . \qquad (3.89)
\end{aligned}
$$

The function $\mathrm{erfi}(z)$ has the following asymptotic relation for large positive, real argument

$$
\mathrm{erfi}(z) = \mathrm{erf}(iz)/i = \frac{2}{\sqrt{\pi}} \int_0^z e^{x^2} dx \overset{z\gg 1}{\approx} \frac{1}{\sqrt{\pi} z} e^{z^2} . \qquad (3.90)
$$

The spectrum is rescaled $x \to ax'$ to accommodate the scaling in (3.16)

$$G_\nu(ax', ay') \overset{a\gg 1}{\approx} (-1)^\nu \frac{a^{2(1+\nu)}}{16} \frac{y'^{2\nu} + x'^{2\nu}}{y'^2 - x'^2} e^{-2(x'^2+y'^2)}\,, \tag{3.91}$$

$$g_\nu(y) \overset{a\gg 1}{\approx} \frac{i^{1+\nu} a^2}{(2\pi)^{\nu/2}} \sqrt{\frac{\pi}{8}} \exp\left[-2\frac{y^2}{a^{2(\nu-1)}}\right]\,. \tag{3.92}$$

The two-point weight function formally vanishes for $x' = y'$, and was obtained through (3.90). The second term of it, the one involving an integral, was dealt with as follows

$$\begin{aligned}
&\int_{\sqrt{2(a^2-1)}x'}^{\sqrt{2(a^2-1)}y'} du\, \mathrm{erfi}\left[\sqrt{2(a^2-1)}(x'+y') - u\right] e^{u^2} \\
= \quad & \frac{4(a^2-1)}{\sqrt{\pi}} \int_{x'}^{y'} du' \int_0^1 dv \left(x'+y'-u'\right) \exp\left[2(a^2-1)[u'^2 + (x'+y'-u')^2 v^2]\right] \\
\overset{a\gg 1}{\approx} \quad & \frac{1}{\sqrt{\pi}} \int_{x'}^{y'} \frac{du'}{x'+y'-u'} \exp\left[2(a^2-1)[u'^2 + (x'+y'-u')^2]\right] \\
\overset{a\gg 1}{\approx} \quad & \frac{1}{4\sqrt{\pi}(a^2-1)} \frac{y'+x'}{y'x'(y'-x')} e^{2(a^2-1)(x'^2+y'^2)}.
\end{aligned} \tag{3.93}$$

First the definition of the erfi-function is used and a rescaling $u = \sqrt{2(a^2-1)}u'$ is done. Thereafter a saddle-point approximation is performed for the integrals. The maxima are $v = 1$ and $u' = x', y'$. The integral is therefore a sum of the two cases.

These weight functions are inserted in the jpdf. For even $n = 2m$

$$\begin{aligned}
a^{2m} P_{2m}^{(\nu)}(a\lambda'_1, \ldots, a\lambda'_{2m}) \overset{a\gg 1}{\approx} \quad & a^{2m} C_{2m,\nu}\, \Delta_{2m}\left(\{a^2\lambda^2\}\right) \\
& \times \mathrm{Pf}\left[(1-\delta_{jk})(-1)^\nu \frac{a^{2(1+\nu)}}{16} \frac{{\lambda'_k}^{2\nu} + {\lambda'_j}^{2\nu}}{{\lambda'_k}^2 - {\lambda'_j}^2} e^{-2({\lambda'_j}^2 + {\lambda'_k}^2)}\right]_{j,k=1}^{2m} \\
\overset{a\gg 1}{\approx} \quad & 2^{m(2m+\nu-1)} \prod_{j=0}^{2m-1} \frac{1}{\Gamma\left(\frac{j+3}{2}\right)\Gamma\left(\frac{j+\nu+1}{2}\right)} \Delta_{2m}\left(\{\lambda^2\}\right) \prod_{j=1}^{2m} e^{-2{\lambda'_j}^2} \\
& \times \mathrm{Pf}\left[\frac{{\lambda'_k}^{2\nu} + {\lambda'_j}^{2\nu}}{{\lambda'_k}^2 - {\lambda'_j}^2}(1-\delta_{jk})\right]_{j,k=1}^{2m}.
\end{aligned} \tag{3.94}$$

The Kronecker δ ensures that the weight function disappears for equal argument. I expand the Pfaffian

$$\begin{aligned}
\mathrm{Pf}\left[\frac{{\lambda'_k}^{2\nu} + {\lambda'_j}^{2\nu}}{{\lambda'_k}^2 - {\lambda'_j}^2}(1-\delta_{jk})\right]_{j,k=1}^{2m} &= \frac{1}{2^m m!} \sum_{\omega\in\mathcal{S}_{2m}} \mathrm{sign}(\omega) \prod_{j=1}^{m} \frac{(\lambda'_{\omega(2j)})^{2\nu} + (\lambda'_{\omega(2j-1)})^{2\nu}}{(\lambda'_{\omega(2j)})^2 - (\lambda'_{\omega(2j-1)})^2} \\
&= \frac{1}{(m!)^2} \sum_{\sigma\in\mathcal{S}_m} \mathrm{sign}(\sigma) \sum_{\omega\in\mathcal{S}_{2m}} \mathrm{sign}(\omega) \prod_{j=1}^{m} \frac{(\lambda'_{\omega(2j)})^{2\nu}}{(\lambda'_{\omega(2j)})^2 - (\lambda'_{\omega(\sigma(2j-1))})^2} \\
&= \frac{1}{(m!)^2} \sum_{\omega\in\mathcal{S}_{2m}} \mathrm{sign}(\omega) \det\left[\frac{(\lambda'_{\omega(2k)})^{2\nu}}{(\lambda'_{\omega(2k)})^2 - (\lambda'_{\omega(2j-1)})^2}\right]_{j,k=1}^{m}.
\end{aligned} \tag{3.95}$$

Here $\mathcal{S}_{2m}$ is the symmetric group permuting $2m$ elements and $\mathrm{sign}(\omega)$ is -1 for odd permutations and 1 for even ones. The first equality is the definition of the Pfaffian. The second one exploits the invariance under pairwise permutation of each pair $(\lambda'_{\omega(2j)}, \lambda'_{\omega(2j-1)})$ and the invariance under the permutation of the variables $\lambda'_{\omega(1)}, \lambda'_{\omega(3)}, \ldots, \lambda'_{\omega(2m-1)}$. This changes the overall combinatorial factor. In the final line the sum has been identified as a determinant.

Denote by $\lambda^{(\omega,o)}$ and $\lambda^{(\omega,e)}$ the set of odd and even eigenvalues $\lambda'_{\omega(1)}, \ldots, \lambda'_{\omega(2m-1)}$ and $\lambda'_{\omega(2)}, \ldots, \lambda'_{\omega(2m)}$, respectively, and pull out the factor $(\lambda'_{\omega(2k)})^{2\nu}$ of the determinant in the last line of (3.95). The resulting Cauchy determinant [89] is

$$\det\left[\frac{1}{(\lambda'_{\omega(2k)})^2-(\lambda'_{\omega(2j-1)})^2}\right]_{j,k=1}^{m} = \mathrm{sign}(\omega)\frac{\Delta_m^2(\{(\lambda^{(\omega,o)})^2\})\Delta_m^2(\{(\lambda^{(\omega,e)})^2\})}{\Delta_{2m}(\{\lambda'^2\})}. \quad (3.96)$$

The additional $\mathrm{sign}(\omega)$ on the right-hand side comes from reordering the arguments of the larger Vandermonde determinant in the denominator to $\lambda'_1, \lambda'_2 \ldots, \lambda'_{2m}$.

So far the jpdf reads

$$\begin{aligned} a^{2m}P_{2m}^{(\nu)}(a\lambda'_1,\ldots,a\lambda'_{2m}) &\overset{a\gg 1}{\approx} \frac{1}{(2m)!}\sum_{\omega\in\mathcal{S}_{2m}}\frac{\Delta_m^2(\{(\lambda^{(\omega,o)})^2\})}{m!\prod_{j=0}^{m-1}\sqrt{\pi}2^{-4j-3/2}(2j)!} \\ &\times\frac{\Delta_m^2(\{(\lambda^{(\omega,e)})^2\})}{m!\prod_{j=0}^{m-1}\sqrt{\pi}2^{-4j-2\nu-3/2}(2j+\nu)!}\prod_{j=1}^{m}(\lambda'_{\omega(2j)})^{2\nu}e^{-2((\lambda'_{\omega(2j)})^2+(\lambda'_{\omega(2j-1)})^2)}. \end{aligned} \quad (3.97)$$

The factor a^{2m} comes from the Jacobian of the rescaling $\lambda \to a\lambda'$. The contents of the sum is the product of two GAOE jpdf of dimensions $2m$ and $2m+\nu$. The sums reflects the fact that the eigenvalues from the two ensembles cannot be distinguished. This is exactly the expected limit.

The limit for odd $n = 2m'+1$ is similar. The Pfaffian is

$$\begin{aligned} &\mathrm{Pf}\left[\begin{array}{c|c} (1-\delta_{jk})(-1)^{\nu}\frac{a^{2(1+\nu)}}{16}\frac{{\lambda'_k}^{2\nu}+{\lambda'_j}^{2\nu}}{{\lambda'_k}^2-{\lambda'_j}^2}e^{-2({\lambda'_j}^2+{\lambda'_k}^2)} & \frac{i^{1+\nu}}{(2\pi)^{\nu/2}}\sqrt{\frac{\pi a^4}{8}}e^{-\frac{2}{a^{2(\nu-1)}}{\lambda'_j}^2} \\ \hline -\frac{i^{1+\nu}}{(2\pi)^{\nu/2}}\sqrt{\frac{\pi a^4}{8}}e^{-\frac{2}{a^{2(\nu-1)}}{\lambda'_k}^2} & 0 \end{array}\right]_{j,k=1}^{2m'+1} \\ &= \frac{i^{1+\nu}(-1)^{m'\nu}}{(2\pi)^{\nu/2}}\sqrt{\frac{\pi a^4}{8}}\left(\frac{a^{2(1+\nu)}}{16}\right)^{m'}\frac{1}{(2m')!}\sum_{\sigma\in\mathcal{S}_{2m'+1}}\mathrm{sign}(\sigma)\mathrm{Pf}\left[\frac{(\lambda'_{\sigma(k)})^{2\nu}+(\lambda'_{\sigma(j)})^{2\nu}}{(\lambda'_{\sigma(k)})^2-(\lambda'_{\sigma(j)})^2}(1-\delta_{jk})\right]_{j,k=1}^{2m'} \\ &\quad\times e^{-\frac{2}{a^{2(\nu-1)}}(\lambda'_{\sigma(2m'+1)})^2}\prod_{j=1}^{2m'}e^{-2(\lambda'_{\sigma(k)})^2} \\ &= \frac{i^{1+\nu}(-1)^{m'\nu}}{(2\pi)^{\nu/2}}\sqrt{\frac{\pi a^4}{8}}\left(\frac{a^{2(1+\nu)}}{16}\right)^{m'}\frac{1}{(m'!)^2}\sum_{\sigma\in\mathcal{S}_{2m'+1}}\mathrm{sign}(\sigma)\det\left[\frac{(\lambda'_{\sigma(2k)})^{2\nu}}{(\lambda'_{\sigma(2k)})^2-(\lambda'_{\sigma(2j-1)})^2}\right]_{j,k=1}^{m'} \\ &\quad\times e^{-\frac{2}{a^{2(\nu-1)}}(\lambda'_{\sigma(2m'+1)})^2}\prod_{j=1}^{2m'}e^{-2(\lambda'_{\sigma(k)})^2}. \end{aligned} \quad (3.98)$$

First the Pfaffian is expanded in the last row, and the expression is symmetrised with respect to the symmetric group $\mathcal{S}_{2m'+1}$ which gives the normalising factor $1/(2m')!$ and (3.95) is used

again. The sum over the permutation $\omega \in \mathcal{S}_{2m'}$ is absorbed in the permutation σ. This gives a combinatorial factor equal to the number of elements ω takes, $(2m')!$.

$$
\begin{aligned}
& a^{2m'+1} P^{(\nu=0)}_{2m'+1}(a\lambda'_1, \ldots, a\lambda'_{2m'+1}) \\
\overset{a\gg 1}{\approx} \quad & \frac{1}{(2m'+1)!} \sum_{\sigma \in \mathcal{S}_{2m'+1}} \sqrt{\frac{8a^2}{\pi}} e^{-2a^2 (\lambda'_{\sigma(2m'+1)})^2} \frac{\Delta^2_{m'}(\{(\lambda^{(\sigma,o)})^2\}) \prod_{k=1}^{m'} ((\lambda'_{\sigma(2k-1)})^2 - (\lambda'_{\sigma(2m'+1)})^2)}{m'! \prod_{j=0}^{m'-1} \sqrt{\pi} 2^{-4j-7/2} (2j+1)!} \\
& \times \frac{\Delta^2_{m'}(\{(\lambda^{(\sigma,e)})^2\}) \prod_{k=1}^{m'} ((\lambda'_{\sigma(2k)})^2 - (\lambda'_{\sigma(2m'+1)})^2)}{m'! \prod_{j=0}^{m'-1} \sqrt{\pi} 2^{-4j-7/2} (2j+1)!} \prod_{j=1}^{m'} e^{-2((\lambda'_{\sigma(2j)})^2 + (\lambda'_{\sigma(2j-1)})^2)} \\
\overset{a\gg 1}{\approx} \quad & \frac{1}{(2m'+1)!} \sum_{\sigma \in \mathcal{S}_{2m'+1}} \delta(\lambda'_{\sigma(2m'+1)}) \prod_{j=1}^{m'} (\lambda'_{\sigma(2j)} \lambda'_{\sigma(2j-1)})^2 e^{-2((\lambda'_{\sigma(2j)})^2 + (\lambda'_{\sigma(2j-1)})^2)} \\
& \times \frac{\Delta^2_{m'}(\{(\lambda^{(\sigma,o)})^2\})}{m'! \prod_{j=0}^{m'-1} \sqrt{\pi} 2^{-4j-7/2} (2j+1)!} \frac{\Delta^2_{m'}(\{(\lambda^{(\sigma,e)})^2\})}{m'! \prod_{j=0}^{m'-1} \sqrt{\pi} 2^{-4j-7/2} (2j+1)!} \, .
\end{aligned}
\tag{3.99}
$$

The cases $\nu = 0$ and $\nu = 1$ have to be treated separately. Denote again the set of eigenvalues $\lambda'_{\sigma(1)}, \ldots, \lambda'_{\sigma(2m'-1)}$ and $\lambda'_{\sigma(2)}, \ldots, \lambda'_{\sigma(2m')}$ by $\lambda^{(\sigma,o)}$ and $\lambda^{(\sigma,e)}$ respectively. The jpdf (3.7) for $\nu = 0$ becomes

$$
\begin{aligned}
& a^{2m'+1} P^{(\nu=0)}_{2m'+1}(a\lambda'_1, \ldots, a\lambda'_{2m'+1}) \\
\overset{a\gg 1}{\approx} \quad & \frac{1}{(2m'+1)!} \sum_{\sigma \in \mathcal{S}_{2m'+1}} \sqrt{\frac{8a^2}{\pi}} e^{-2a^2 (\lambda'_{\sigma(2m'+1)})^2} \frac{\Delta^2_{m'}(\{(\lambda^{(\sigma,o)})^2\}) \prod_{k=1}^{m'} ((\lambda'_{\sigma(2k-1)})^2 - (\lambda'_{\sigma(2m'+1)})^2)}{m'! \prod_{j=0}^{m'-1} \sqrt{\pi} 2^{-4j-7/2} (2j+1)!} \\
& \times \frac{\Delta^2_{m'}(\{(\lambda^{(\sigma,e)})^2\}) \prod_{k=1}^{m'} ((\lambda'_{\sigma(2k)})^2 - (\lambda'_{\sigma(2m'+1)})^2)}{m'! \prod_{j=0}^{m'-1} \sqrt{\pi} 2^{-4j-7/2} (2j+1)!} \prod_{j=1}^{m'} e^{-2((\lambda'_{\sigma(2j)})^2 + (\lambda'_{\sigma(2j-1)})^2)} \\
\overset{a\gg 1}{\approx} \quad & \frac{1}{(2m'+1)!} \sum_{\sigma \in \mathcal{S}_{2m'+1}} \delta(\lambda'_{\sigma(2m'+1)}) \prod_{j=1}^{m'} (\lambda'_{\sigma(2j)} \lambda'_{\sigma(2j-1)})^2 e^{-2((\lambda'_{\sigma(2j)})^2 + (\lambda'_{\sigma(2j-1)})^2)} \\
& \times \frac{\Delta^2_{m'}(\{(\lambda^{(\sigma,o)})^2\})}{m'! \prod_{j=0}^{m'-1} \sqrt{\pi} 2^{-4j-7/2} (2j+1)!} \frac{\Delta^2_{m'}(\{(\lambda^{(\sigma,e)})^2\})}{m'! \prod_{j=0}^{m'-1} \sqrt{\pi} 2^{-4j-7/2} (2j+1)!} \, .
\end{aligned}
\tag{3.100}
$$

Note that in the jpdf represents three ensembles, two GAOE of dimension $(2m'+1) \times (2m'+1)$ and one of dimension 2×2 on the scale $1/a$. The latter acts as a perturbative coupling of order $1/a$ between the larger ensembles. Compare with the structure in (3.16). This is the only case where the topology changes, see Chapter 4 for treatment of such systems.

For $\nu = 1$ the Pfaffian (3.98) is modified to

$$
\begin{aligned}
\mathrm{Pf} \left[\begin{array}{c|c} (\delta_{jk}-1) \frac{a^4}{16} \frac{{\lambda'_k}^2 + {\lambda'_j}^2}{{\lambda'_k}^2 - {\lambda'_j}^2} e^{-2({\lambda'_j}^2 + {\lambda'_k}^2)} & -\frac{a^2}{4} e^{-2{\lambda'_j}^2} \\ \hline \frac{a^2}{4} e^{-2{\lambda'_k}^2} & 0 \end{array} \right]_{j,k=1}^{2m'+1} &= \frac{(-1)^{m'+1} a^2}{4\, m'!(m'+1)!} \left(\frac{a}{2}\right)^{4m'} \\
\times \sum_{\sigma \in \mathcal{S}_{2m'+1}} \mathrm{sign}(\sigma) \prod_{j=1}^{2m'+1} e^{-2(\lambda'_{\sigma(k)})^2} \det \left[\begin{array}{c|c} \frac{(\lambda'_{\sigma(2k)})^2}{(\lambda'_{\sigma(2k)})^2 - (\lambda'_{\sigma(2j-1)})^2} & \vec{1} \end{array} \right]_{\substack{j=1,\ldots,m'+1 \\ k=1,\ldots,m'}} .
\end{aligned}
\tag{3.101}
$$

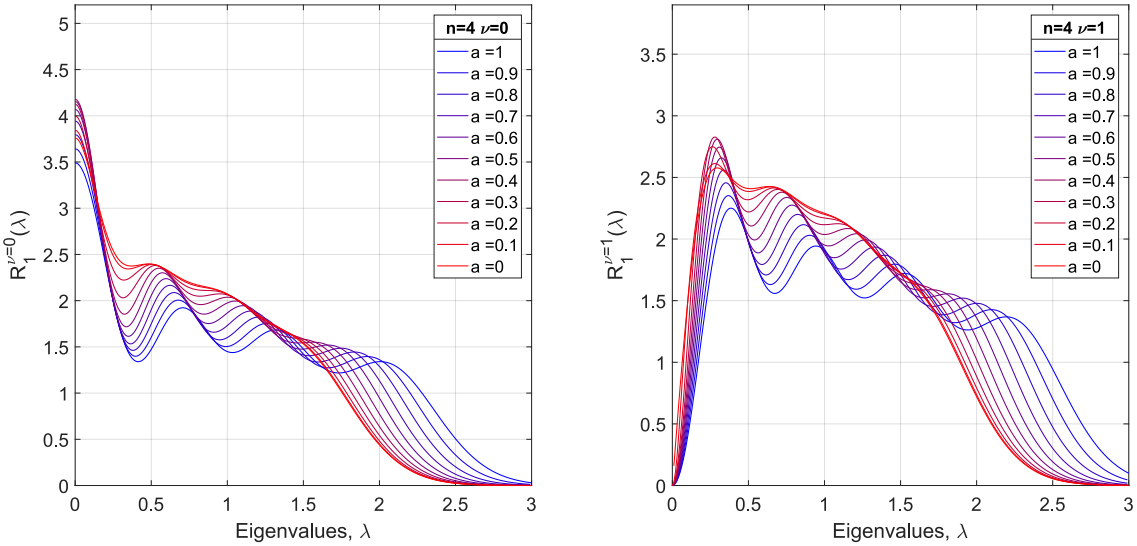

Figure 3.3: The spectral density (3.107) is shown for $n = 4$ with $\nu = 0$ (left) and $\nu = 1$ (right). The parameter a increases from the most narrow distribution at $a = 0$ (red), corresponding to the density of the chGOE in (2.65), to the broadest distribution at $a = 1$ (blue), corresponding to the density of the GAOE in (2.47). This figure is also published in [AKMV].

The factors $(\lambda'_{\sigma(2k)})^2$ are now pulled out of the determinant. The Cauchy determinant is instead a Cauchy-Vandermonde determinant, see [90],

$$\det\left[\left.\frac{1}{(\lambda'_{\sigma(2k)})^2-(\lambda'_{\sigma(2j-1)})^2}\;\right|\;\vec{1}\right]_{\substack{j=1,\dots,m'+1\\k=1,\dots,m'}}=\mathrm{sign}(\sigma)\frac{\Delta^2_{m'}(\{(\lambda^{(\sigma,e)})^2\})\Delta^2_{m'+1}(\{(\lambda^{(\sigma,o)})^2\})}{\Delta_{2m'+1}(\{\lambda^2\})}\,, \tag{3.102}$$

with $\lambda^{(\sigma,o)}=\mathrm{diag}(\lambda'_{\sigma(1)},\dots,\lambda'_{\sigma(2m'+1)})$ and $\lambda^{(\sigma,e)}=\mathrm{diag}(\lambda'_{\sigma(2)},\dots,\lambda'_{\sigma(2m')})$. The asymptotics of the jpdf is

$$\begin{aligned}&a^{2m'+1}P^{(\nu=1)}_{2m'+1}(a\lambda'_1,\dots,a\lambda'_{2m'+1})\\ \overset{a\gg1}{\approx}\;&\frac{1}{(2m'+1)!}\sum_{\sigma\in\mathcal{S}_{2m'+1}}\left(\prod_{j=1}^{m'}(\lambda'_{\sigma(2j)})^2e^{-2(\lambda'_{\sigma(2j)})^2}\right)\left(\prod_{j=1}^{m'+1}e^{-2(\lambda'_{\sigma(2j-1)})^2}\right)\\ &\times\frac{\Delta^2_{m'+1}(\{(\lambda^{(\sigma,e)})^2\})}{m'!\prod_{j=0}^{m'-1}\sqrt{\pi}2^{-4j-7/2}(2j+1)!}\frac{\Delta^2_{m'}(\{(\lambda^{(\sigma,o)})^2\})}{(m'+1)!\prod_{j=0}^{m'}\sqrt{\pi}2^{-4j-3/2}(2j)!}\,.\end{aligned} \tag{3.103}$$

The contents of the sum is two GAOE of sizes $(2m'+1)\times(2m'+1)$ and $(2m'+2)\times(2m'+2)$ respectively. It is clear that the zero mode of J comes from the matrix block A, see (3.16).

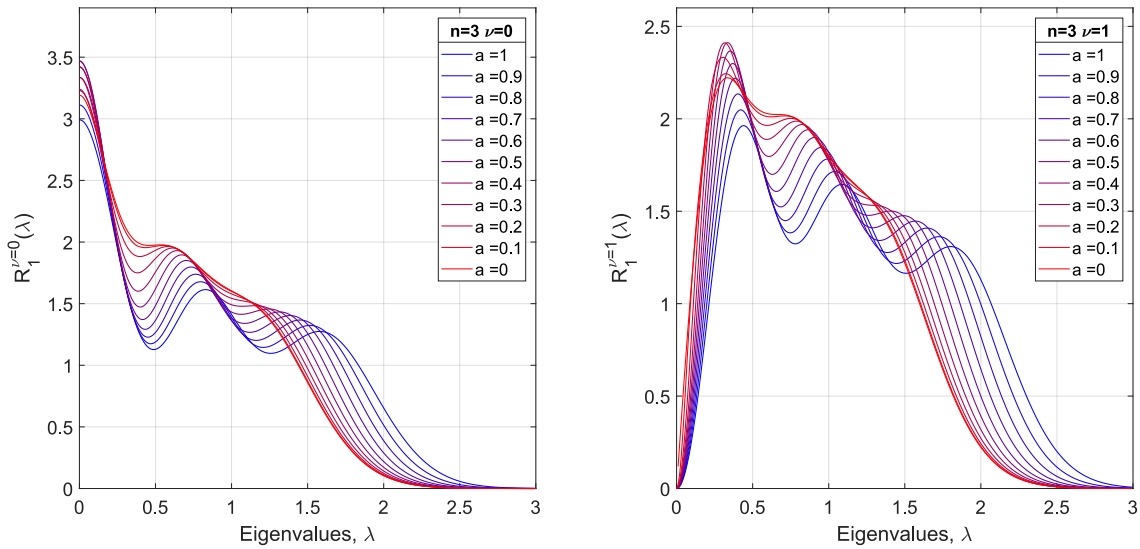

Figure 3.4: The spectral density for odd $n = 3$ from (3.108) is plotted for $\nu = 0$ (left) and $\nu = 1$ (right). As in Figure 3.3, the parameter a varies from a narrow distribution at $a = 0$ (red, chGOE) to the broad distribution which corresponds to $a = 1$ (blue, GAOE, see (2.47)). This plot is also published in [AKMV].

3.4.2 Limiting Polynomials

I again start with the limit $a \to 0$. The Laguerre representation of $p_j^{(\nu)}(x)$ (3.69) and the identity (3.76) leads to

$$\lim_{a\to 0} p_j^{(\nu)}(x) = \frac{j!}{(-4)^j} \int_{-\infty}^{\infty} dy\, L_j^{(\nu)}\left(4x^2 + 2y^2\right) \delta(y) = \frac{j!}{(-4)^j}\, L_j^{(\nu)}\left(4x^2\right) \ . \tag{3.104}$$

These agree with (2.62) as they should. Starting from (3.70), the same may be done for $q_j^{(\nu)}(x)$ to arrive at (2.63).

For the limit $a \to 1$, I use the Gaussian representation (3.59) to write

$$\begin{aligned} \lim_{a\to 1} x^\nu p_j^{(\nu)}(x) &= \frac{2}{\sqrt{2\pi}} \int_{-\infty}^{\infty} dy \int_{-\infty}^{\infty} dz\, e^{-2y^2} (iy + z + x)^j (iy - z + x)^{j+\nu} \delta(z) \\ &= \frac{1}{\sqrt{\pi}} \int_{-\infty}^{\infty} du\, e^{-u^2} \left(\frac{iu}{\sqrt{2}} + x\right)^{2j+\nu} \\ &= \frac{1}{2^{3(2j+\nu)/2}} H_{2j+\nu}\left(\sqrt{2}\, x\right) \ , \end{aligned} \tag{3.105}$$

In the final line the integral representation of the Hermite polynomials (3.63) has been used. These are the orthogonal polynomials of the GAOE [8], only the even or only the odd Hermite polynomials for $\nu = 0, 1$, respectively.

The final limit $a \to \infty$ is taken for the Hermite representation (3.61). The spectrum is again rescaled $x \to ax'$, which yields

$$\lim_{a\to\infty} a^{-2j} x^\nu p_j^{(\nu)}(ax) = \frac{1}{2^{3(2j+\nu)/2}} H_j\left(\sqrt{2}x\right) H_{j+\nu}\left(\sqrt{2}x\right) \ . \tag{3.106}$$

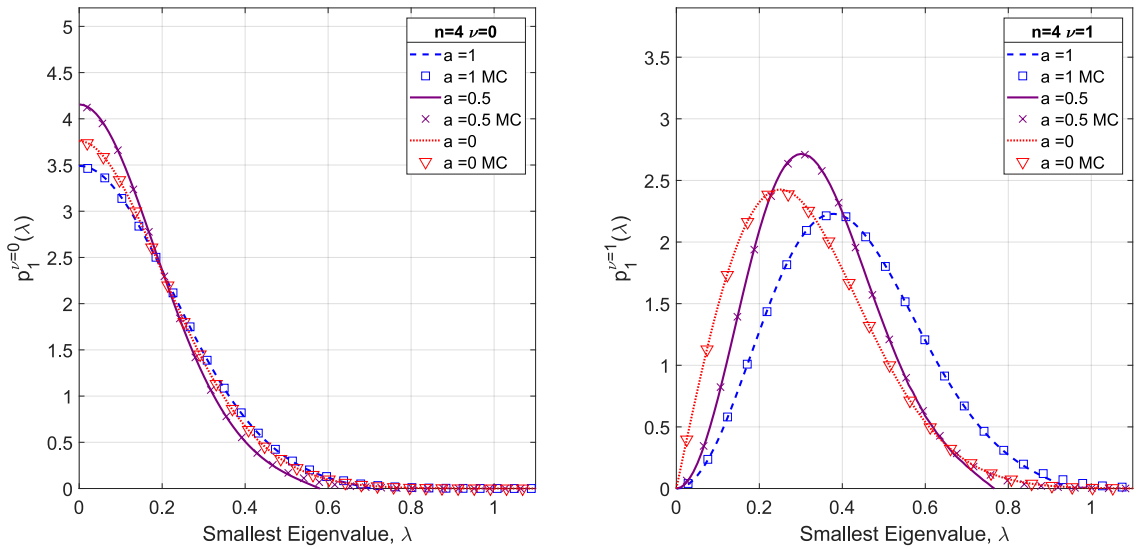

Figure 3.5: The approximate distribution of the smallest eigenvalue $p_1^\nu(s)$, see (3.109), (curves) is compared to Monte-Carlo (MC) simulations (symbols). This plot shows the results for $n = 4$ with $\nu = 0$ (left) and $\nu = 1$ (right). The ensemble size is 10^6 and the bin size is 0.05. For $a = 0$ the exact curves for $p_1^\nu(s)$ are drawn, see (3.111) and (3.112). This plot is also published in [AKMV].

The overall constant (3.11) provides the convergence. The rest of the terms are suppressed by $1/a^2$. The factorisation of (3.106) reflects the factorisation of the model into the matrices A and B, and the polynomials $H_j\left(\sqrt{2}x\right)$ and $H_{j+\nu}\left(\sqrt{2}x\right)$ represent these two matrices respectively. The polynomials $q_j^{(\nu)}(x)$ are omitted for the same reasons as above; these are determinantal point processes.

This concludes the consistency check of the limits of a. The final two sections will deal with an analysis of the smallest eigenvalue and the limit of large matrix size.

3.5 Spectral Density and Distribution of Smallest Eigenvalue

In this section I take a closer look at the spectral density of the transition ensemble. All the k-point correlation functions are given by inserting the polynomials (3.14) in the standard form (2.57) and (2.73).

Spectral Density for Even Matrix Size

For even matrix size the density is

$$R_1^\nu(\lambda) \quad = \quad S_{2m}(\lambda, \lambda)\,. \tag{3.107}$$

See Figure 3.3 for a plot of this for $n = 4$ even and different values of a. The local maxima roughly correspond to the individual eigenvalues. At $a = 1$ the eigenvalues have the greatest repulsion, corresponding to Dyson index $\beta = 2$, and the local maxima are therefore most pronounced. The density flattens out when decreasing a, and for $a = 0$, the level repulsion

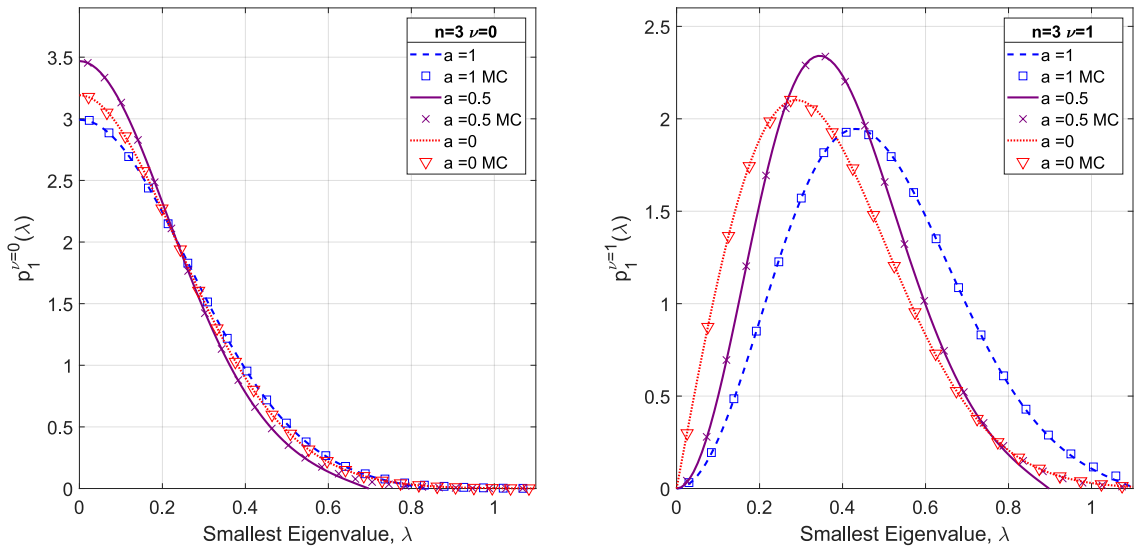

Figure 3.6: The analytical approximation (3.109) ($a > 0$) and the exact distributions (3.111) and (3.112) ($a = 0$) (curves) as well as Monte-Carlo simulations (symbols) of the smallest eigenvalue $p_1^\nu(s)$ for $n = 3$ with $\nu = 0$ (left) and $\nu = 1$ (right). As before the ensemble size is 10^6 and the bin size is 0.05. This plot is also published in [AKMV].

corresponds to Dyson index $\beta = 1$ where it is at its weakest. For $\nu = 1$ the extra eigenvalue at the origin also pushes away the spectrum. The density for the limits $a \to 1$ and $a \to 0$ may be found in (2.47) and (2.65) respectively.

Spectral Density for Odd Matrix Size

Similarly, the spectral density (2.77) for $n = 2m - 1$ odd is given by

$$R_1^\nu(\lambda) \quad = \quad S_{2m-1}(\lambda, \lambda)\,. \tag{3.108}$$

A plot for $n = 3$ is given in Figure 3.4.

Both Figures 3.3 and 3.4 show an interesting behaviour for the smallest eigenvalue (the left-most peak). It has its maximum peak between $a = 0$ and $a = 1$. That is, the behaviour is not monotonic. I therefore take a closer look at the smallest eigenvalue by itself. It should be noted that these results are only universal in the limit on $N \to \infty$. The support of the density also changes with a, which may influence the result. I outline the method for doing this limit in Section 3.6.

Distribution of Smallest Eigenvalue

I expand the smallest eigenvalue in terms of the k-point density correlation functions.

$$p_1^\nu(s) \quad = \quad \sum_{l=1}^{n} \frac{(-1)^{l-1}}{(l-1)!} \int_0^s dx_1 \dots dx_{l-1} R_l^\nu(s, x_1, \dots, x_{l-1}) = R_1^\nu(s) - \int_0^s dx_1 R_2^\nu(s, x_1) + \dots\,. \tag{3.109}$$

This may be done in general for the l-th gap probability at the origin and the resulting distribution of the l-th smallest eigenvalue, see [91]. The expansion converges quite quickly. For $l = 1$ we have no integral in the sum. More sophisticated methods for the approximation of Fredholm determinant, see e.g. [78], but for finite (and small) n, (3.109) is sufficient.

See Figures 3.5 and 3.6 for a comparison of Monte-Carlo simulations to (3.109) truncated after the first two terms. The expansion breaks down at the latest when the density becomes negative, though this is almost at the edge of the support, which makes this a good approximation.

An additional advantage of looking at this expansion is that it includes the 2-point correlation function and thus the off-diagonal kernels $I_n^\nu(x,y)$ and $D_n^\nu(x,y)$ in (2.48), as well as $S_n^\nu(x,y)$ at unequal argument

$$R_2^\nu(x,y) \;=\; S_n^\nu(x,x)S_n^\nu(y,y) - I_n^\nu(x,y)D_n^\nu(x,y) - S_n^\nu(x,y)^2 \;. \tag{3.110}$$

The expansion therefore acts as a more thorough numerical check of these kernels.

The non-monotonous behaviour is clear for the smallest eigenvalue, but it is still unclear whether this is also true for the limit $n \to \infty$.

The smallest eigenvalue is known exactly for chGOE for finite n [92, 93]. For $\nu = 1$

$$p_1^{\nu=1}(s)\big|_{a=0} \;=\; 4ns\, e^{-2ns^2} \;, \tag{3.111}$$

and for $\nu = 0$

$$p_1^{\nu=0}(s)\big|_{a=0} = n\sqrt{\frac{8}{\pi}}\,\Gamma\left(\frac{n+1}{2}\right) e^{-2ns^2} U\left(\frac{n-1}{2}, -\frac{1}{2}, 2s^2\right) \;, \tag{3.112}$$

where U is Tricomi's confluent hypergeometric function. These are valid for both even and odd n. These make up the curves for $a = 0$ in Figures 3.5 and 3.6.

The analytical distribution of GAOE ($a \to 1$) is an open problem, though it is known that it is proportional to the expectation value of a characteristic polynomial to half-integer power, see e.g. [94] for the corresponding expression for the chGOE. The curves for $a = 1$ in Figures 3.5 and 3.6 are generated with the significantly simpler k-point correlation functions for GAOE, see e.g. [8].

3.6 Limit of Large Matrix Size

The Gaussian choice of weight in the above was arbitrary. Universal results should only be expected in the limit of large matrix size. At the time of writing these are not finished results, but I shall endeavour to outline the steps necessary.

The limit I look at is $n \to \infty$ while rescaling $x = \lambda/\sqrt{n}$ with different scalings of a. This is the microscopic limit. The scaling $a = \alpha/\sqrt{n}$ is a small perturbation of the chGOE. One may also choose $a \sim 1$ or $a = \alpha\sqrt{n}$. I will focus on $a = \alpha/\sqrt{n}$ for illustration.

3.6.1 Rewriting Polynomials and Kernels

The three kernels for even $n = 2m$ and rescaling $x = \lambda/\sqrt{n}$, $a = \alpha/\sqrt{n}$ are

$$S^{\nu}_{2m}\left(\frac{x}{\sqrt{n}},\frac{y}{\sqrt{n}}\right) = \sum_{j=0}^{m-1}\int_0^{\infty} dw\, G_{\nu}\left(\frac{y}{\sqrt{n}},w\right)\frac{p^{(\nu)}_{2j}\left(\frac{x}{\sqrt{n}}\right)q^{(\nu)}_{2j}(w)-q^{(\nu)}_{2j}\left(\frac{x}{\sqrt{n}}\right)p^{(\nu)}_{2j}(w)}{h^{(\nu)}_{2j}}\,, \tag{3.113}$$

$$D^{\nu}_{2m}\left(\frac{x}{\sqrt{n}},\frac{y}{\sqrt{n}}\right) = G_{\nu}\left(\frac{x}{\sqrt{n}},\frac{y}{\sqrt{n}}\right)+\sum_{j=0}^{m-1}\int_0^{\infty} dw_1dw_2\, G_{\nu}\left(\frac{x}{\sqrt{n}},w_1\right)G_{\nu}\left(\frac{y}{\sqrt{n}},w_2\right) \times\frac{\bar{q}^{(\nu)}_{2j}(w_1)\bar{p}^{(\nu)}_{2j}(w_2)-\bar{p}^{(\nu)}_{2j}(w_1)\bar{q}^{(\nu)}_{2j}(w_2)}{h^{(\nu)}_{2j}}\,, \tag{3.114}$$

$$I^{\nu}_{2m}\left(\frac{x}{\sqrt{n}},\frac{y}{\sqrt{n}}\right) = \sum_{j=0}^{m-1}\frac{q^{(\nu)}_{2j}\left(\frac{x}{\sqrt{n}}\right)p^{(\nu)}_{2j}\left(\frac{y}{\sqrt{n}}\right)-p^{(\nu)}_{2j}\left(\frac{x}{\sqrt{n}}\right)q^{(\nu)}_{2j}\left(\frac{y}{\sqrt{n}}\right)}{h^{(\nu)}_{2j}}\,. \tag{3.115}$$

The challenge is to keep the convergence. In this sense, $I^{\nu}_{2m}\left(\frac{x}{\sqrt{n}},\frac{y}{\sqrt{n}}\right)$ is the simplest to calculate. In all cases I will write the sum as an integral

$$\lim_{n\to\infty}\frac{2}{n}\sum_{j=0}^{m-1} = \int_0^1 dt\,, \tag{3.116}$$

that is, I look at the integration variable $t = j/n$ for $j, n \to \infty$.

I first do some preliminary work on each polynomial. I wish to simplify the expressions for $p^{(\nu)}_t\left(\frac{x}{\sqrt{n}}\right), q^{(\nu)}_t\left(\frac{x}{\sqrt{n}}\right), q^{(\nu)}_t(w), p^{(\nu)}_t(w)$ for $a = \alpha/\sqrt{n}$ in the limit $n \to \infty$.

Expression for $p^{(\nu)}_t\left(\frac{x}{\sqrt{n}}\right)$

I use the representation (3.59).

$$\begin{aligned} p^{(\nu)}_t\left(\frac{x}{\sqrt{n}}\right) &= \left(\frac{\sqrt{n}}{x}\right)^{\nu}\frac{4}{\pi\sqrt{1-\alpha^4/n^2}}\int_{-\infty}^{\infty}dy_1dy_2\, e^{-\frac{4}{1+\alpha^2/n}{y_1}^2-\frac{4}{1-\alpha^2/n}{y_2}^2} \\ &\quad\times\left(iy_1+y_2+\frac{x}{\sqrt{n}}\right)^{j}\left(iy_1-y_2+\frac{x}{\sqrt{n}}\right)^{j+\nu} \\ &= (-1)^{nt}\left(\frac{\sqrt{n}}{x}\right)^{\nu}\frac{4n^{nt+1}}{\pi\sqrt{1-\alpha^4/n^2}}\int_{-\infty}^{\infty}dy_1dy_2\, e^{-\frac{4n}{1+\alpha^2/n}{y_1}^2-\frac{4n}{1-\alpha^2/n}{y_2}^2} \\ &\quad\times({y_1}^2+{y_2}^2)^{nt}\left(1+\frac{x}{n(iy_1+y_2)}\right)^{nt}\left(1+\frac{x}{n(iy_1-y_2)}\right)^{nt}\left(i\sqrt{n}y_1+\frac{x}{\sqrt{n}}\right)^{\nu} \end{aligned}$$

I have rescaled the integration variables and now use the relation

$$\lim_{n\to\infty}\left(1+\frac{x}{n}\right)^n = e^x\,, \tag{3.117}$$

and change to polar coordinates

$$\begin{aligned} p_t^{(\nu)}\left(\frac{x}{\sqrt{n}}\right) &\overset{n\gg 1}{=} (-1)^{nt}\left(\frac{\sqrt{n}}{x}\right)^{\nu}\frac{4n^{nt+1}}{\pi}\int_{-\infty}^{\infty}dy_1dy_2\,\exp\left\{-4n({y_1}^2+{y_2}^2)+nt\ln\left({y_1}^2+{y_2}^2\right)\right\} \\ &\quad\times\exp\left\{-\frac{2itxy_1}{{y_1}^2+{y_2}^2}\right\}\left(i\sqrt{n}y_1+\frac{x}{\sqrt{n}}\right)^{\nu} \\ &= (-1)^{nt}x^{-\nu}\frac{4n^{nt+1}}{\pi}\int_0^{\infty}dr\,r\int_{-\pi}^{\pi}d\theta\,\exp\left\{-4nr^2+2nt\ln\left(r\right)\right\} \\ &\quad\times\exp\left\{-\frac{2itx\cos(\theta)}{r}\right\}\left(i\sqrt{n}r\cos(\theta)+\frac{x}{\sqrt{n}}\right)^{\nu} \end{aligned} \tag{3.118}$$

I now perform a saddle point approximation for the integral over r. As the leading order will cancel, the higher order terms of the saddle point approximation, see Appendix A.3. Along with the polynomials $q_t^{(\nu)}\left(\frac{x}{\sqrt{n}}\right)$ shown in the following subsection and the constants, these should then be plugged in to (3.114-3.115).

Expression for $q_t^{(\nu)}\left(\frac{x}{\sqrt{n}}\right)$

I again use the Gaussian representation (3.60). First make the same rescaling as before

$$\begin{aligned} q_t^{(\nu)}\left(\frac{x}{\sqrt{n}}\right) &= (-1)^{nt}\left(\frac{\sqrt{n}}{x}\right)^{\nu}\frac{4n^{nt+1}}{\pi\sqrt{1-\alpha^4/n^2}}\int_{-\infty}^{\infty}dy_1dy_2\,e^{-\frac{4n}{1+\alpha^2/n}{y_1}^2-\frac{4n}{1-\alpha^2/n}{y_2}^2} \\ &\quad\times({y_1}^2+{y_2}^2)^{nt}\left(1+\frac{x}{n(iy_1+y_2)}\right)^{nt}\left(1+\frac{x}{n(iy_1-y_2)}\right)^{nt}\left(i\sqrt{n}y_1+\frac{x}{\sqrt{n}}\right)^{\nu} \\ &\quad\times\left[\frac{4x^2}{n}-\frac{(nt+\nu-1)(nt+\nu)}{4n(x/n+iy_1-y_2)^2}-\frac{(nt-1)nt}{4n(x/n+iy_1+y_2)^2}\right. \\ &\quad-\frac{nt(nt+\nu)}{2n(iy_1+y_2+x/n)(iy_1-y_2+x/n)} \\ &\quad\left.-2\frac{\alpha^6/n^3-4n{y_1}^2+4n{y_2}^2-4\alpha^4/n({y_1}^2+{y_2}^2)+\alpha^2(8{y_1}^2+8{y_2}^2-1/n)}{\alpha^4/n^2-1}\right] \\ &\overset{n\gg 1}{=} (-1)^{nt}\left(\frac{\sqrt{n}}{x}\right)^{\nu}\frac{4n^{nt+1}}{\pi}\int_0^{\infty}dr\,r\int_{-\pi}^{\pi}d\theta\,\exp\left\{-4nr^2+2nt\ln\left(r\right)\right\} \\ &\quad\times\exp\left\{-\frac{2itx\cos(\theta)}{r}\right\}\left(i\sqrt{n}r\cos(\theta)+\frac{x}{\sqrt{n}}\right)^{\nu} \\ &\quad\times\left[\frac{4x^2}{n}-\frac{(nt+\nu-1)(nt+\nu)}{4nr^2(i\cos(\theta)-\sin(\theta))^2}-\frac{(nt-1)t}{4r^2(i\cos(\theta)+\sin(\theta))^2}\right. \\ &\quad-\frac{t(nt+\nu)}{2r^2(i\cos(\theta)+\sin(\theta))(i\cos(\theta)-\sin(\theta))} \\ &\quad\left.+2(\alpha^6/n^3+4nr^2(\sin^2(\theta)-\cos^2(\theta))-4\alpha^4r^2/n+\alpha^2(8r^2-1/n))\right] \end{aligned}$$

$$
\begin{aligned}
&= (-1)^{nt}\frac{4n^{nt+1}}{\pi}\int_0^\infty dr\, r\int_{-\pi}^{\pi} d\theta\, \exp\left\{-4nr^2+2nt\ln(r)\right\} \\
&\times \exp\left\{-\frac{2itx\cos(\theta)}{r}\right\}\left(\frac{inr\cos(\theta)}{x}+1\right)^{\nu} \\
&\times\left[\frac{4x^2}{n}+\frac{e^{-2i\theta}(nt+\nu-1)(nt+\nu)}{4nr^2}+\frac{e^{2i\theta}(nt-1)t}{4r^2}+\frac{t(nt+\nu)}{2r^2}\right. \\
&\left.+2(\alpha^6/n^3+4nr^2(\sin^2(\theta)-\cos^2(\theta))-4\alpha^4r^2/n+\alpha^2(8r^2-1/n))\right]\,.
\end{aligned}
\tag{3.119}
$$

Note that the first two lines are the same as $p_t^{(\nu)}\left(\frac{x}{\sqrt{n}}\right)$ and rest do not contribute to the saddle point equation.

Expression for $p_t^{(\nu)}(x)$

The representation (3.54) is used, including the weight and integral. For $\nu=0$

$$
\begin{aligned}
&\int_{-\infty}^{+\infty} dw\, G_0\left(\frac{x}{\sqrt{n}},w\right)\, p_t^{(0)}(w) \\
&= \frac{(j!)^2\pi\alpha^2}{8n}\int_{-\infty}^{+\infty} dw\, e^{-2(x^2/n+w^2)}\,\mathrm{erf}\left[\sqrt{\frac{n}{\alpha^2}-1}(w-x/\sqrt{n})\right]\mathrm{erf}\left[\sqrt{\frac{n}{\alpha^2}-1}(x/\sqrt{n}+w)\right] \\
&\int_0^{2\pi}\frac{d\varphi_L}{2\pi}e^{-ij\varphi_L}\int_0^{2\pi}\frac{d\varphi_R}{2\pi}e^{-ij\varphi_R}\exp\left[-\frac{\alpha^2}{8n}(e^{2i\varphi_L}+e^{2i\varphi_R})-w(e^{i\varphi_L}+e^{i\varphi_R})-\frac{1}{4}e^{i(\varphi_L+\varphi_R)}\right] \\
&\overset{n\gg 1}{=} \frac{(j!)^2\pi\alpha^2}{8n}\int_{-\infty}^{+\infty} dw\, e^{-2(x^2/n+w^2)}\int_0^{2\pi}\frac{d\varphi_L}{2\pi}e^{-ij\varphi_L}\int_0^{2\pi}\frac{d\varphi_R}{2\pi}e^{-ij\varphi_R} \\
&\exp\left[-\frac{\alpha^2}{8n}(e^{2i\varphi_L}+e^{2i\varphi_R})-w(e^{i\varphi_L}+e^{i\varphi_R})-\frac{1}{4}e^{i(\varphi_L+\varphi_R)}\right]
\end{aligned}
\tag{3.120}
$$

First the Gaussian integral over w is performed

$$
\begin{aligned}
&\int_{-\infty}^{+\infty} dw\, G_0\left(\frac{x}{\sqrt{n}},w\right)\, p_t^{(0)}(w) \\
&\overset{n\gg 1}{=} \sqrt{\frac{\pi}{2}}\frac{(j!)^2\pi\alpha^2}{8n}\int_0^{2\pi}\frac{d\varphi_L}{2\pi}e^{-ij\varphi_L}\int_0^{2\pi}\frac{d\varphi_R}{2\pi}e^{-ij\varphi_R}\exp\left[-\frac{\alpha^2}{8n}(e^{2i\varphi_L}+e^{2i\varphi_R})\right] \\
&\times\exp\left[\frac{1}{8}(e^{i\varphi_L}+e^{i\varphi_R})^2-\frac{1}{4}e^{i(\varphi_L+\varphi_R)}\right]\,.
\end{aligned}
\tag{3.121}
$$

Rescale $e^{i\varphi}\to 2i\sqrt{j}e^{i\varphi_{L/R}}$ and perform a saddle-point approximation

$$
\begin{aligned}
&\int_{-\infty}^{+\infty} dw\, G_0\left(\frac{x}{\sqrt{n}},w\right)\, p_t^{(0)}(w) \\
&\overset{n\gg 1}{=} \sqrt{\frac{\pi}{2}}\frac{(j!)^2\pi\alpha^2}{8n(-4j)^j}\int_0^{2\pi}\frac{d\varphi_L}{2\pi}e^{-ij\varphi_L}\int_0^{2\pi}\frac{d\varphi_R}{2\pi}e^{-ij\varphi_R}\exp\left[\frac{\alpha^2 t}{2}(e^{2i\varphi_L}+e^{2i\varphi_R})\right] \\
&\times\exp\left[-\frac{j}{2}(e^{i\varphi_L}+e^{i\varphi_R})^2+je^{i(\varphi_L+\varphi_R)}\right]\,.
\end{aligned}
\tag{3.122}
$$

The saddle-point equations are

$$
0 = ie^{2i\phi_{L/R}}+i\,,
\tag{3.123}
$$

which have the solutions $\{\phi_L = \frac{\pi}{2}, \phi_R = \frac{\pi}{2}\}$, $\{\phi_L = \frac{\pi}{2}, \phi_R = \frac{3\pi}{2}\}$, $\{\phi_L = \frac{3\pi}{2}, \phi_R = \frac{\pi}{2}\}$, and $\{\phi_L = \frac{3\pi}{2}, \phi_R = \frac{3\pi}{2}\}$. Note that these will give the same for even j, so there will be an overall factor of 4.

Expression for $q_t^{(\nu)}(x)$

I again use the contour integral representation (3.56) and include the weight and integral. For $\nu = 0$

$$\begin{aligned}
&\int_{-\infty}^{+\infty} dw\, G_0\left(\frac{x}{\sqrt{n}}, w\right)\, q_t^{(0)}(w) \qquad (3.124)\\
\overset{n\gg 1}{=}\;& \frac{(j!)^2\pi\alpha^2}{8n}\int_{-\infty}^{+\infty} dw\, e^{-2(x^2/n+w^2)}\,\mathrm{erf}\left[\sqrt{\frac{n}{\alpha^2}-1}(w - x/\sqrt{n})\right]\mathrm{erf}\left[\sqrt{\frac{n}{\alpha^2}-1}(x/\sqrt{n}+w)\right]\\
&\int_0^{2\pi}\frac{d\varphi_L}{2\pi}e^{-ij\varphi_L}\int_0^{2\pi}\frac{d\varphi_R}{2\pi}e^{-ij\varphi_R}\exp\left[-\frac{\alpha^2}{8n}(e^{2i\varphi_L}+e^{2i\varphi_R}) - w(e^{i\varphi_L}+e^{i\varphi_R})\right]\\
&\times\exp\left[-\frac{1}{4}e^{i(\varphi_L+\varphi_R)}\right]\left(w^2 - \frac{\alpha^4}{16n^2}(e^{2i\varphi_L}+e^{2i\varphi_R}) - \frac{1}{8}e^{i(\varphi_L+\varphi_R)}\right)\\
\overset{n\gg 1}{=}\;& \frac{(j!)^2\pi\alpha^2}{8n}\int_{-\infty}^{+\infty} dw\, e^{-2(x^2/n+w^2)}\int_0^{2\pi}\frac{d\varphi_L}{2\pi}e^{-ij\varphi_L}\int_0^{2\pi}\frac{d\varphi_R}{2\pi}e^{-ij\varphi_R}\\
&\exp\left[-\frac{\alpha^2}{8n}(e^{2i\varphi_L}+e^{2i\varphi_R}) - w(e^{i\varphi_L}+e^{i\varphi_R}) - \frac{1}{4}e^{i(\varphi_L+\varphi_R)}\right]\left(w^2 - \frac{1}{8}e^{i(\varphi_L+\varphi_R)}\right) \qquad (3.125)
\end{aligned}$$

The Gaussian integral over w is performed

$$\begin{aligned}
&\int_{-\infty}^{+\infty} dw\, G_0\left(\frac{x}{\sqrt{n}}, w\right)\, q_t^{(0)}(w) \qquad (3.126)\\
\overset{n\gg 1}{=}\;& \sqrt{\frac{\pi}{2}}\frac{(j!)^2\pi\alpha^2}{8n}\int_0^{2\pi}\frac{d\varphi_L}{2\pi}e^{-ij\varphi_L}\int_0^{2\pi}\frac{d\varphi_R}{2\pi}e^{-ij\varphi_R}\exp\left[-\frac{\alpha^2}{8n}(e^{2i\varphi_L}+e^{2i\varphi_R})\right]\\
&\times\exp\left[\frac{1}{8}(e^{i\varphi_L}+e^{i\varphi_R})^2 - \frac{1}{4}e^{i(\varphi_L+\varphi_R)}\right]\left(\frac{1}{16}\left(e^{i\phi_L}+e^{i\phi_R}\right)^2 + \frac{1}{4} - \frac{1}{8}e^{i(\varphi_L+\varphi_R)}\right).
\end{aligned}$$

Rescale $e^{i\varphi} \to 2i\sqrt{j}e^{i\varphi_{L/R}}$ and perform a saddle-point approximation

$$\begin{aligned}
&\int_{-\infty}^{+\infty} dw\, G_0\left(\frac{x}{\sqrt{n}}, w\right)\, q_t^{(0)}(w) \qquad (3.127)\\
\overset{n\gg 1}{=}\;& \sqrt{\frac{\pi}{2}}\frac{(j!)^2\pi\alpha^2}{8n(-4j)^j}\int_0^{2\pi}\frac{d\varphi_L}{2\pi}e^{-ij\varphi_L}\int_0^{2\pi}\frac{d\varphi_R}{2\pi}e^{-ij\varphi_R}\exp\left[\frac{\alpha^2 t}{2}(e^{2i\varphi_L}+e^{2i\varphi_R})\right]\\
&\times\exp\left[-\frac{j}{2}(e^{i\varphi_L}+e^{i\varphi_R})^2 + je^{i(\varphi_L+\varphi_R)}\right]\left(\frac{1}{4} - \frac{j}{4}\left(e^{i\phi_L}+e^{i\phi_R}\right)^2 + \frac{j}{2}e^{i(\varphi_L+\varphi_R)}\right).
\end{aligned}$$

The saddle-points are the same as before $\{\phi_L = \frac{\pi}{2}, \phi_R = \frac{\pi}{2}\}$, $\{\phi_L = \frac{\pi}{2}, \phi_R = \frac{3\pi}{2}\}$, $\{\phi_L = \frac{3\pi}{2}, \phi_R = \frac{\pi}{2}\}$, and $\{\phi_L = \frac{3\pi}{2}, \phi_R = \frac{3\pi}{2}\}$.

3.6.2 Expression for Constants $h_t^{(\nu)}$

Finally the limit of constants is calculated. Stirling's approximation yields

$$\begin{aligned} h_t^{(\nu)} &= \frac{\pi\alpha^2(1-\alpha^2/n)^{2nt+2+\nu}}{2^{4nt+2\nu+7}n}(nt)!(nt+\nu)! \\ &\overset{n\gg 1}{=} \frac{2\pi^2\alpha^2 e^{-2t\alpha^2}}{2^{4nt+2\nu+7}}\sqrt{t(nt+\nu)/n}e^{nt\ln(nt)+(nt+\nu)\ln(nt+\nu)-2nt-\nu} \\ &\overset{n\gg 1}{=} \frac{2\pi^2 t\alpha^2 e^{-2t\alpha^2}}{2^{4nt+2\nu+7}}e^{nt\ln(nt)+(nt+\nu)\ln(nt+\nu)-2nt-\nu}\,. \end{aligned} \tag{3.128}$$

This concludes the the list of steps needed to calculate the large-N limit. The different pieces are inserted in (3.113-3.115).

3.7 Conclusion

This chapter has been concerned with the analytical calculation of a parameter-dependent ensemble that transitions between two random matrix models, both with real elements. It connects the chiral Gaussian orthogonal ensemble (chGOE), also called the real Wishart-Laguerre ensemble or Cartan class B|DI, and the Gaussian antisymmetric Hermitian ensemble (GAOE), Cartan class B|D. Noteworthy is that both the ensemble are invariant under the action of subgroups of orthogonal groups, although these are not the same. Because the group integrals are of real type, this would usually constitute a significant problem. In this case, however, the integral is already known and computed by Harish-Chandra.

The case $n = 2m-1$ odd and $\nu = 0$ in the regime $a^2 \propto n$ may help describe topological insulators, especially the disordered system of a quantum wire with two Majorana modes in Section 2.6. The Hamiltonian is antisymmetric and real, and it splits into a direct sum of two identical Hamiltonians with one generic zero eigenvalue each in the unperturbed case. The perturbations in the systems are captured by the off-diagonal matrices. Note that this model has independent diagonal blocks, which makes it analytically viable, but it is likely to capture the important features.

It is also likely that this model will find other applications due to the ubiquity of random matrices, especially the topological protection.

Going forward, note that this is an example of a system where topology is broken by a perturbation, namely the matrix $X/\sqrt{n}$. These systems are investigated further in the following chapter.

Chapter 4

Universal Broadening of Zero Modes in a General Setting

I now consider broadening of zero modes in a more general setting. It has been observed [28, 29, 95, 96, 97] that for specific ensembles, perturbed topological zero modes spread out as a finite size Gaussian ensemble and that the distribution is universal. This is surprising as universality is usually only found in the limit of infinite matrix size, but with several results in this direction and corroboration by lattice simulations [32, 98, 99, 100], it is obvious to investigate the underlying mechanism further. This scaling property was first observed for lattice QCD in [32] and understood within that context in [28, 29]. A similar behaviour was found for outliers above the bulk of the spectrum, see, e.g., the mathematical review [101]. This chapter is based on [KMS].

The main results of this chapter are exactly these two statements. Perturbed zero modes decouple from the rest of the spectrum to first order in perturbation theory, and the modes spread out according to a finite size random matrix ensemble.

As treated in the previous chapter, systems that transition between two symmetry classes may be treated with two-matrix models. In the vicinity of one of the symmetry classes, the other may be viewed as a perturbation. Any properties inherently dependent on the symmetry class (such as zero modes) are very susceptible to such perturbations. This is heuristically speaking the reason a decoupling of the spectra occurs to lowest order. The zero modes feel the perturbation much earlier than the bulk.

In this chapter no assumptions are made about the nature of the zero modes. They may be of topological origin, like antisymmetry or chirality (see Chapter 3), or be given by peculiarities of the unperturbed system. In physical terms, the main assumption is that there is sufficient mixing of the states: The zero modes must be sufficiently delocalised in the eigenbasis of the perturbation. The physical ensemble average is modelled by an average over the Haar measure of the unitary matrix that transition between the eigenbases of the unperturbed system and the perturbation. This could be an average over gauge fields, as in QCD, or an average over disorder in solid state systems. This framework is motivated by the fact that a perturbation that affects topology must be on a global scale. That the former zero modes behave like a Gaussian ensemble is a mechanism similar to the central limit-theorem.

The intuition that the zero modes interacts with a whole ensemble has other applications. It has been pointed out [102] that it is difficult in experiments to distinguish between perturbed topological modes and a simple accumulation of eigenvalues around the origin. In [KMS],

we propose to look at the different scaling behaviour of the eigenvalues with the system size. Accumulated eigenvalues around the origin will be part of the same ensemble as the first excited state, whereas the perturbed zero modes feel a completely separate ensemble. This means that the scaling behaviour of the eigenvalues at the origin will only differ from the first excited state if they are former zero modes.

It is also likely that the limit of large number of zero modes is relevant for analysis of correlation matrices when applying a power map, see [103].

Because the framework in this chapter is more general, I start out on an operator level before presenting the random matrix setup. Consider the model where a Hermitian operator $\hat{A}$ is perturbed by another Hermitian operator $\hat{S}$,

$$\hat{K} \quad = \quad \hat{A} + \alpha \hat{S} \, . \tag{4.1}$$

Of interest is still the spectrum of eigenvalues for $\hat{K}$ after an ensemble average, though note that the spectra of $\hat{A}$ and $\hat{S}$ are not averaged over. The average instead comes from the change of basis between the eigenbases of $\hat{A}$ and $\hat{S}$. The coupling α is chosen small enough for first order perturbation theory to apply.

The approach is as follows. In Section 4.1 I specify what the conditions on α are. I also show how to relate Equation (4.1) to a matrix model. The limit $N \to \infty$ will relate the matrix model back to the operator equation. The decoupling of the spectra and the more precise clarification of the conditions on $\hat{A}$, $\hat{S}$, and α is done in Section 4.2. Section 4.3 is dedicated to calculating the central limit theorem for matrices for all symmetry classes, see Section 2.3. This is then applied to the aforementioned average over the eigenbasis change between $\hat{A}$ and $\hat{S}$. Further analysis of the scaling and applications, along with numerical checks, is done in Section 4.4.

4.1 Estimate of Scales with Perturbation Theory

Consider the general Hermitian operator $\hat{A}$. It may be a Hamiltonian, a Euclidean Dirac operator, or some other quantity. It can be decomposed in its eigenvalues λ_j and its normalised eigenvectors $|\psi_j\rangle$

$$\hat{A} = \sum_j \lambda_j \, |\psi_j\rangle \, \langle \psi_j| \, . \tag{4.2}$$

Zeros as well as degeneracies are included. The operator may also have a continuous spectrum, in which case a UV cut-off is performed and the volume V is sent to infinity afterwards. On a technical level, the dimension N of the Hilbert space is sent to infinity, but the dimension is proportional to the volume of the system $N \propto V$. This relation is known from QCD [28, 29, 95, 96] and is expected to hold in condensed matter systems [97]. Other quantities such as the number of colours and the representation of the gauge group or the size of the spins and the number of particles enter into N as well.

Assume now that A has a fixed number $\nu > 0$ of eigenvalues at the origin. I order them such that $|\lambda_k| > |\lambda_N|$ for all $k > N$ and $|\psi_j\rangle$ for $j = 1, \ldots, \nu$ form an orthonormal basis of the zero mode space. In other words, the first N eigenvalues are also the N smallest. This means that the UV cut-off may be written as

$$\hat{A}^{(N)} \quad = \quad \sum_{j=\nu+1}^{N} \lambda_j \, |\psi_j\rangle \, \langle \psi_j| \, . \tag{4.3}$$

This operator may be represented by a matrix

$$\sum_j \lambda_j \left|\psi_j\right\rangle \left\langle\psi_j\right| \quad \hat{=} \quad \left(\begin{array}{c|c} A' = \mathrm{diag}(\lambda_{\nu+1}, \ldots, \lambda_N) & 0 \\ \hline 0 & 0 \end{array}\right) \tag{4.4}$$

The notation "$\hat{=}$" will be used to indicate representation of the truncated operator $\hat{A}$ as a finite-dimensional matrix. This operator is perturbed by a generic additive Hermitian perturbation $\hat{S}$ which broadens the zero modes of $\hat{A}$

$$\hat{K} \quad = \quad \hat{A} + \alpha\hat{S} = \lim_{N\to\infty} (\hat{A}^{(N)} + \alpha\hat{S}^{(N)}) = \lim_{N\to\infty} \hat{K}^{(N)} \,. \tag{4.5}$$

The coupling constant α is small, and the the perturbation $\hat{S}$ of the form

$$\hat{S}^{(N)} \quad = \quad \sum_{j,k=1}^{N} \left\langle\psi_j\right| \hat{S} \left|\psi_k\right\rangle \left|\psi_j\right\rangle \left\langle\psi_k\right| . \tag{4.6}$$

Note that $|\psi_j\rangle$ are still the eigenstates of $\hat{A}$.

Because I only look at leading order effects of $\hat{S}$ on the zero modes, I work in a perturbative regime. This requires an estimate of the scale of α in terms of $\hat{A}$, $\hat{S}$, and N, as well as how $\hat{S}$ describes a generic perturbation.

I start with an estimate in standard perturbation theory. This does not take into account that the spectra of $\hat{A}$ and $\hat{S}$ may vary over different scales, but gives a sense of the problem. See Section 4.2 for the full estimate.

The first order perturbation of the zero eigenvalues is given by the eigenvalues of the perturbation matrix

$$\hat{K}_1^{(\mathrm{zero})} \quad = \quad \alpha \sum_{j',j=1}^{\nu} \left\langle\psi_j\right| \hat{S} \left|\psi_{j'}\right\rangle \;\; \left|\psi_j\right\rangle \left\langle\psi_{j'}\right| \;, \tag{4.7}$$

where the subscript denotes the order of the perturbation. The first order only dominates if it contributes more than the second order given by the eigenvalues of

$$\hat{K}_2^{(\mathrm{zero})} \quad = \quad -\alpha^2 \sum_{j',j=1}^{\nu} \left(\sum_{k=\nu+1}^{N} \frac{\left\langle\psi_j\right| \hat{S} \left|\psi_k\right\rangle \left\langle\psi_k\right| \hat{S} \left|\psi_{j'}\right\rangle}{\lambda_k} \right) \left|\psi_j\right\rangle \left\langle\psi_{j'}\right| \;. \tag{4.8}$$

They become of the same magnitude when the largest singular value of $\hat{K}_2^{(\mathrm{zero})}$ is of the same order as the smallest singular value of $\hat{K}_1^{(\mathrm{zero})}$.

Note that each matrix entry of $\hat{K}_1^{(\mathrm{zero})}$ can be expressed as a sum

$$\langle\psi_j|\hat{S}|\psi_{j'}\rangle = \sum_{l=1}^{N} s_l \langle\psi_j|\phi_l\rangle\langle\phi_l|\psi_{j'}\rangle. \tag{4.9}$$

The perturbation matrix for the zero modes is the part $j, j' = 1, \ldots, \nu$. The central limit theorem says that for uncorrelated and identically distributed summands, the sum would be Gaussian.

In Section 4.3 I show that this may be extended, and that the entries $\langle\psi_j|\,\hat{S}\,|\psi_{j'}\rangle$ follow a Gaussian distribution on the scale $\sqrt{\mathrm{Tr}\left(\hat{S}^{(N)}\right)^2}/N$ for large N and sufficient mixing between the eigenbases of $\hat{A}$ and $\hat{S}$. The estimates of the first and second order follow from

$$\begin{aligned}\left\|\left(\{\langle\psi_j|\,\hat{S}\,|\psi_{j'}\rangle\}_{j,j'=1,\ldots,\nu}\right)^{-1}\right\|_{\mathrm{op}} &\propto \frac{\sqrt{\mathrm{Tr}\left(\hat{S}^{(N)}\right)^2}}{N}\,,\\ \left\|\left\{\sum_{k=\nu+1}^{N}\frac{\langle\psi_j|\,\hat{S}\,|\psi_k\rangle\,\langle\psi_k|\,\hat{S}\,|\psi_{j'}\rangle}{\lambda_k}\right\}_{j,j'=1,\ldots,\nu}\right\|_{\mathrm{op}} &\leq \frac{\mathrm{Tr}\left(\hat{S}^{(N)}\right)^2}{N^2|\lambda_{\nu+1}|}\,,\end{aligned} \tag{4.10}$$

where $\|\cdot\|_{\mathrm{op}}$ denotes the operator norm, the largest singular value of the operator. This leads to the estimate

$$\frac{1}{N}\frac{\sqrt{\mathrm{Tr}\left(\hat{S}^{(N)}\right)^2}}{|\lambda_{\nu+1}|}\,\alpha \;\ll\; 1 \tag{4.11}$$

for the coupling constant α.

Note that if the non-zero eigenvalues of $\hat{S}$ are of order 1 and the smallest eigenvalue of $\hat{A}$ is of order $1/N$, the estimate becomes $\sqrt{N}\alpha \ll 1$, which is a well-known relation in lattice QCD [28, 29, 95, 96]. For certain ensembles the second order disappears due to symmetry. Consider for instance the complex Wilson ensemble (1.3)

$$K \;=\; \begin{pmatrix} \alpha A & W \\ W^\dagger & \alpha B\end{pmatrix} \tag{4.12}$$

and recall that the eigenvalues come in $\pm$ pairs. This means that denominator of the inner sum in Equation (4.8) comes in $\pm$ pairs as well. That is, there are two eigenvalues k_+, k_-, where $k_+ = -k_-$. So if $\langle\psi_j|\,\hat{S}\,|\psi_k\rangle\,\langle\psi_k|\,\hat{S}\,|\psi_{j'}\rangle$ is the same for these pairs, the summands cancel pairwise. To show this, note that the perturbation commutes with γ_5.

$$\begin{aligned}\langle\psi_j|\,S\,|\psi_{k_+}\rangle\,\langle\psi_{k_+}|\,S\,|\psi_{j'}\rangle &= \langle\psi_j|\,S{\gamma_5}^2\,|\psi_{k_+}\rangle\,\langle\psi_{k_+}|\,S{\gamma_5}^2\,|\psi_{j'}\rangle\\ &= \langle\psi_j|\,\gamma_5 S\gamma_5\,|\psi_{k_+}\rangle\,\langle\psi_{k_+}|\,\gamma_5 S\gamma_5\,|\psi_{j'}\rangle\;.\end{aligned} \tag{4.13}$$

Using $\gamma_5\,|\psi_{k_+}\rangle = |\psi_{k_-}\rangle$, one can write

$$\langle\psi_j|\,S\,|\psi_{k_+}\rangle\,\langle\psi_{k_+}|\,S\,|\psi_{j'}\rangle \;=\; \langle\psi_j|\,\gamma_5 S\,|\psi_{k_-}\rangle\,\langle\psi_{k_-}|\,S\gamma_5\,|\psi_{j'}\rangle\;. \tag{4.14}$$

Note that all zero modes have the same chirality $\gamma_5\,|\psi'_j\rangle = |\psi'_j\rangle$, which means that

$$\langle\psi_j|\,S\,|\psi_{k_+}\rangle\,\langle\psi_{k_+}|\,S\,|\psi_{j'}\rangle \;=\; \langle\psi_j|\,S\,|\psi_{k_-}\rangle\,\langle\psi_{k_-}|\,S\,|\psi_{j'}\rangle\;. \tag{4.15}$$

In this case the first order has to be compared to even higher orders. The discussion in Section 4.3 is unaffected by whether or not the second order perturbation theory disappears.

It should be noted that this approach does not take into account that $\hat{A}$ and $\hat{S}$ may have several parts of their spectra that scale differently. The smallest non-zero eigenvalue of $\hat{A}^{(N)}$ is usually of the order $1/N$, see [10, 16, 23, 25, 24, 22, 26, 69, 70]. The largest eigenvalue of $\hat{S}$ can even exceed the one of $\hat{A}$ as is the case for the Wilson-Dirac operator [27]. If that is the case, α can never be perturbative for the whole spectra but only for a certain subspectrum like the zero modes. The scale where perturbation theory applies is set by Equation (4.10).

4.2 Conditions on Operators and Decoupling

A crucial quantity to consider is the number of eigenvalues $\hat{S}^{(N)}$ that are of the same order as its maximal singular value $\sigma_{\max}^{(N)} = \left\|\hat{S}^{(N)}\right\|_{\mathrm{op}}$ when N goes to infinity. This may be estimated by the ratio between the l^2-norm and the operator norm

$$q^{(N)} = \frac{\sqrt{\mathrm{Tr}\left(\hat{S}^{(N)}\right)^2}}{\left\|\hat{S}^{(N)}\right\|_{\mathrm{op}}} \in [1, \sqrt{N}] \,. \tag{4.16}$$

This is akin to a participation ratio for eigenvalues. With this, the following conditions may be introduced

$$\mathrm{Tr}\,\hat{S}^{(N)} = 0, \tag{4.17}$$

$$\lim_{N\to\infty} q^{(N)} = \infty, \tag{4.18}$$

$$\alpha = o\left(\frac{1}{\left\|\hat{S}^{(N)}\right\|_{\mathrm{op}}}\sqrt{\frac{N}{\mathrm{Tr}(A')^{-2}}}\right) \,. \tag{4.19}$$

The first condition is not mandatory, but makes the notation below simpler. Shifting the spectrum by $\hat{S}^{(N)} - (\mathrm{Tr}\,\hat{S}^{(N)}/N)\mathbb{1}_N \to \hat{S}^{(N)}$ gives 4.17, if it is not already fulfilled. It also helps avoid the completely degenerate case $\hat{S} \propto \mathbb{1}$, where the Gaussian broadening collapses to a δ-function because the spectrum is only shifted. This also means that the results hold for any exact mode in a spectral gap. (That is, it does not have to be at the origin.)

I will indicate below in Section 4.3 where Condition (4.18) is used on a technical level. On a physical level, it ensures that there are enough eigenvalues inducing the self-average through the relative change of eigenbasis between $\hat{A}$ and $\hat{S}$ for the Matrix Central Limit Theorem to be valid. In other words, there is sufficient delocalisation. Since $q^{(N)}$ is scale-invariant, this condition does not say anything about the strength of the perturbation. This is instead captured by Condition (4.19). It gives a harder bound than Inequality (4.11)

$$\frac{N}{\|(A')^{-1}\|_{\mathrm{op}}\sqrt{\mathrm{Tr}\left(\hat{S}^{(N)}\right)^2}} \geq \frac{N}{q^{(N)}\sqrt{\mathrm{Tr}(A')^{-2}}\left\|\hat{S}^{(N)}\right\|_{\mathrm{op}}} \geq \frac{\sqrt{N}}{\sqrt{\mathrm{Tr}(A')^{-2}}\left\|\hat{S}^{(N)}\right\|_{\mathrm{op}}} \,, \tag{4.20}$$

and is necessary to truncate the series after the first term in Section 4.2.1. It ensures that the former zero modes are unperturbed by the spectrum of A'. (That is, they reside in a spectral gap.)

4.2.1 Decoupling of Eigenvalue Equation

In this section I show how the spectrum of the perturbed eigenvalues decouples from the bulk of the operator. As before I work in the eigenbasis of the truncated Hermitian operator $\hat{A}^{(N)}$. The transformation between the eigenbases of $\hat{A}^{(N)}$ and $\hat{S}^{(N)}$ is unitary and denoted by U. That is, diagonalising $\hat{S}^{(N)} = \sum_{l=1}^{N} s_l|\phi_l\rangle\langle\phi_l|$, one may write $U = \{\langle\psi_j|\phi_l\rangle\}_{j,l=1,\ldots,N}$. The matrices U will be drawn from the Stiefel manifold corresponding to the considered symmetry

class, see Table 2.2. To motivate this form of the average, note that almost regardless what the eigenvalues s_l are, the coefficients $\langle\psi_j|\phi_l\rangle\langle\phi_l|\psi_{j'}\rangle$ behave in a generic case like random variables. "Generic" here means that these statements hold when averaging over the eigenvectors. In this basis $\hat{S}^{(N)}$ takes the block form

$$US^{(N)}U^\dagger \;=\; \left(\begin{array}{c|c} S_1 & S_2 \\ \hline S_2^\dagger & S_3 \end{array}\right) . \tag{4.21}$$

Here and in the rest of the analysis I represent the operators as $N \times N$ matrices $\hat{S}^{(N)} \hat{=} S^{(N)}$. The unitary matrix $U_{i,k} = \langle\psi_i|\phi_k\rangle$ which changes from the eigenbasis of $S^{(N)}$ to $A^{(N)}$ is written out explicitly, that is,

$$[US^{(N)}U^\dagger]_{i,j} = U_{i,k}S^{(N)}_{k,k'}[U^\dagger]_{k',j} = \langle\psi_i|\phi_k\rangle\langle\phi_k|\Big(\sum_{l=1}^{N} s_l|\phi_l\rangle\langle\phi_l|\Big)|\phi_{k'}\rangle\langle\phi_{k'}|\psi_j\rangle \;, \tag{4.22}$$

where k and k' are summed over and the zero modes are associated with S_3. It is also useful to introduce a corresponding structure for U. The part associate with the zero modes is U_2, i.e., $[U]_{l,k} = [U_2]_{l,k} = \langle\psi_l|\phi_k\rangle$, where $l = N-\nu+1,\ldots,N$. Similarly, U_1 denotes the rest of U, i.e., $[U]_{m,k} = [U_1]_{m,k} = \langle\psi_m|\phi_k\rangle$, where $m = 1,\ldots,N-\nu$. Note that I do not require all of U to be Haar-distributed, but only U_2.

Consider now the secular equation of the whole system $K^{(N)} = A^{(N)} + \alpha US^{(N)}U^\dagger$

$$\det\Big(K^{(N)} - \lambda\mathbb{1}_N\Big) \;=\; 0 \,. \tag{4.23}$$

This may be written out in terms of the block structure (4.21)

$$\begin{aligned}
\det\Big(K^{(N)} - \lambda\mathbb{1}_N\Big) \;&=\; \det\left(\begin{array}{c|c} A' + \alpha S_1 - \lambda\mathbb{1}_{N-\nu} & \alpha S_2 \\ \hline \alpha S_2^\dagger & \alpha S_3 - \lambda\mathbb{1}_\nu \end{array}\right) \qquad (4.24)\\
&=\; \det\big(A' - \lambda\mathbb{1}_{N-\nu}\big)\,\det\left(\begin{array}{c|c} \mathbb{1}_{N-\nu} + \alpha(A'-\lambda\mathbb{1}_{N-\nu})^{-1}S_1 & \alpha(A'-\lambda\mathbb{1}_{N-\nu})^{-1}S_2 \\ \hline \alpha S_2^\dagger & \alpha S_3 - \lambda\mathbb{1}_\nu \end{array}\right) .\\
&=\; \det\left(A' - \lambda\mathbb{1}_{N-\nu}\right)\det\left(\mathbb{1}_{N-\nu} + \alpha(A'-\lambda\mathbb{1}_{N-\nu})^{-1}U_1SU_1^\dagger\right)\\
&\quad\times\det\Big[\alpha U_2SU_2^\dagger - \lambda\mathbb{1}_\nu - \alpha U_2SU_1^\dagger\left(\mathbb{1}_{N-\nu} + \alpha\left(A'-\lambda\mathbb{1}_{N-\nu}\right)^{-1}U_1SU_1^\dagger\right)^{-1}\\
&\quad\times\alpha\left(A'-\lambda\mathbb{1}_{N-\nu}\right)^{-1}U_1SU_2^\dagger\Big]
\end{aligned}$$

In the second line the factor $(A' - \lambda\mathbb{1}_{N-\nu})$ has been pulled out in the first $N-\nu$ rows of the determinant. Then the second determinant has been expanded, and $S_{1,2,3}$ have been written out explicitly. The inverse matrix may be written as a Neumann series

$$\left(\mathbb{1}_{N-\nu} + \alpha\left(A'-\lambda\mathbb{1}_{N-\nu}\right)^{-1}U_1SU_1^\dagger\right)^{-1} \;=\; \sum_{j=0}^{\infty}(-\alpha)^j\left[\left(A'-\lambda\mathbb{1}_{N-\nu}\right)^{-1}U_1SU_1^\dagger\right]^j .$$

This is used to rewrite the terms in that determinant and identifying a new Neumann series

$$\begin{aligned} & \alpha U_2 S \left(\mathbb{1}_{N-\nu} - \alpha U_1^\dagger \left(\mathbb{1}_{N-\nu} + \alpha \left(A' - \lambda \mathbb{1}_{N-\nu} \right)^{-1} U_1 S U_1^\dagger \right)^{-1} \left(A' - \lambda \mathbb{1}_{N-\nu} \right)^{-1} U_1 S \right) U_2^\dagger \\ = \; & \alpha U_2 S \left(\mathbb{1}_{N-\nu} + \sum_{j=1}^{\infty} (-\alpha)^j \left[U_1^\dagger \left(A' - \lambda \mathbb{1}_{N-\nu} \right)^{-1} U_1 S \right]^j \right) U_2^\dagger \\ = \; & \alpha U_2 S \left[\mathbb{1}_{N-\nu} + \alpha U_1^\dagger \left(A' - \lambda \mathbb{1}_{N-\nu} \right)^{-1} U_1 S \right]^{-1} U_2^\dagger \, . \end{aligned}$$

Inserting this result in Equation (4.24), one finds

$$\begin{aligned} \det\Big(K^{(N)} - \lambda \mathbb{1}_N \Big) \; = \; & \det\left(A' - \lambda \mathbb{1}_{N-\nu} \right) \det\Big(\mathbb{1}_N + \alpha S^{(N)} U_1^\dagger (A' - \lambda \mathbb{1}_{N-\nu})^{-1} U_1 \Big) \\ & \times \det\Big(\alpha U_2 [\mathbb{1}_N + \alpha S^{(N)} U_1^\dagger (A' - \lambda \mathbb{1}_{N-\nu})^{-1} U_1]^{-1} S^{(N)} U_2^\dagger - \lambda \mathbb{1}_\nu \Big) \, . \end{aligned} \tag{4.25}$$

So far this is an exact rewriting, but here the bounds on α become relevant. Two mechanisms come into play at the same time.

First of all the smallest eigenvalues of A' must not be allowed to interact with the spectrum of the zero modes. This is achieved if the smallest singular value of A', which is $\frac{1}{\|(A')^{-1}\|_{\mathrm{op}}}$, is much bigger than the largest singular value of $\alpha U_2 [\mathbb{1}_N + \alpha S^{(N)} U_1^\dagger (A')^{-1} U_1]^{-1} S U_2^\dagger$. This means that $A' - \lambda \mathbb{1}_{N-\nu} \approx A'$ for the λ of interest. This leaves

$$\begin{aligned} \det\Big(K^{(N)} - \lambda \mathbb{1}_N \Big) \; \overset{\lambda \text{ former zero mode}}{\approx} \; & \det\left(A' \right) \det\Big(\mathbb{1}_N + \alpha S^{(N)} U_1^\dagger (A')^{-1} U_1 \Big) \\ & \times \det\Big(\alpha U_2 [\mathbb{1}_N + \alpha S^{(N)} U_1^\dagger (A')^{-1} U_1]^{-1} S^{(N)} U_2^\dagger - \lambda \mathbb{1}_\nu \Big) \, . \end{aligned} \tag{4.26}$$

Simultaneously, one has to make sure that $\alpha U_2 [\mathbb{1}_N + \alpha S^{(N)} U_1^\dagger (A')^{-1} U_1]^{-1} S^{(N)} U_2^\dagger$ is under control to justify dropping $\lambda \mathbb{1}_{N-\nu}$. The goal is to be left with only $S_3 - \lambda \mathbb{1}_\nu$ in the final determinant, so showing that on average $\mathbb{1}_N + \alpha S^{(N)} U_1^\dagger (A')^{-1} U_1 \approx \mathbb{1}_N$ is left. Choose an arbitrary vector $|\chi\rangle \in \mathbf{C}^N$. Then the square norm of $\alpha U_1^\dagger (A')^{-1} U_1 S^{(N)} |\chi\rangle$ is on average

$$\begin{aligned} \int_{\mathcal{K}} d\mu(U) \alpha^2 \langle \chi | S^{(N)} U_1^\dagger (A')^{-2} U_1 S^{(N)} | \chi \rangle \; &= \; \frac{\alpha^2 \operatorname{Tr}(A')^{-2}}{N} \langle \chi | (S^{(N)})^2 | \chi \rangle \\ &\leq \; \frac{\alpha^2 \operatorname{Tr}(A')^{-2} \left\| S^{(N)} \right\|_{\mathrm{op}}^2}{N} \ll 1 \, . \end{aligned}$$

Each of the groups $\mathcal{K}$ comprises the symmetric group of permutations, which leads to the first equality. (Note the invariance of the matrices $(A')^{-2}$ and $S^{(N)}$, which gives this structure. The constant comes from considering $(A')^{-2} = \mathbb{1}$.) Note that this gives the condition (4.19) and means that $\alpha S^{(N)} U_1^\dagger (A')^{-1} U_1$ may be disregarded in comparison to $\mathbb{1}_N$.

The decoupling

$$\det\Big(K^{(N)} - \lambda \mathbb{1}_N \Big) \; \overset{\lambda \text{ former zero mode}}{\approx} \; \det\left(A' \right) \det\Big(\alpha U_2 S^{(N)} U_2^\dagger - \lambda \mathbb{1}_\nu \Big) \tag{4.27}$$

is found, which is the main result of this section.

The symmetry classes of $\hat{A}$ and $\hat{S}$ are still open and will be discussed in the following section. (See also Section 2.3.) This means that the group $\mathcal{K}$ from where the unitary matrix U are drawn via the corresponding Haar measure has not been chosen either, see Table 2.2.

4.3 Central Limit Theorem for Matrices

As described above, the ensemble average is an average over the part of the transformation between the eigenbases of $\hat{A}$ and $\hat{S}$ associated with the zero modes. In this section I show the extension of the central limit theorem for large N, where the perturbation matrix for the zero modes becomes independent of the exact values of the eigenvalues s_l of $\hat{S}$. This requires the inverse participation ratio $\sum_{l=1}^{N} |\langle\psi_j|\phi_l\rangle|^4$ to be sufficiently small for $j = 1, \ldots, \nu$. I show that all matrix entries with $j, j' = 1, \ldots, \nu$ become Gaussian independent up to some symmetry relations due to the sum

$$\langle\psi_j|\hat{S}|\psi_{j'}\rangle = \sum_{l=1}^{N} s_l \langle\psi_j|\phi_l\rangle\langle\phi_l|\psi_{j'}\rangle. \tag{4.28}$$

That is, I show that this sum and therefore also the matrix entries are Gaussian. It means that the eigenvalues obey a $\nu \times \nu$ Gaussian RMT.

I ignore the overall factor α as the perturbative expansion of the zero modes has already taken place and simply focus on the distribution of the matrix $S_3 = U_2 S^{(N)} U_2^\dagger$ of finite size $\nu \times \nu$ is when N becomes large. The non-chiral, the classical chiral, and the Bogoliubov–de Gennes classes will be treated separately in Subsections 4.3.1, 4.3.2, and 4.3.3. In all cases a Gaussian distribution is found for S_3 under the conditions (4.17-4.19) and U_2 Haar distributed. Results from effective field theory [96, 97] suggest that the following statements also hold in a more general setting such as a deformed or truncated Haar measure.

4.3.1 Gaussian Limit for Non-Chiral S_3

Let the distribution of $S' = \kappa S_3$, with $\kappa = N/\sqrt{\mathrm{Tr}\big(S^{(N)}\big)^2}$, be defined via a Dirac δ-function,

$$p(S') \;=\; \int_{\mathcal{K}_\nu} d\mu(U_2)\, \delta\left(S' - \kappa U_2 S^{(N)} U_2^\dagger\right), \tag{4.29}$$

where $d\mu(U_2)$ is the normalised Haar measure of the Stiefel manifold $\mathcal{K}_\nu$. (See the first five rows of Tables 2.1, 2.2, and 2.3.) The scaling is contained explicitly in κ to simplify later calculations. The Haar measure may also be represented as a Dirac measure on the larger set $\mathcal{G}_\nu$,

$$\int_{\mathcal{K}_\nu} d\mu(U_2) f(U_2) = \frac{\int_{\mathcal{G}_\nu} dU_2 f(U_2) \delta(\mathbb{1}_\nu - U_2 U_2^\dagger)}{\int_{\mathcal{G}_\nu} dU_2 \delta(\mathbb{1}_\nu - U_2 U_2^\dagger)}. \tag{4.30}$$

with an arbitrary integrable function f. Both Dirac δ-functions can be expressed as Gaussian integrals over the symmetric spaces $\mathcal{H}_\nu$ for Equation (4.29) and $\mathcal{P}_\nu$ for Equation (4.30), see Tables 2.2 and 2.3.

The starting point is therefore the expression

$$\begin{aligned} p(S') \;&=\; \lim_{\epsilon\to 0} \frac{\int_{\mathcal{G}_\nu} dU_2 \int_{\mathcal{P}_\nu} dP\, f_\epsilon(U_2, S') \exp\Big[\epsilon\gamma N \,\mathrm{Tr}(\mathbb{1}_\nu - iP)^2 + \gamma N \,\mathrm{Tr}\Big(\mathbb{1}_\nu - U_2 U_2^\dagger\Big)(\mathbb{1}_\nu - iP)\Big]}{\int_{\mathcal{G}_\nu} dU_2 \int_{\mathcal{P}_\nu} dP \exp\Big[\epsilon\gamma N \,\mathrm{Tr}(\mathbb{1}_\nu - iP)^2 + \gamma N \,\mathrm{Tr}\Big(\mathbb{1}_\nu - U_2 U_2^\dagger\Big)(\mathbb{1}_\nu - iP)\Big]}, \\ f_\epsilon(U_2, S') \;&=\; \frac{\int_{\mathcal{H}_\nu} dH \exp\Big[-\epsilon \,\mathrm{Tr}\, H^2 + i \,\mathrm{Tr}\Big(S' - \kappa U_2 S^{(N)} U_2^\dagger\Big) H\Big]}{\int_{\mathcal{H}_\nu} d\bar{S} \int_{\mathcal{H}_\nu} dH \exp\big[-\mathrm{Tr}\, H^2 - \mathrm{Tr}\, \bar{S}^2/4\big]}. \end{aligned} \tag{4.31}$$

The shift in P guarantees that the integral over U_2 is absolutely integrable and the denominators normalise the integrals properly. The factor γN in the P-dependent part of the exponent is introduced to simplify the saddle point approximation later. The parameter γ depends on the symmetry class and can be found in Table 2.3. It is essentially the exponent of the determinant when performing a multivariate Gaussian integral.

The absolute integrability of the integrals means they can be interchanged. The now $\nu \times N$ Gaussian integral over U_2 can be performed, which gives a determinant with the exponent γ

$$\begin{aligned} p(S') &= \lim_{\epsilon\to 0} \frac{\int_{\mathcal{P}_\nu} dP \widetilde{f}_\epsilon(P,S') \exp\Big[\epsilon\gamma N \operatorname{Tr}(\mathbb{1}_\nu - iP)^2 + \gamma N \operatorname{Tr}(\mathbb{1}_\nu - iP)\Big]}{\int_{\mathcal{P}_\nu} dP \exp\Big[\epsilon\gamma N \operatorname{Tr}(\mathbb{1}_\nu - iP)^2 + \gamma N \operatorname{Tr}(\mathbb{1}_\nu - iP)\Big] \det{}^{-\gamma N}[\gamma N(\mathbb{1}_\nu - iP)]}\,, \\ \widetilde{f}_\epsilon(P,S') &= \frac{\int_{\mathcal{H}_\nu} dH \exp\big[-\epsilon \operatorname{Tr} H^2 + i \operatorname{Tr} S'H\big] \det{}^{-\gamma}[\gamma N \mathbb{1}_N \otimes (\mathbb{1}_\nu - iP) + i\kappa S^{(N)} \otimes H]}{\int_{\mathcal{H}_\nu} d\bar{S} \int_{\mathcal{H}_\nu} dH \exp\big[-\operatorname{Tr} H^2 - \operatorname{Tr} \bar{S}^2/4\big]}\,. \end{aligned} \tag{4.32}$$

The determinant also guaranties convergence for the integral over P in the limit $\epsilon \to 0$ if N is large enough. The integral over H still needs regularisation. The saddle point is therefore performed on this slightly rewritten version

$$\begin{aligned} p(S') &= \frac{\int_{\mathcal{P}_\nu} dP g(P,S') \exp[-i\gamma N \operatorname{Tr} P] \det{}^{-\gamma N}[\mathbb{1}_\nu - iP]}{\int_{\mathcal{P}_\nu} dP \exp[-i\gamma N \operatorname{Tr} P] \det{}^{-\gamma N}[\mathbb{1}_\nu - iP]}\,, \\ g(P,S') &= \lim_{\epsilon\to 0} \frac{\int_{\mathcal{H}_\nu} dH \exp\big[-\epsilon \operatorname{Tr} H^2 + i \operatorname{Tr} S'H\big]}{\int_{\mathcal{H}_\nu} d\bar{S} \int_{\mathcal{H}_\nu} dH \exp\big[-\operatorname{Tr} H^2 - \operatorname{Tr} \bar{S}^2/4\big]} \\ &\quad \times \det{}^{-\gamma}[\mathbb{1}_{N\nu} + i\gamma^{-1} S^{(N)} / \sqrt{\operatorname{Tr}\big(S^{(N)}\big)^2} \otimes H(\mathbb{1}_\nu - iP)^{-1}]\,, \end{aligned} \tag{4.33}$$

where κ has been written out, and the rescaling $P \to P/\sqrt{\gamma N}$ is done. This implies that the P-integrand becomes the Gaussian $\exp\big[-\operatorname{Tr} P^2/2\big]$ via a Taylor expansion. Integration yields

$$\begin{aligned} \lim_{N\to\infty} p(S') &= \lim_{N\to\infty} \lim_{\epsilon\to 0} \frac{\int_{\mathcal{H}_\nu} dH \exp\big[-\epsilon \operatorname{Tr} H^2 + i \operatorname{Tr} S'H\big]}{\int_{\mathcal{H}_\nu} d\bar{S} \int_{\mathcal{H}_\nu} dH \exp\big[-\operatorname{Tr} H^2 - \operatorname{Tr} \bar{S}^2/4\big]} \\ &\quad \times \det{}^{-\gamma}[\mathbb{1}_{N\nu} + i\gamma^{-1} S^{(N)} / \sqrt{\operatorname{Tr}\big(S^{(N)}\big)^2} \otimes H]\,. \end{aligned} \tag{4.34}$$

The limit of the integral over H is done with an expansion of the determinant which is

$$\ln \det{}^{-\gamma}\left[\mathbb{1}_{N\nu} + i\frac{S^{(N)}}{\gamma\sqrt{\operatorname{Tr}\big(S^{(N)}\big)^2}} \otimes H\right] = \gamma \sum_{j=1}^{\infty} \frac{1}{j} \operatorname{Tr}\left(-i\frac{S^{(N)}}{\gamma\sqrt{\operatorname{Tr}\big(S^{(N)}\big)^2}}\right)^j \operatorname{Tr} H^j\,. \tag{4.35}$$

The first term ($j = 1$) vanishes because of Condition (4.17) and the coefficient for $j = 2$ becomes $-1/(2\gamma)$. The other terms for $j > 2$ can be estimated as follows

$$\left|\frac{\operatorname{Tr}\big(S^{(N)}\big)^j}{(\operatorname{Tr}\big(S^{(N)}\big)^2)^{j/2}}\right| \leq \frac{\big\|S^{(N)}\big\|_{\mathrm{op}}^{j-2} \operatorname{Tr}\big(S^{(N)}\big)^2}{(\operatorname{Tr}\big(S^{(N)}\big)^2)^{j/2}} = \frac{1}{(q^{(N)})^{j-2}} \overset{N\to\infty}{\to} 0\,. \tag{4.36}$$

The limit follows from (4.18). The determinant can therefore be approximated by a Gaussian and ϵ may be set to 0. The integral over H may now be calculated

$$\lim_{N\to\infty} p(S') = \frac{\int_{\mathcal{H}_\nu} dH \exp\left[-\operatorname{Tr} H^2/(2\gamma) + i \operatorname{Tr} S'H\right]}{\int_{\mathcal{H}_\nu} d\bar{S} \int_{\mathcal{H}_\nu} dH \exp\left[-\operatorname{Tr} H^2 - \operatorname{Tr} \bar{S}^2/4\right]} = \frac{\exp\left[-\gamma \operatorname{Tr} S'^2/2\right]}{\int_{\mathcal{H}_\nu} d\bar{S} \exp\left[-\gamma \operatorname{Tr} \bar{S}^2/2\right]} \quad (4.37)$$

This means that the former zero eigenvalues are broadened by the matrix αS_3 which is distributed like a Gaussian random matrix with standard deviation $\alpha\sqrt{\operatorname{Tr}\left(S^{(N)}\right)^2/(\gamma N^2)}$ for large N, which is the main result of the section.

4.3.2 Gaussian Limit of S_3 for one of the three Standard Chiral Classes

For the three classical chiral ensembles, can be dealt with in a similar way. The normalised Haar measure of $\mathcal{K}_\nu$ is again replaced by a Gaussian integral over $\mathcal{G}_\nu$ and $\mathcal{P}_\nu$ and the Dirac δ-function in S' by a Gaussian integral on $\mathcal{H}_\nu$. Equation (4.31) therefore still holds, but with the respective spaces, see the sixth to eighth row of the Table 2.2. The structure of the matrices is different for the chiral matrices. The matrix $\gamma N(\mathbb{1}_N - iP) = \operatorname{diag}(\gamma(n+\nu)(\mathbb{1}_{n'+\nu'} - iP_1), \gamma n(\mathbb{1}_{n'} - iP_2))$ is block diagonal, one block is of size $(n'+\nu') \times (n'+\nu')$ and the other of size $n' \times n'$, and the matrices

$$S^{(N)} = \begin{pmatrix} 0 & W \\ W^\dagger & 0 \end{pmatrix} \text{ as well as } H = \begin{pmatrix} 0 & X \\ X^\dagger & 0 \end{pmatrix} \quad (4.38)$$

consist of off-diagonal blocks of size $(n+\nu) \times n$ and $n \times (n+\nu)$ as well as $(n'+\nu') \times n'$ and $n' \times (n'+\nu')$, respectively. The dimensions satisfy $n'+\nu' \le n+\nu$, $n' \le n$, $2n+\nu = N$, and $2n'+\nu' = \nu$, and ν' denotes the number of non-broadened zero modes. The two blocks of $\gamma N(\mathbb{1}_N - iP)$ are weighted differently to simplify the saddle point later. The integral over $U_2 = \operatorname{diag}(\widetilde{V}_1, \widetilde{V}_2)$ may now be performed, which leads to the counterpart of Equation (4.32) with the appropriate matrix spaces and the exponent γ as given in Table 2.3. The following identity is also needed

$$\begin{aligned} &\int_{\mathcal{G}_\nu} d(\widetilde{V}_1, \widetilde{V}_2) \exp\Big[-\gamma(n+\nu) \operatorname{Tr} \widetilde{V}_1^\dagger (\mathbb{1}_{n'+\nu'} - iP_1)\widetilde{V}_1 - \gamma n \operatorname{Tr} \widetilde{V}_2^\dagger (\mathbb{1}_{n'} - iP_2)\widetilde{V}_2 \\ &-i\kappa \operatorname{Tr} \widetilde{V}_1^\dagger X \widetilde{V}_2 W^\dagger - i\kappa \operatorname{Tr} \widetilde{V}_2^\dagger X^\dagger \widetilde{V}_1 W \Big] \\ \propto\ &\det{}^{-\gamma} \begin{bmatrix} \gamma(n+\nu)\mathbb{1}_{n+\nu} \otimes (\mathbb{1}_{n'+\nu'} - iP_1) & i\kappa W \otimes X \\ i\kappa W^\dagger \otimes X^\dagger & \gamma n \mathbb{1}_n \otimes (\mathbb{1}_{n'} - iP_2) \end{bmatrix}. \end{aligned} \quad (4.39)$$

To get the statistics of the cut-out S_3 I assume that the projection is symmetry-preserving, which means that S and S_3 share the same symmetry class though they are of different dimensions, see Table 2.1. Therefore the matrix S_3 is chiral as well,

$$S_3 \mathrel{\hat{=}} \begin{pmatrix} 0 & W_3 \\ W_3^\dagger & 0 \end{pmatrix} \quad (4.40)$$

where W_3 is $(n'+\nu') \times n'$ dimensional. The notation "$\hat{=}$" here has the additional meaning that there is a unitary matrix for the ensemble from which $S^{(N)}$ is drawn that allows it to be written in this form. The matrix $U = \operatorname{diag}(V_1, V_2)$ can be chosen in a block diagonal form with $(V_1, V_2) \in \mathcal{K} = \mathrm{O}(n+\nu) \times \mathrm{O}(n), \mathrm{U}(n+\nu) \times \mathrm{U}(n), \mathrm{USp}(n+\nu) \times \mathrm{USp}(n)$.

The rest of the derivation is very similar to the non-chiral case. First the limit $\epsilon \to 0$ is taken in the P-integral because convergence is given by the determinant. The limit $N \to \infty$ implies that $(n+\nu)/N$ and n/N are fixed, since the number of zero modes is fixed. After rescaling $P_1 \to P_1/\sqrt{\gamma(n+\nu)}$ and $P_2 \to P_2/\sqrt{\gamma n}$, the P-integral can be done. The remaining determinant is expanded

$$\begin{aligned} & \det{}^{-\gamma}\left[\mathbb{1}_{N\nu} + \begin{pmatrix} 0 & i\frac{\kappa}{\gamma\sqrt{(n+\nu)n}} W \otimes X \\ i\frac{\kappa}{\gamma\sqrt{(n+\nu)n}} W^\dagger \otimes X^\dagger & 0 \end{pmatrix}\right] \\ = \;& \gamma \sum_{j=1}^{\infty} \frac{1}{j} \operatorname{Tr}\left(-\frac{N^2}{\gamma^2(n+\nu)n \operatorname{Tr}\left(S^{(N)}\right)^2} WW^\dagger\right)^j \operatorname{Tr}\left(XX^\dagger\right)^j . \end{aligned} \tag{4.41}$$

Using $2\operatorname{Tr}\left(WW^\dagger\right)^j = \operatorname{Tr}\left(S^{(N)}\right)^{2j}$, the same estimate as in Equation (4.36) can be made leaving only $j = 2$. The leftover Gaussian integral over H is done, which yields

$$\lim_{N\to\infty} p(S') \;=\; \frac{\exp\left[-\gamma(n+\nu)n \operatorname{Tr}\{S'\}^2/N^2\right]}{\int_{\mathcal{H}_\nu} d\bar{S} \exp\left[-\gamma(n+\nu)n \operatorname{Tr} \bar{S}^2/N^2\right]} . \tag{4.42}$$

This shows that the matrix αS_3 again is distributed according to a Gaussian random matrix with standard deviation $\alpha\sqrt{\operatorname{Tr}\left(S^{(N)}\right)^2/(2\gamma(n+\nu)n)}$.

4.3.3 Gaussian Limit for the Boguliubov–de Gennes types of S_3

The two Boguliubov–de Gennes cases are again very similar to the other three chiral classes except that for $U_2 = \operatorname{diag}(\widetilde{V}_1, \widetilde{V}_2)$ there is the additional condition $\widetilde{V}_2 = \widetilde{V}_1^*$. Therefore the matrix P has the diagonal block form $P = \operatorname{diag}(\widetilde{P}, \widetilde{P}^*)$ with $\widetilde{P} \in \operatorname{Herm}(\nu/2)$. The matrices $S^{(N)}$ and H have the chiral forms (4.38) with the additional conditions $W^T = \pm W$ and $X^T = \pm X$, both relations with the same sign. Start with Equation (4.31) and the corresponding matrix spaces (the last two rows of Tables 2.1, 2.2, and 2.3), replace N by $N/2$, and set $\gamma = 1/2$ in the exponential functions. The counterpart of Equation (4.39) is

$$\begin{aligned} & \int_{\mathcal{G}_\nu} d\widetilde{V}_1 \exp\left[-N \operatorname{Tr} \widetilde{V}_1^\dagger(\mathbb{1}_{\nu/2} - i\widetilde{P})\widetilde{V}_1/2 - i\kappa \operatorname{Tr} \widetilde{V}_1^\dagger X \widetilde{V}_1^* W^\dagger - i\kappa \operatorname{Tr} \widetilde{V}_1^T X^\dagger \widetilde{V}_1 W\right] \\ \propto \;& \det{}^{-1/2}\left[\frac{N}{2}\mathbb{1}_2 \otimes \mathbb{1}_{N/2} \otimes (\mathbb{1}_{\nu/2} - i\widetilde{P}) + i\kappa(\tau_3 - i\tau_1) \otimes X \otimes W^\dagger + i\kappa(\tau_3 + i\tau_1) \otimes X^\dagger \otimes W\right] \\ = \;& \det{}^{-1/2}\begin{bmatrix} \frac{N}{2}\mathbb{1}_{N/2} \otimes (\mathbb{1}_{\nu/2} - i\widetilde{P}) & 2i\kappa X^\dagger \otimes W \\ 2i\kappa X \otimes W^\dagger & \frac{N}{2}\mathbb{1}_{N/2} \otimes (\mathbb{1}_{\nu/2} - i\widetilde{P}) \end{bmatrix} , \end{aligned} \tag{4.43}$$

where τ_j is the three Pauli matrices. The second line comes from decomposing $\widetilde{V}_1$ into real and imaginary part, and the third line is found by performing a rotation with $\exp[i\pi(\mathbb{1}_2 - \tau_3)/4] \exp[i\pi\tau_2/4]$. For the saddle point expansion I rescale $\widetilde{P} \to \widetilde{P}/\sqrt{\gamma N}$, and the Taylor expansion of the determinant works as in Equation (4.41). The Gaussian distribution is again found

$$\lim_{N\to\infty} p(S') \;=\; \frac{\exp\left[-\operatorname{Tr}\{S'\}^2\right]}{\int_{\mathcal{H}_\nu} d\bar{S} \exp\left[-\operatorname{Tr} \bar{S}^2\right]} , \tag{4.44}$$

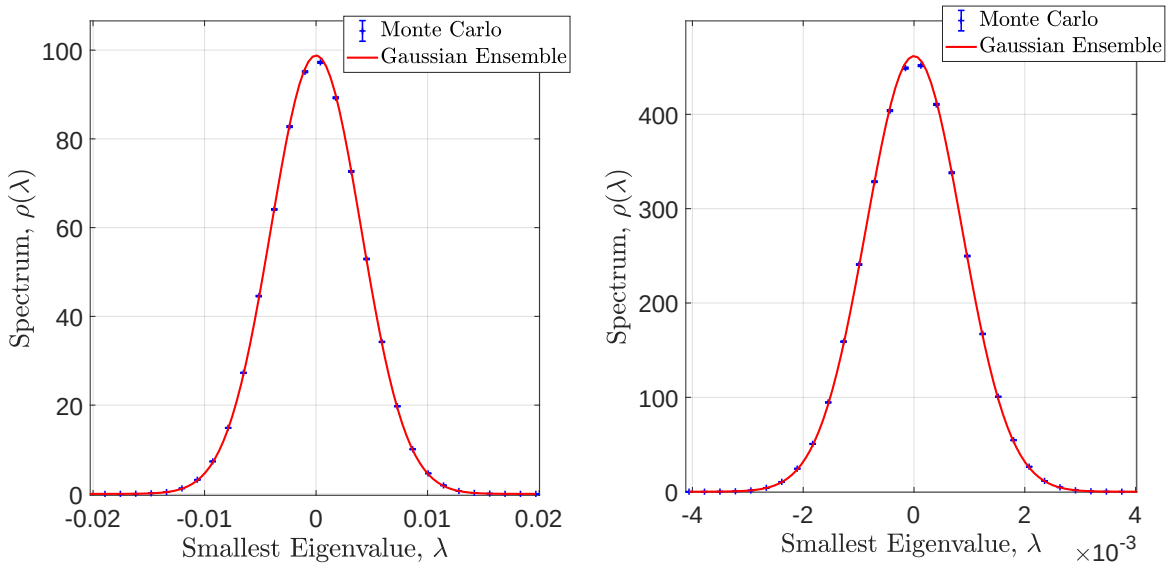

Figure 4.1: Distribution of the two smallest eigenvalues of *Ensemble 1* (left plot) and *Ensemble 3* (right plot) in Section 4.4.2. In both ensembles the unperturbed Hamiltonian A is imaginary, antisymmetric and block-diagonal of dimension $N = 134$ so that it has two zero eigenvalues. The perturbation S is a full generic imaginary matrix $i\alpha W$ (*Ensemble 1*) on the off-diagonal block and a constant matrix $i\alpha\mathbb{1}$ (*Ensemble 3*) with $\alpha = 0.01$. The Monte Carlo simulations (blue error bars, 10^6 matrices generated) are compared with the theoretical RMT predictions that are Gaussian distributions with the variances derived in Section 4.3 (red solid curves). This figure is also published in [KMS].

which implies that αS_3 is a Gaussian random matrix with standard deviation $\alpha\sqrt{\mathrm{Tr}\big(S^{(N)}\big)^2/(2N^2)}$ in the limit $N \to \infty$.

4.4 Scaling and Application

In this section I take a closer look at the scaling behaviour of the spectra. As discussed in Section 4.1, the smallest eigenvalue of $A^{(N)}$ is typically on the scale N^{-1}. This means that in the rescaled eigenvalues

$$x = N\lambda\,, \tag{4.45}$$

where λ are the eigenvalues of $K^{(N)}$, in the limit $N \to \infty$, one zooms in on the microscopic spectrum around the origin.

Following (4.11), the width of the former zero eigenvalues is $\alpha\sqrt{\mathrm{Tr}\,S^2}/N$ and the smallest eigenvalues of A are $1/N$. So rescaling the eigenvalues as in (4.45) gives a broadening of $\alpha\sqrt{\mathrm{Tr}\,S^2}$. Assuming $\mathrm{Tr}\,S^2 \sim N$ and fixed α, the width of the rescaled broadened zero modes scale as $\sqrt{N}$. I will demonstrate the applicability of this in more detail below. See also Figure 4.2 (left plot) and Figure 4.3.

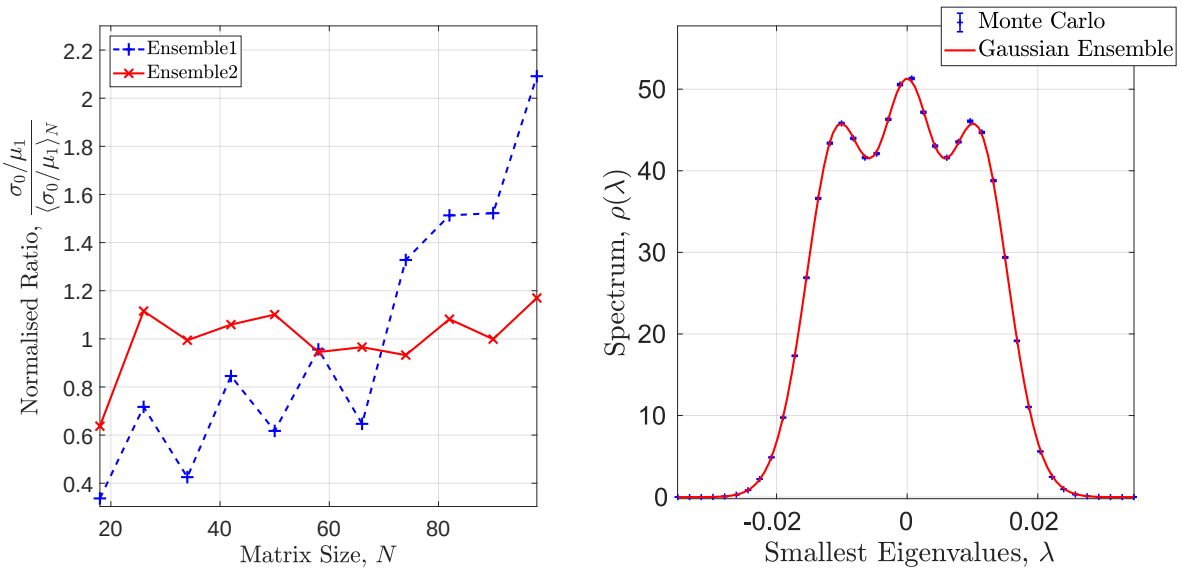

Figure 4.2: Left: Identification of former topological modes. Plotted is a comparison of the ratio between the width of the smallest eigenvalue and the position of the second smallest eigenvalue as a function of the matrix size N for *Ensemble 1* ($\nu = 1$) and *Ensemble 2* ($\nu = 0$) in Section 4.4.2. The mean of each curve has been normalised, and the coupling constant is set to $\alpha = 0.01\sqrt{\mathrm{Tr}\, A^{-2}}\|S\|_{\mathrm{op}}/\sqrt{N}$ according to (4.19). The ensemble size is 10^5. **Right:** The density of the smallest eigenvalues for *Ensemble 4* with $n = 33$ and $\nu = 3$ from Section 4.4.2. The Monte Carlo simulation (blue error bars, 10^6 matrices generated) and the theoretical distribution of the GUE of size 3×3 (red solid curve) are compared, see (4.50). This figure is also published in [KMS].

4.4.1 Application to Experiments

Let me relate the scaling with N to physical quantities. As discussed in the Chapter 1, the matrix scales linearly with the volume of the system $V \sim N$. This means that under the above assumptions, the width of the broadened modes scale as $\sqrt{V}$. This relation is a result from the ϵ-regime of effective field theory and applies to the low-energy modes around the origin, where dynamics decouple [16, 17, 18]. The potential term becomes the most important here.

We therefore propose the ratio σ_0/μ_1 as an experimental identifier in [KMS]. Here σ_0 is the width of the ground state distribution, and μ_1 is the mean position of the first excited state. If this scales significantly different from 1, it is safe to conclude a system with a broadened zero mode. This scaling is also found in the literature of lattice QCD and has helped to explain the unusual behaviour observed in lattice simulations [28, 29].

On a more heuristic note, the Gaussian behaviour of a finite submatrix when the size of the whole matrix becomes large lends further intuition to the ubiquity of Gaussian distributions. (It is a priori unlikely that such a chaotic phenomenon as noise comes from independent sources only.)

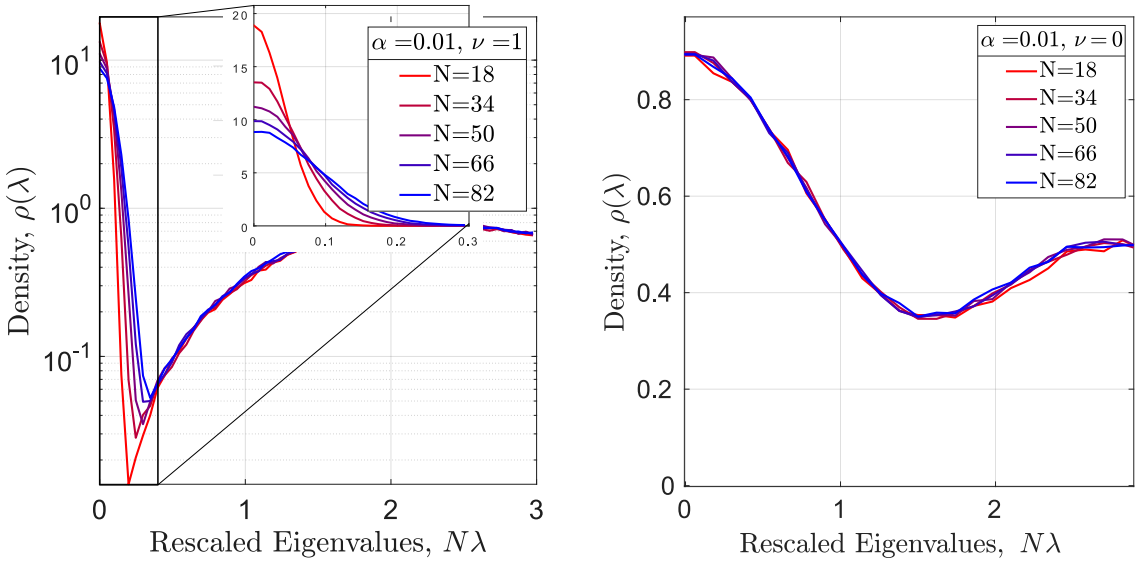

Figure 4.3: The microscopic density for Monte Carlo simulations of an ensemble with a single topological mode (left, see (4.46)) and one without (right, see (4.47)) for different matrix sizes. Here I have also averaged over the spectrum for visual clarity of the bulk. The eigenvalues have been rescaled as in (4.45) to keep the distance between the smallest eigenvalues of the order 1. Note the difference between a topological and a non-topological mode, namely that the former topological mode broadens with N. The ensemble size is 10^5 and the bin size is roughly 0.2 for the left plot and 0.1 for the right plot. The density in the left plot is shown on logarithmic scale to keep both peaks visible in the same plot, but a zoom-in is provided. This figure is also published in [KMS].

4.4.2 Example Ensembles

For numerical checks I use the following example ensembles. In each case I draw a fixed $A^{(N)}$ and $S^{(N)}$ and then average over U for the Hamiltonian $K^{(N)} = A^{(N)} + \alpha U S^{(N)} U^\dagger$.

Ensemble 1: Consider a direct sum of two antisymmetric matrices that are the same up to a sign. This corresponds to particle-hole-symmetry [34, 37, 65] and is chosen to illustrate a particular condensed matter application. The ensemble is perturbed by off-diagonal blocks in order to model topological superconductors carrying Majorana modes. This has the form

$$K^{(N)} = \begin{pmatrix} iM & 0 \\ 0 & -iM \end{pmatrix} + \alpha O \begin{pmatrix} 0 & iW \\ -iW^T & 0 \end{pmatrix} O^T \,,\; M = -M^T \,. \tag{4.46}$$

The matrices M and W are real and of dimension $2n + \nu$, and M is antisymmetric. So for $\alpha = 0$ and $\nu = 1$ the model exhibits two generic zero modes. This is the ensemble is the one considered in Chapter 3, but for $A = B$ and in the regime $1/a \ll 1$. The matrices are generated once via i.i.d. entries uniform on the interval $[-1, 1]$ and then kept fixed. The ensemble average is only done via the orthogonal matrix O. The full matrix $K^{(N)}$ is of size $N = 4n + 2\nu$ and imaginary antisymmetric, and for $\alpha > 0$ no exact modes are present. For $\nu = 1$ the two zero modes are broadened by the coupling. They form a 2×2 imaginary antisymmetric Gaussian ensemble.

Ensemble 2: To compare the different scalings of broadened zero eigenvalues and bulk eigenvalues, I also consider an ensemble for comparison of the form

$$K^{(N)} = iA^{(N)} + i\alpha O S^{(N)} O^T \ , \ K^{(N)} = K^{(N)\dagger} = -K^{(N)T} \tag{4.47}$$

with matrix size $N = 2n$ and no further substructure. This ensemble never has exact zero modes in contrast to the models covered by our discussion. All matrix entries of A and S are drawn i.i.d. once, uniformly from the interval $[-1, 1]$. Afterwards they are kept fixed, and the average is over the orthogonal matrices O only.

See Figure 4.3 for a comparison between the microscopic densities about the origin for *Ensembles 1* and *2*. In both plots the eigenvalues have been rescaled according to (4.45) to keep the mean inter-eigenvalue distance of order 1. To contrast the scaling of the eigenvalues with the volume $V \sim N$, I also average over the spectrum of A and S. As predicted in Section 4.4.1, the perturbed zero mode in *Ensemble 1* changes with the volume in the rescaled variables, whereas the same does not happen for the smallest eigenvalue in *Ensemble 2*.

It is, however, not necessary to average over the spectrum, see Figure 4.2 (left plot). Here the ratio σ_0/μ_1 is plotted as a function of the matrix size N. This is the experimental identifier we propose in [KMS]. The rescaling $\alpha \|S\|_{\text{op}} \sqrt{\text{Tr}\, A^{-2}}/\sqrt{N} \to \alpha$ has been made to keep the coupling constant on the same scale for all matrix sizes, see (4.19). As there is no average over the spectrum, the variance of the individual modes partially obscures the scaling, but it is still visible. If an average over the spectrum is also performed, the difference becomes even clearer, see Figure 4.3.

Ensemble 3: To illustrate that degeneracy of the perturbation is irrelevant as long as it satisfies the conditions (4.17-4.19), consider an ensemble very similar to *Ensemble 1*, except that the perturbation is proportional to the second Pauli matrix. That is,

$$\begin{aligned} K^{(N)} &= \begin{pmatrix} iM_1 & 0 \\ 0 & iM_2 \end{pmatrix} + i\alpha O \begin{pmatrix} 0 & \mathbb{1} \\ -\mathbb{1} & 0 \end{pmatrix} O^T \ , \\ & M_1 = -{M_1}^T \ , \ M_2 = -{M_2}^T \ . \end{aligned} \tag{4.48}$$

M_1 and M_2 are real antisymmetric, but independent as the eigenvalues would otherwise be shifted rather than perturbed. These are chosen fixed with i.i.d. entries on the interval $[-1, 1]$ while the average is over the orthogonal matrix O. This ensemble emphasises the generality of the conditions (4.17-4.19). That is, the matrix central limit theorem stated above describes the limit for a broad class of ensembles. This similarity is illustrated in Figure 4.1 where I compare Monte Carlo simulations to the corresponding theoretical curves derived in Section 4.3.

Ensemble 4: As an application to lattice QCD, where chirality is broken by a perturbation [28, 29, 95, 96, 98, 99], consider the following model

$$K^{(N)} = \begin{pmatrix} 0 & M \\ M^\dagger & 0 \end{pmatrix} + \alpha U S U^\dagger \ . \tag{4.49}$$

M is a complex $(n + \nu) \times n$ matrix with no further symmetries, S is a complex hermitian matrix, and U is unitary and Haar-distributed. As before the only average is over U. The index ν determines the number of exact zero modes, which allows any number of broadened modes, unlike the antisymmetric ensembles. The ν zero modes from the chiral ensemble are all broadened by the perturbation, which is hermitian and has no further symmetry.

This means that the former zero modes are distributed according to a Gaussian unitary ensemble of size $\nu \times \nu$

$$\begin{aligned} \rho^{\nu}_{\mathrm{GUE}}(\lambda) &= \frac{1}{2\sigma}\sum_{j=0}^{\nu-1}\varphi_j\left(\frac{\lambda}{\sigma}\right)^2, \\ \varphi_j(\lambda) &= \frac{1}{\sqrt{2^j j!\sqrt{\pi}}}e^{-\lambda^2/2}H_j(\lambda) \end{aligned} \tag{4.50}$$

with $\sigma = \alpha\sqrt{\mathrm{Tr}\big(S^{(N)}\big)^2/(\gamma N^2)}$ and $H_j(\lambda)$ the Hermite polynomials corresponding to the weight $e^{-\lambda^2}$. This may also be found in Equation (2.28) and in [8]. In Figure 4.2 (right plot) the broadening of this ensemble to the theoretical prediction is compared to the width found in Section 4.3.1.

4.5 Conclusion

In this chapter I presented a general mechanism for the universal decoupling and broadening of former zero modes under a generic perturbation. The broadened zero follows the statistics of finite-dimensional Gaussian random matrix ensemble, which is surprising because one usually expects that spectral universality only holds in the limit of large matrix dimensions. The new universality relies on a self-average of the change of basis $U_2 = \{\langle\psi_j|\phi_l\rangle\}_{j,l=N-\nu+1,\ldots,N}$ between the unperturbed operator A and the perturbation S associated with the zero modes of A. I worked under the assumption that all bases transformations U_2 are drawn from the Haar measure of the group associated to the respective symmetry class, but lattice simulations in QCD [32, 98, 99, 100] and special cases from effective field theory [96, 97] strongly suggest that the measure can be relaxed to something non-uniform.

I quantified under which conditions this decoupling and universality applies. This includes an extension of the central limit theorem to the elements of a finite submatrix when the size of the whole matrix becomes infinite. The three conditions (4.17-4.19) are rather mild and have natural physical interpretations such as whether the coupling strength α allows a spectral gap. The critical scaling of α found in lattice QCD with Wilson fermions [32, 98, 99, 100] and in the RMT-models for Majorana modes in disordered quantum wires [97] is recovered here.

Note that the limit $\nu \to \infty$ may be taken naïvely by letting the Gaussian ensemble of the former zero modes go to infinite size. This does not take into account how ν scales with N, and the limit may therefore be viewed as $N \to \infty, \nu \to \infty$ while keeping $\nu \ll N$. At the time of writing, we are also working on extending these results to non-hermitian perturbations.

A possible application of these results is to distinguish topological modes in the bulk from modes in the bulk. The two kinds of modes scales very differently with the system size and the coupling parameter α. The scaling may therefore provide a useful indicator for experiments.

Chapter 5

Universal Spacing Distributions in 2D and Comparison to Data

Let me now focus more on the nearest neighbour spacing distributions of eigenvalues. As discussed in the introduction, the spacing distribution of random variables holds information about the degree of correlation. For real eigenvalues, the uncorrelated variables (Poisson) follow an exponential distribution, whereas the correlated ones (Wigner) exhibit a repulsion between each other. This behaviour has been observed in nature several places and is very characteristic. For quantum chaos, the spacing of eigenvalues also identifies integrable and chaotic systems, because they behave as Poisson and Wigner variables respectively. This was proposed in [3, 4] and observed in [6]. The was also better through a semi-classical expansion [104].

It is important to emphasise the universality of the spacing distributions, but also that this only applies to a uniform spectrum. If an area is more dense, the average spacing will naturally be smaller. A non-uniform spectrum will therefore give several overlapping distributions, which cannot be compared meaningfully to Wigner and Poisson. It is therefore necessary to make a change of coordinates that makes the density uniform. This process is called unfolding.

It is natural to extend these notions to the complex plane. For correlated variables, this corresponds to processes in 2D and for quantum chaos, it is relevant for open systems. The extension for quantum chaos was proposed in [105], where it was suggested that integrable and chaotic systems should have the same repulsion as Poisson and Ginibre respectively.

In this chapter I further extend this result to the full distribution as well as consider distributions between Poisson and Ginibre. I also compare to other real-world data. First of all, I go through the known results for Ginibre ensembles (non-Hermitian matrices with no symmetries) and I show how the complex spectrum differs from the real one. I then discuss how to unfold in 2D, and show how to apply this to the relevant datasets, of which there are two: Simulations of an open spin chains that transition from integrable to chaotic and buzzard nests from the Teutoburger forest. The goal for the first set is to see the transition in the eigenvalue spacing of the Liouville operator, and the goal of the second set is to get a sense of territorial behaviour.

This chapter is based partially on [AKMP]. Section 5.3.3 is based on unpublished work with Oliver Krüger and Rebecca Werdehausen and became part of the latter's bachelor's thesis [40].

5.1 Spacing Distribution of Eigenvalues

As discussed in Chapter 2.1, the spacing approximate distribution for real eigenvalues is given by the Wigner surmise, see Equation (2.15). I repeated here for convenience

$$p_\beta(s) = 2\frac{\Gamma\left(\frac{\beta+2}{2}\right)^{\beta+1}}{\Gamma\left(\frac{\beta+1}{2}\right)^{\beta+2}} s^\beta \exp\left\{-\left(\frac{\Gamma\left(\frac{\beta+2}{2}\right)}{\Gamma\left(\frac{1+\beta}{2}\right)}s\right)^2\right\} . \tag{5.1}$$

This also works as an approximation for the intermediate values of β given by the corresponding log-gasses, which I will return to in Section 5.1.3. See Figure 5.1 (left plot) for a plot of the Wigner surmise for different β along with the corresponding log-gasses. Also included is the exponential distribution that arises for Poisson variables. Remarkably, although it is only an exact result for 2×2-matrices, the Wigner surmise is a good approximation for larger matrices if either β or the spacing is small. It of course does not hold very close to $\beta = 0$, as

$$\lim_{\beta\to 0} p_\beta(s) \neq e^{-s} . \tag{5.2}$$

For the interpolation between Poisson and Wigner, other approximations are used instead, such as the Brody distribution [106]

$$p_q(s) = c_q s^q \exp\left(-\frac{c_q}{q+1}s^{q+1}\right) , \text{ where } \quad c_q = \tfrac{\Gamma(1/(q+1))^{q+1}}{q+1} , \tag{5.3}$$

and $q \in [0, 1]$. See for instance [107].

That the $N = 2$ result is a good approximation for $N \to \infty$ does not hold in the complex plane, and therefore the whole expression for the spacing distribution is needed. I first show the analytic result for complex Ginibre and argue that this distribution should also hold for real and quaternion Ginibre as long as only the bulk is considered.

5.1.1 Nearest Neighbour Spacing Distribution for Complex Ginibre

The approach for complex Ginibre is as follows. Fix an eigenvalue at the origin. The distribution of the smallest non-zero eigenvalue for this ensemble will then correspond to the nearest neighbour spacing distribution at the origin of complex Ginibre without a fixed eigenvalue. I start with the gap probability, because it is a simpler object to work with. The distribution of the smallest eigenvalue may be found by taking the derivative. From here the translational symmetry of the spectrum generalises the result at the origin to the whole bulk.

The starting point is therefore the gap probability of complex Ginibre with 1 eigenvalue fixed at the origin, see [9]

$$G_N(s) \propto \int_s^\infty dr_1 r_1 \dots dr_{N-1} r_{N-1} \int_0^{2\pi} d\theta_1 \dots d\theta_{N-1} e^{-\sum_{j=1}^{N-1} r_j^2} |\Delta_{N-1}(\{z\})|^2 \prod_{j=1}^{N-1} {r_j}^2 \tag{5.4}$$

Note the structure similar to GUE. Applying the Andréief identity [108]

$$\int d\mu(x_1)\dots d\mu(x_N) \det_{j,k=1,\dots,N}[\phi_j(x_k)] \det_{j,k=1,\dots,N}[\psi_j(x_k)] = N! \det_{j,k=1,\dots,N}\left[\int d\mu(x)\phi_j(x)\psi_k(x)\right] , \tag{5.5}$$

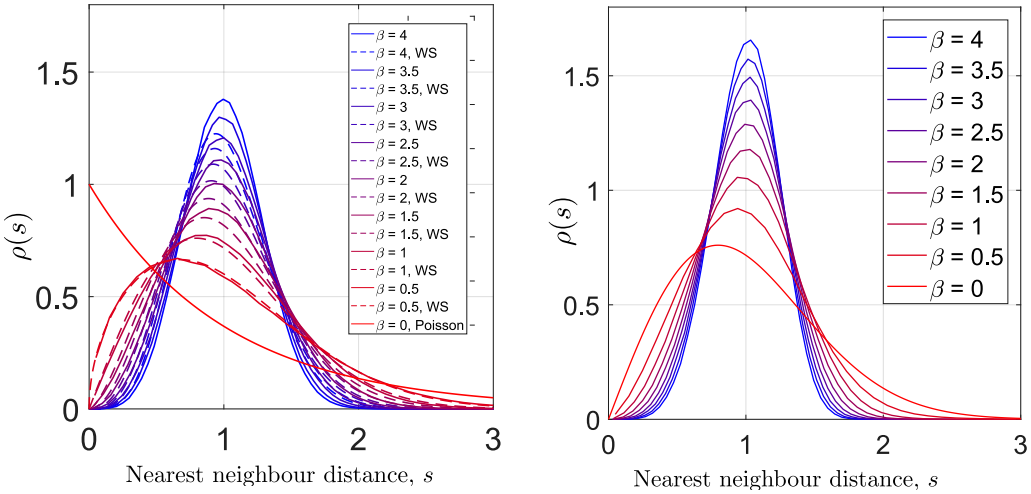

Figure 5.1: The spacing distributions for Coulomb gasses at different inverse temperature β showing the transition for 1D (left) and 2D (right). Plotted is the numerically computed spacing of Coulomb gasses with the method described in Section 5.1.3. The number of particles considered is 200 for 1D and 300 for 2D. The ensemble size is 10^4. For 1D the Wigner surmise (WS) has also been plotted (Equation (5.1)), which is an approximation of the spacing in 1D for $N > 2$, but a good one for low β. The analytical spacing distribution for Poisson variables ($\beta = 0$) is also plotted in both cases.

Equation (5.4) may be written as

$$G_N(s) \quad \propto \quad \det_{j,k=1,\ldots,N-1} \left[\int_s^\infty dr\, r^{3+j+k-2} e^{-r^2} \int_0^{2\pi} d\theta\, e^{i\theta(j-k)} \right] . \tag{5.6}$$

The angular integral enforces $j = k$ and reduces the expression to

$$\begin{aligned} G_N(s) \quad &\propto \quad \prod_{j=1}^{N-1} \int_s^\infty dr\, r^{2j+1} e^{-r^2} \\ &= \quad \prod_{j=1}^{N-1} \Gamma\left(j+1, s^2\right) . \end{aligned} \tag{5.7}$$

The normalisation is $G_N(0) = 1$, which gives

$$G_N(s) \quad = \quad \prod_{j=1}^{N-1} \frac{\Gamma\left(j+1, s^2\right)}{j!} . \tag{5.8}$$

To find the distribution of the nearest eigenvalue, the derivative is taken

$$\begin{aligned} p_N(s) \quad &= \quad -\partial_s G(s) \\ &= \quad 2s \sum_{j=1}^{N-1} \frac{s^{2j}}{\Gamma(1+j, s^2)} \exp\left\{ \sum_{k=0}^{N-1} \ln\left(\frac{\Gamma(1+k, s^2)}{k!} \right) \right\} . \end{aligned} \tag{5.9}$$

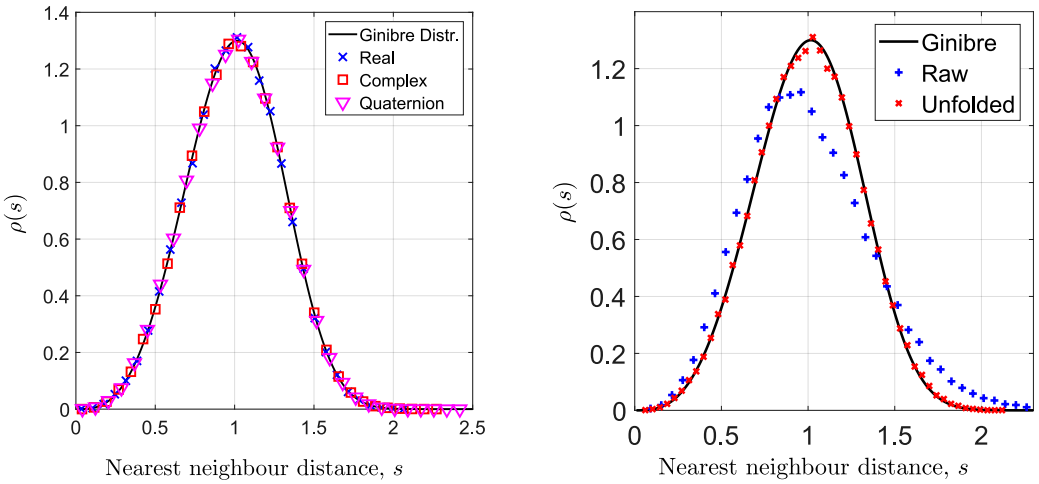

Figure 5.2: Left: A comparison of the bulk spacing distribution for real, complex, and quaternion Ginibre to show that these agree. Plotted is Monte Carlo simulations of the respective ensembles along with the analytic distribution from (5.10). The matrix size is 500 and the ensemble size is 1000. Only eigenvalues away from the real line and the edge have been included. Unfolding is trivial in this case, because the density is flat in all cases. This figure has also been published in [AKMP]. **Right:** The effect of the unfolding method described in Section 5.2.2. Plotted is the spacing distribution of a product of two 200×200 complex Ginibre matrices, which does not have a uniform macroscopic spectrum, but has the spacing (5.10) after unfolding and therefore serves as a good check of the method, see Section 5.1.5. The ensemble size is 1000 and the width has been chosen as 4.5 times the mean level spacing. This figure has also been included in [AKMP].

The zeroth term in the exponential along with the term s^{2j} come from the derivative of the Γ-function in front. I normalise the first moment to 1 numerically when implementing it. The limit $N \to \infty$ is easily taken

$$p_(s) \quad = \quad 2s \sum_{j=1}^{\infty} \frac{s^{2j}}{\Gamma(1+j, s^2)} \exp\left\{ \sum_{k=0}^{\infty} \ln\left(\frac{\Gamma(1+k, s^2)}{k!} \right) \right\} \tag{5.10}$$

and converges very quickly. Note that $G_N(s)$ is the cumulative distribution, which is needed later when comparing distributions.

5.1.2 Extension to Other Ginibre Ensembles

As it turns out, the real and quaternion Ginibre ensembles have the same bulk distribution as the complex case. This may be realised heuristically as follows. Consider the jpdf of both ensembles [8, 9, 109, 110]

$$\begin{aligned} P_{\text{real}}(\lambda) \quad \propto \quad & |\Delta_M(\{z\})|^2 \Delta(\{x\}) \prod_{i,j=1}^{M} (z_i - z_j^*) \prod_{i=1}^{k} \prod_{j=1}^{M} |z_j - x_i|^2 \prod_{j=1}^{k} e^{-\frac{1}{2}x_j^2} \\ & \times \prod_{j=1}^{M} \operatorname{sign}\left(\operatorname{Im}(z_j)\right) \operatorname{erfc}\left(\sqrt{2}\operatorname{Im}(z_j)\right) \exp\left(-\frac{1}{2}\left(z_j^2 + z_j^{*2}\right)\right) \end{aligned} \tag{5.11}$$

$$P_{\text{quat}}(\{z\}) \propto \prod_{j<k} |z_j - z_k|^2 |z_j - z_k^*|^2 \prod_{j=1}^{N} |z_j - z_j^*|^2 \exp\left(-|z_j|^2\right) , \tag{5.12}$$

where for the k real eigenvalues are denoted x and the $2M$ complex ones λ, and the matrix size is $2M+k = N$. For the quaternion ensemble there are no real eigenvalues, so $k = 0$. For the real ensemble the eigenvalues are ordered such that the density is positive. Note that the factors including the complex conjugate cannot vanish far away from the real axis. As discussed, the origin of the level repulsion is the vanishing jpdf, which means the dominant local effect in the bulk is $\prod_{j\neq k} |z_j - z_k|^2$ for the real and quaternion ensembles as well. The more rigorous statement would be on the level of the kernels, see [111] for real Ginibre. This means that the different symmetry classes cannot be distinguished in their bulk. It is possible at the real axis, however. See Figure 5.2 (left plot) for a numerical check of this. The macroscopic density is flat for both real and quaternion Ginibre [9], and the unfolding discussed in Section 5.2 is not needed yet.

5.1.3 Coulomb Gasses

The spacing distributions may be extended beyond matrix ensembles by considering Coulomb gasses. Consider the following for real eigenvalues: Rewriting the partition function of GOE, GUE, and GSE in one

$$\begin{aligned} Z_N^\beta &\propto \int \prod_{j=1}^{N} d\lambda_j e^{-\frac{\beta}{2}\lambda_j^2} \, |\Delta_N(\{\lambda\})|^\beta \\ &= \int \prod_{j=1}^{N} d\lambda_j \exp\left\{ -\frac{\beta}{2} \sum_{j=1}^{N} \lambda_j^2 + \beta \sum_{N\geq j>k\geq 1} \log|\lambda_j - \lambda_k| \right\} , \end{aligned} \tag{5.13}$$

it may be identified as the partition function of a static gas with logarithmic interaction in a harmonic oscillator potential and inverse temperature β, confer with $Z = \int e^{-\beta H}$. For general β, the rescaling $\beta\lambda^2 \to \lambda^2$ such that the limit $\beta \to 0$ is meaningful. It is of course slightly artificial to call it a Coulomb gas for real eigenvalues, because the Coulomb interaction is only logarithmic in 2D. Nonetheless, it is a useful picture for understanding the local and global interactions. See for instance [112] for more on Coulomb gasses. The complex case has the same structure

$$Z_N^\beta \propto \int \prod_{j=1}^{N} d^2\lambda_j \exp\left\{ -\frac{\beta}{2} \sum_{j=1}^{N} |\lambda_j|^2 + \beta \sum_{N\geq j>k\geq 1} \log|\lambda_j - \lambda_k| \right\} , \tag{5.14}$$

and here the logarithmic interaction is more natural. For 1D some approximations are available, but for 2D there is neither analytic result nor approximation for the spacing of eigenvalues for general β, and I instead generated the ensembles numerically with Monte Carlo simulations through what is known as the Metropolis algorithm, see [114] for more details. The idea is to generate a random configuration X (in this case they are picked Gaussian) and explore the space as follows. Let $H(X)$ be the energy associated with the configuration X.

- Generate a new configuration X'. (In this case as a small Gaussian perturbation of X. The width of the Gaussian is chosen as $N^{-1/3}$ in accordance with [114].)

- Accept the new configuration with probability

$$p = \begin{cases} e^{-(H(X')-H(X))} & \text{if } H(X') > H(X) \\ 1 & \text{otherwise} \end{cases} \tag{5.15}$$

- Repeat this process until convergence. (In this case I simply make $100N$ perturbations of individual points, corresponding to roughly 100 iterations of this process. I can verify convergence comparing $\beta = 2$ to Ginibre.)

See Figure 5.1 for a plot of the spacing distributions for different β as well as the Wigner surmise for 1D. Again, unfolding is not necessary here, because the macroscopic density is flat, see for instance [113].

5.1.4 Poisson Variables in 2D

As they will be relevant for later comparison, I briefly go through how to derive the spacing distribution of 2D Poisson variables, see also [115]. Assume a uniform distribution of N independent points on a disk of radius R and look at the gap probability at the centre. (As the points are uncorrelated, it is unnecessary to place a point there.)

$$G_N(s) \propto \left(\int_s^R r\, dr \int_0^{2\pi} d\theta \right)^N = \left(R^2 \pi \left(1 - \frac{s^2}{R^2} \right) \right)^N . \tag{5.16}$$

To keep the density uniform in the limit $N \to \infty$, I rescale $R = \widetilde{R}\sqrt{N}$. This leaves

$$\lim_{N\to\infty} G_N(s) \propto \lim_{N\to\infty} \left(1 - \frac{s^2}{\widetilde{R}^2 N} \right)^N = \exp\left(-\frac{s^2}{\widetilde{R}^2} \right) . \tag{5.17}$$

This makes the nearest neighbour spacing

$$\begin{aligned} p(s) &= -\partial_s \lim_{N\to\infty} G_N(s) \\ &\propto s \exp\left(-\frac{s^2}{\widetilde{R}^2} \right) . \end{aligned} \tag{5.18}$$

Normalising both zeroth and first moments leads to

$$p(s) = \frac{\pi}{2} s \exp\left(-\frac{\pi}{4} s^2 \right) . \tag{5.19}$$

Note that this is the Wigner Surmise for $\beta = 1$, though in this case it is an exact result. The above approach works in any dimension if the scaling is taken into account.

5.1.5 Products of Ginibre Matrices

Because they provide a good test for the unfolding method I present in Section 5.2, I want to emphasise the following properties of the product of k independent Ginibre matrices. Firstly, the macroscopic density in the limit $N \to \infty$ takes the form [117, 41, 118]

$$\rho^k(\lambda) = \frac{|\lambda|^{\frac{2}{k}-2}}{k\pi} \Theta(1 - |\lambda|) , \tag{5.20}$$

where $\Theta(x)$ is the Heaviside step function. Note that the spectrum is flat for $k = 1$, but for $k > 1$ a singularity is present at the origin, which grows in strength for larger k. Secondly, they share the same microscopic spacing distribution [118], so the result for $k = 1$, Equation (5.10), may be used for all k after unfolding. This means the product of independent Ginibre matrices are an example of a non-uniform spectrum which follows a known local nearest neighbour spacing. I therefore use it to judge the validity of the unfolding method.

5.2 Unfolding of the Spectrum

Let me now turn to the problem of making a density uniform, which is necessary for comparison with the spacing distributions. In 1D, the transformation is understood and, as I will show, it is simply the cumulative distribution. In 2D, some work has been done, see for instance [116], but I will take a different approach than the literature.

5.2.1 One Dimension

Let me start by going through the methods already known for 1D. The goal is to find coordinates $\widetilde{x} = f(x)$ such that

$$\rho_{un}(\widetilde{x}) = \rho\left(f^{-1}(\widetilde{x})\right)(f^{-1})'(\widetilde{x}) = 1 \tag{5.21}$$

up to normalisation. This implies

$$\begin{aligned} \rho\left(f^{-1}(\widetilde{x})\right) &= \frac{1}{(f^{-1})'(\widetilde{x})} && (5.22)\\ &= f'\left(f^{-1}(\widetilde{x})\right) . && (5.23) \end{aligned}$$

Rearranging and integrating on either side yields

$$\begin{aligned} \widetilde{x}_0 &= \int_0^{\widetilde{x}_0} \frac{\rho\left(f^{-1}(\widetilde{x})\right)}{f'\left(f^{-1}(\widetilde{x})\right)} d\widetilde{x} && (5.24)\\ &= \int_0^{f^{-1}(\widetilde{x}_0)=x} \rho(x)dx \\ &= N(x) , \end{aligned}$$

where $N(x)$ is the cumulative distribution. If this is known analytically, it can be applied directly, but otherwise it can be approximated by a smoothing of the empirical cumulative distribution. I denote this by $\bar{N}(x)$, and the smoothing method is

$$\bar{N}(x) = \sum_{j=1}^{N} \frac{1 + \mathrm{erf}(a(x - x_j))}{2} , \tag{5.25}$$

where a is a smoothing parameter to be chosen. Note that (5.25) come from the regularisation $\Theta(x) \approx (\mathrm{erf}(x) + 1)/2$. The parameter a may be chosen by applying the transformation to a known spectrum such as GUE. It will in general depend on the amount of points and the support of the spectrum.

5.2.2 Two Dimensions

For two dimensions it is natural to extend the above result, which would mean to find a set of coordinates

$$\begin{pmatrix} \widetilde{x} \\ \widetilde{y} \end{pmatrix} = \begin{pmatrix} f_1(x,y) \\ f_2(x,y) \end{pmatrix} , \tag{5.26}$$

that satisfies

$$\begin{aligned} 1 &= \rho_{un}(\widetilde{x},\widetilde{y}) \\ &= \rho(f^{-1}(\widetilde{x},\widetilde{y})) \det \begin{pmatrix} \partial_{\widetilde{x}} f_1^{-1}(\widetilde{x},\widetilde{y}) & \partial_{\widetilde{y}} f_1^{-1}(\widetilde{x},\widetilde{y}) \\ \partial_{\widetilde{x}} f_2^{-1}(\widetilde{x},\widetilde{y}) & \partial_{\widetilde{y}} f_2^{-1}(\widetilde{x},\widetilde{y}) \end{pmatrix} . \end{aligned} \tag{5.27}$$

I now make the ansatz

$$f_2^{-1}(\widetilde{x},\widetilde{y}) = \widetilde{y} , \tag{5.28}$$

which leaves

$$1 = \rho(f^{-1}(\widetilde{x},\widetilde{y}))\partial_{\widetilde{x}} f_1^{-1}(\widetilde{x},\widetilde{y}) . \tag{5.29}$$

This is then solved as in the 1D-case, which leaves the transformation

$$f(x,y) = \begin{pmatrix} \partial_y N(x,y) \\ y \end{pmatrix} , \tag{5.30}$$

This was proposed in [116]. The implementation in [116] is to unfold in strips and fit a low-order polynomial in 1D along these strips. A different implementation is to choose an empirical cumulative density in two dimensions

$$N(x,y) = \sum_{j=1}^{N} \Theta(x-x_j)\Theta(y-y_j) . \tag{5.31}$$

This is not unique as it may be taken from any direction. If a symmetry is present in the data, it is advisable to take the cumulative distribution along this symmetry (this should be done in the ansatz). The empirical distribution is then smoothed out as before (5.25)

$$\bar{N}(x,y) = \frac{1}{4N} \sum_{j=1}^{N} \left[1+\mathrm{erf}(a(x-x_j))\right] \left[1+\mathrm{erf}(a(y-y_j))\right] , \tag{5.32}$$

where a is again a smoothing parameter chosen appropriately. This leaves

$$\partial_y \bar{N}(x,y) = \frac{a}{2N\sqrt{\pi}} \sum_{j=1}^{N} \left[1+\mathrm{erf}(a(x-x_j))\right] \exp\left\{-a^2(y-y_j)^2\right\} , \tag{5.33}$$

which is numerically simple to implement. The parameter a may be determined by considering the unfolding of a product of two complex Ginibre matrices. Because the spacing of the unfolded spectrum is already known, an appropriate smoothing parameter will map the raw spectrum to an unfolding, where the spacing is correct.

A crucial part of the above derivation that I unfold on a global scale. This is not a problem in 1D, but when extending to a manifold such as a 2D density, a global transformation is not guaranteed to preserve the local behaviour. This is a fundamental result in differential geometry and is known to all who have tried to make a flat map of the Earth that faithfully represents local distances. It is simply not possible. The method presented above should therefore be viewed as an approximate unfolding that is only applicable to distributions already close to uniform.

A general unfolding has to be on a local scale. That is, the measure

$$ds^2 \quad = \quad \rho(x,y)\left(dx^2+dy^2\right) \tag{5.34}$$

is used rather than a change of variables. The density at each point is estimated the same way as in (5.32). That is, assuming each point is a Gaussian with a given width

$$\bar{\rho}(x,y) \quad = \quad \frac{1}{2\pi\sigma^2 N}\sum_{j=1}^{N}\exp\left(-\frac{(x-x_j)^2+(y-y_j)^2}{2\sigma^2}\right) . \tag{5.35}$$

I use the products of Ginibre matrices to determine σ by requiring that all products have the same unfolded spectrum, see Section 5.1.5. I find that a width of $\sigma = 4.5\mu_s$, where μ_s is the mean spacing, gives the best result. See Figure 5.2 (right plot) for the effects of unfolding the spectrum for a product of 2 matrices. The products of 3-5 matrices give similar results, which supports the choice of unfolding and parameter σ.

5.3 Comparison to Data

These methods are applied to two different data sets, where the spacings are expected to hold information about the system. First I consider an open spin chain and investigate the extension to complex eigenvalues of the integrable/chaotic distinction proposed in [3, 4]. Secondly I look at buzzard nests in the local forest around Bielefeld. Here the spacing may give some understanding of their territorial behaviour. It is expected that the nests should at least not follow Poisson spacing, but the strength of the repulsion is still to be determined.

5.3.1 Fitting of Distributions

Let me give a short introduction on the fitting techniques used for comparison in this section, see also [119, 120] for more on data analysis. The main measure I use for comparing two distributions f, g is the Kolmogorov distance

$$D \quad = \quad \max|F(x)-G(x)| \in [0,1] , \tag{5.36}$$

where F and G are the cumulative distributions of f and g respectively. The Kolmogorov distance is a more natural choice for fitting distributions than something like a χ^2-fit, because it already takes normalisation into account. The downside is that it becomes more difficult to quantify the uncertainty on β than it would be for a χ^2-fit.

As I only fit the same distribution to each dataset, I can simply minimise the distance. I generate Coulomb gasses for equidistant values of β (intervals of 0.1) and compare each to the data to find the smallest Kolmogorov distance. The Coulomb gas ensembles I use for comparison

consist of 200 particles and the ensemble size is 1000. If I had to compare different distributions to the same dataset (as may be necessary for extending the analysis), the goodness of fit (GoF) would be required. It is defined as the probability of getting a larger Kolmogorov distance with a data set of the same size. If the distribution is known, this may in principle be calculated analytically. For a fit, however, the curve and data will be correlated, and therefore bootstrapping is needed. Generating a data set of the same size according to the fitted distribution and fitting the result, the correlation may be circumvented. Regarding the amount of test ensembles, [120] states that a precision of ϵ on the probability requires $\frac{1}{4}\epsilon^{-2}$ tests. So for $\epsilon = 0.01$ it is necessary to generate 2500 test ensembles. However, the Kolmogorov distance without the goodness of fit will suffice here.

5.3.2 Integrable and Chaotic Systems

The spectral distinction between integrable and chaotic proposed in [3, 4] was extended by Grobe, Haake, and Sommers (GHS) [105] to dissipative open quantum systems, but where [105] consider the exponent of the repulsion and only Poisson/Ginibre, I here extend the comparison to both the full spacing distribution and to repulsions between Poisson and Ginibre.

The physical operator under consideration here is the Liouville operator of an open spin chain consisting of N spin $\frac{1}{2}$. Open systems may be viewed as part of a larger closed system. Given a dissipative system S connected to a heat bath R and starting with the equations of motion for $S+R$, one may derive a general form for the equations of motion for S [115]. Exactly this property allows description of S on its own. Consider the Lindblad master equation

$$\frac{d\rho}{dt}(t) \;=\; \widehat{L}\rho(t)\,, \tag{5.37}$$

where $\widehat{L}$ is the Liouville operator and ρ the density operator. This describes the time evolution of the density operator, and it is exactly the eigenvalues of $\widehat{L}$ viewed as an operator on the vector space of density operators I analyse to find a spectral signature of chaos. See [115] for more on chaos in dissipative quantum systems. The Hamiltonian of this open spin chain is

$$\begin{aligned} H \;=\; & J\sum_{l=1}^{N-1}(\sigma_l^x\sigma_{l+1}^x + \sigma_l^y\sigma_{l+1}^y + \Delta\sigma_l^z\sigma_{l+1}^z) \\ & + J'\sum_{l=1}^{N-2}(\sigma_l^x\sigma_{l+2}^x + \sigma_l^y\sigma_{l+2}^y + \Delta'\sigma_l^z\sigma_{l+2}^z)\,, \end{aligned} \tag{5.38}$$

where $J, J', \Delta, \Delta' \in \mathbf{R}$, σ_l^α and $\alpha = x, y, z$ the Pauli matrices for each single spin $l = 1, \ldots, N$. To each spin a I associate a dephasing operator

$$L_l = \sqrt{\gamma}\sigma_l^z,\ l = 1, \ldots, N \text{ and } \gamma > 0\,. \tag{5.39}$$

A dephasing at the two ends of the spin-chain is introduced via the Lindblad operators

$$\begin{aligned} L_{-1} \;&=\; \sqrt{\gamma_{\mathrm{L}}^+}\sigma_1^+,\ L_0 = \sqrt{\gamma_{\mathrm{L}}^-}\sigma_1^-\,, \\ L_{N+1} \;&=\; \sqrt{\gamma_{\mathrm{R}}^+}\sigma_N^+,\ L_{N+2} = \sqrt{\gamma_{\mathrm{R}}^-}\sigma_N^-\,, \end{aligned} \tag{5.40}$$

where $\gamma_{\rm L}^{\pm}, \gamma_{\rm R}^{\pm} > 0$ and $\sigma_l^{\pm} = \sigma_l^x \pm i\sigma_l^y$. Going back to the master equation (5.37), the Liouville operator $\widehat{L}$ acting on a density operator ρ is given by [121, 122]

$$\widehat{L}\rho \;\; = \;\; -i[H,\rho] + \sum_{l=-1}^{N+2} \left(2L_l\rho L_l^\dagger - \{L_l^\dagger L_l, \rho\}\right) , \tag{5.41}$$

where the commutator and anticommutator are denoted by $[\cdot,\cdot]$ and $\{\cdot,\cdot\}$, respectively.

I consider the Liouville operator $\widehat{L}$ as a $(4^N-1)\times(4^N-1)$ real matrix acting on the vector space of density operators. This missing dimension results from the fixed trace condition of ρ. The operator $\widehat{L}$ is real because $\rho \to \widehat{L}\rho$ preserves the Hermiticity.

For $\gamma = \gamma_{\rm L}^{\pm} = \gamma_{\rm R}^{\pm} = 0$ (no dephasing noise), the operator $\widehat{L}$ is a real antisymmetric (because $\mathrm{Tr}\,\rho_1[H,\rho_2] = -\,\mathrm{Tr}[H,\rho_1]\rho_2$) and chiral (because $[H,\rho]^T = -[H,\rho^T]$) matrix, which means the spectrum is completely imaginary and symmetric around the origin. When the next-to-nearest neighbour interactions are switched off as well ($J' = 0$) the spectrum is completely integrable. With increasing J' the system becomes more chaotic and one would expect Wigner statistics with $\beta = 1$ in the bulk of the spectrum.

When including the dephasing noise ($\gamma, \gamma_{\rm L}^{\pm}, \gamma_{\rm R}^{\pm} \neq 0$), the Liouville operator $\widehat{L}$ becomes a real asymmetric matrix and its eigenvalues spread into the complex plane. There is still a good quantum number to consider, namely the total spin polarization $S = \sum_{l=1}^{N} \sigma_l^z$, which satisfies $[H,S] = 0$ and gives the Liouvillian weak symmetry [122]

$$[\widehat{L}(\rho), S] \;\; = \;\; \widehat{L}([\rho, S]) \, . \tag{5.42}$$

This is equivalent to the vanishing commutator of the $(4^N-1)\times(4^N-1)$ matrix representations of $\widehat{L}$ and of $[S,\cdot]$.

Let $|s,n\rangle$ be an eigenstate of H with $S|s,n\rangle = s|s,n\rangle$ where $s = -N/2, -(N-2)/2, \ldots, N/2$. This makes the eigenvalue equation of the state $|s,n\rangle\langle s',n'|$ under the adjoint action of S

$$[S, |s,n\rangle\langle s',n'|] \;\; = \;\; (s-s')|s,n\rangle\langle s',n'|. \tag{5.43}$$

Defining $M = N - s + s' \in \{0,1,\ldots,2N\}$, the dimension of the eigenspace of the fixed quantum number $s - s' = N - M$ is given by $\binom{2N}{M} - \delta_{MN}$, where the Kronecker δ represents the missing identity matrix which belongs to the $M = N$ state space. The operator $\widehat{L}$ therefore decomposes into block matrices and it becomes necessary to study the spectral statistics of each of these matrices separately. To get a good statistical error one should choose M close to N.

I analyse four situations of the Liouville operator (5.41) where $N = 10$ and $M = 7$ for all cases. This gives 77520 eigenvalues in total per case to analyse. I study only the bulk of the first quadrant, which reduces this number.

Ensemble A The boundary driven XX-chain with bulk dephasing. The numerical parameters are chosen as $J = 1$, $J' = \Delta = \Delta' = 0$, $\gamma_{\rm L}^{+} = 0.5$, $\gamma_{\rm L}^{-} = 1.2$, $\gamma_{\rm R}^{+} = 1$, $\gamma_{\rm R}^{-} = 0.8$, $\gamma = 1$. The model is equivalent to the Fermi–Hubbard chain with imaginary interaction $U = i\gamma$ with off-diagonal boundaries, see [123], which is known to be Bethe ansatz integrable. From the natural extension of the Berry–Tabor conjecture Poisson statistics of the Liouvillian spectrum should be expected, see Figure 5.3 (top left plot).

Ensemble B The isotropic Heisenberg (XXX) chain with pure-source/pure-sink driving. The parameters are $J = \Delta = 1$, $J' = \Delta' = 0$, $\gamma_{\rm L}^{+} = 0.6$, $\gamma_{\rm R}^{-} = 1.4$, $\gamma_{\rm L}^{-} = \gamma_{\rm R}^{+} = \gamma = 0$. The

System	Poisson	Fitted Coulomb β	Ginibre
(a)	0.015	–	0.15
(b)	0.10	0.0092 ($\beta = 1.0$)	0.058
(c)	0.15	–	0.012
(d)	0.16	0.0094 ($\beta = 1.9$)	0.012
Buzzards	0.12	0.052 ($\beta = 0.8$)	0.092

Table 5.1: The Kolmogorov distance between the empirical data shown in Figures 5.3 and 5.4, the Poisson distribution (5.19), fitted value for β (specified in the parenthesis) of the Coulomb gas, and Ginibre spacing distribution (5.10). The best fits for (a) and (c) are $\beta = 0$ and $\beta = 2$ respectively.

steady state (zero-mode) of this problem is known to be exactly solvable [121], but the full Liouvillian spectrum shows non-integrable behaviour. Note that though the next-to-nearest interactions are removed, part of the dephasing noise is non-zero. See Figure 5.3 (top right plot), where it is clear that the spectrum is partially chaotic.

Ensemble C The XXX-chain with arbitrary polarizing boundary driving. Here the parameters are $J = \Delta = 1,\ J' = \Delta' = 0,\ \gamma_{\mathrm{L}}^{+} = 0.5,\ \gamma_{\mathrm{L}}^{-} = 0.3,\ \gamma_{\mathrm{R}}^{+} = 0.3,\ \gamma_{\mathrm{R}}^{-} = 0.9,\ \gamma = 0$. The bulk Hamiltonian of this model is well-known to be integrable via Bethe ansatz, but with the boundary driving not even the steady state seems to be exactly solvable. Compared to Ensemble B, the dephasing noise is larger, and the spectrum in Figure 5.3 (bottom left plot) confirms that its dynamics is chaotic.

Ensemble D The XXZ-chain with nearest neighbour and next-to-nearest neighbour interactions. The parameters are chosen as $J = J' = 1,\ \Delta = 0.5,\ \Delta' = 1.5,\ \gamma_{\mathrm{L}}^{+} = 0.5,\ \gamma_{\mathrm{L}}^{-} = 0.3,\ \gamma_{\mathrm{R}}^{+} = 0.3,\ \gamma_{\mathrm{R}}^{-} = 0.9,\ \gamma = 0$ in this case. This time, even the bulk Hamiltonian is non-integrable (quantum chaotic), though it seems the spacing follows roughly the same statistics as Ensemble C, see Figure 5.3 (bottom right plot).

See Table 5.1 for the Kolmogorov distances of the comparisons to Poisson, Ginibre, and the best Coulomb gas fit.

The dataset and description of the system (also printed in [AKMP]) are provided by Tomaž Prosen and the eigenvalues are treated as follows. As the spectrum is symmetric around the real and imaginary axes, these areas are special and therefore not a part of the bulk. The edge is excluded by considering an ellipse with principle axes proportional to the width of the data in the respective directions.

These nearest neighbours of each of these points is then found with the unfolding method from Section 5.2 and compared to the spacing distributions found in Section 5.1. The comparison to the Coulomb gasses is done by generating a number of realisations for different β and finding the one that gives the smallest Kolmogorov distance. See Figure 5.3 for the comparison. It should be noted that this is no guarantee that the analytic spacing of the Liouville eigenvalues follow the exact same spacing as 2D Coulomb gasses, but the indicators presented here give strong reason to suggest this.

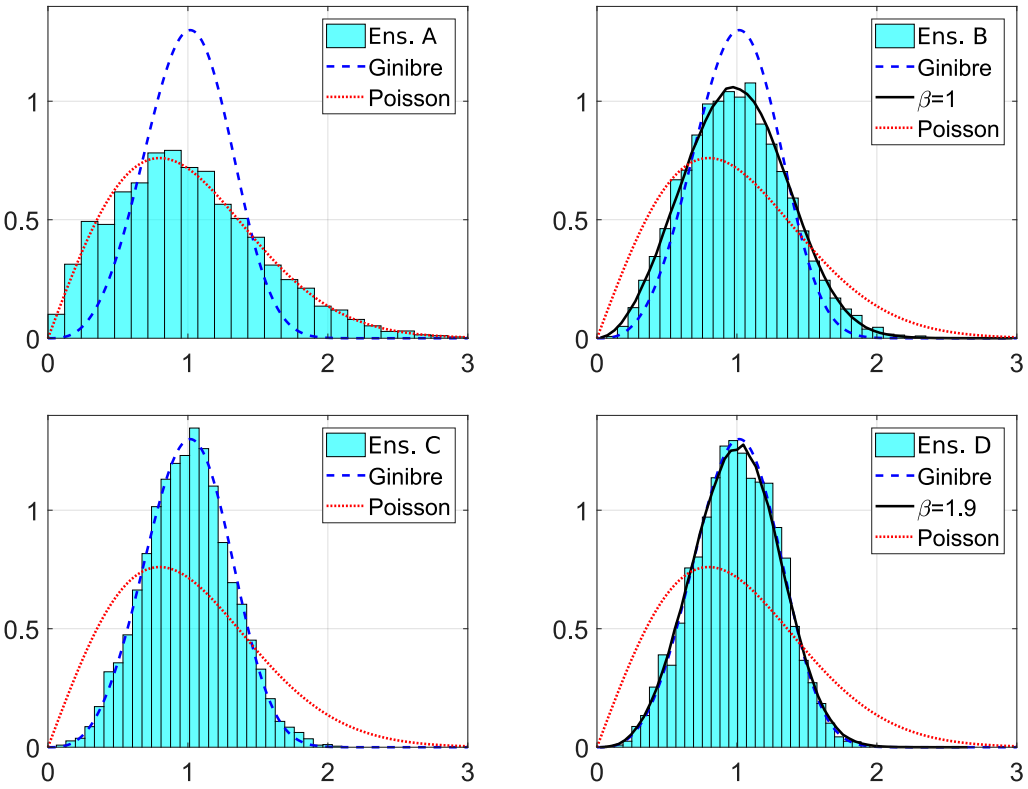

Figure 5.3: Comparison of the nearest neighbour spacing distributions for eigenvalues of the Liouville operator described in Section 5.3.2 to the analytical expressions in Section 5.1. Top left is the integrable system, Configuration A, top right is the slightly chaotic Configuration B, and the bottom row is the chaotic Configurations C and D, all from Section 5.3.2. These have been unfolded with the method described in Section 5.2 and are compared to Ginibre and Poisson spacing, see Equations (5.10) and (5.19) respectively. A fit of the spacings of the Coulomb gasses generated with the method in Section 5.1.3 is also provided, where the best fit is neither $\beta = 0$ nor $\beta = 2$. Note how the transition from integrable to chaotic corresponds to a transition between Poisson spacing and Ginibre. These figures are also published in [AKMP].

5.3.3 Buzzard Nests

The data set of buzzard nests is provided by Oliver Krüger and has the following form. 266 active buzzard nests have been observed in the Teutoburger Forest and their longitude and latitude noted. As longitude and latitude do correspond to the same length far away from the equator, I use the mean of the points as a reference and find the coordinates in kilometres with this as the origin instead. This is joint work with Rebecca Werdehausen [40].

When comparing the positions to a map, it is also clear that smaller villages are responsible for some of the holes in the data, which makes it much less clear what constitutes the bulk than for the Liouville operator. I therefore employ a more complicated method. Drawing a circle around each point (radius here chosen as twice the mean spacing), I exclude each point whose circle touches the edge of the shape described by the circles. See Figure 5.4 (left plot) for an illustration of this method.

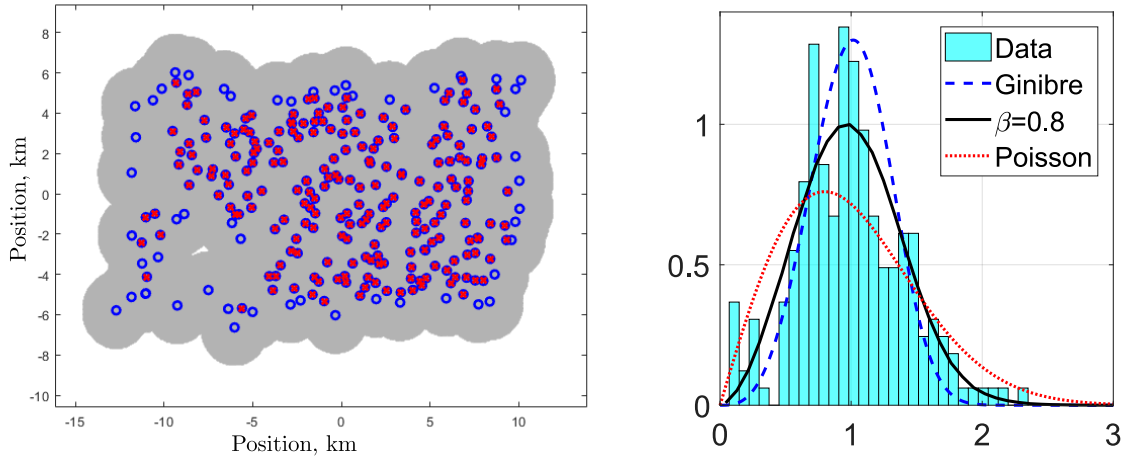

Figure 5.4: The behaviour of the buzzard nests described in 5.3.3. **Left:** The positions relative to the middle point. The blue circles denote all positions, the black area is the mask used to determine where the bulk, and the red crosses are the considered points. Of the original 266 points, 215 are included. **Right:** The nearest neighbour spacing of chosen points unfolded according to the method described in Section 5.2 and compared to the analytical expressions from Section 5.1. Even with the low statistics it seems clear that though the repulsion is weak, it is decidedly stronger than Poisson.

The distances are again calculated as described in Section 5.2, and the result can be found in Figure 5.4 (right plot) with the Kolmogorov distances in Table 5.1. Despite the low statistics, it seems the nests repel each other (a fit to the Coulomb gas gives $\beta = 0.8$).

A possible extension of this analysis would be modelling each point with a different charge, which would give the option of accounting for each territory's attractiveness. This would be at the cost of integrability, but as the analytical expression for the 2D Coulomb gasses is not known either, this would be an option if a reasonable way of fitting the charge of each point can be found. (The space to search here will be very large.)

5.4 Conclusion

The goal of this chapter has been to investigate the understanding that can be gained from analysing the spacing distributions of random points. This is well-understood for real variables, and some results are known in the complex plane. I have endeavoured to extend these by considering the spacings of Ginibre matrices and Poisson variables compared to data.

The first result is a slightly more precise statement of universality for the bulk of real, complex, and quaternion Ginibre ensembles, where all three are found to have the same spacing distribution. This analysis is done on the level of the jpdf and numerically. This universality of course makes distinctions between different matrix ensembles more difficult than the Hermitian cases, but the transition between the Poisson and Ginibre spacings can still be explored numerically through Coulomb gasses.

For comparison to non-uniform densities, it is also necessary to understand how the density affects the spacing. In other words, the spectrum has to be unfolded. In this chapter, I

present a new way of treating this, namely a Gaussian broadening of each point to approximate the local density and let the corresponding distances be calculated.

These methods were then applied to two different data sets to ascertain their behaviour. Firstly, the eigenvalues of a Liouville operator for different open systems that transition between integrable and chaotic. Here the goal was to see the transition reflected in the spacing, reminiscent of the Poisson/Wigner-distinction found in Hermitian ensembles. Here it does indeed seem that an integrable system corresponds to Poisson spacing in two dimension and chaotic to Ginibre. Secondly, the territorial behaviour of buzzards in the local forest was investigated with the same methods. It was expected that the points would not be Poissonian, and the comparison to the Coulomb gas supports this.

For both of these dataset, it may also be interesting to consider other observables such as the statistics of the number of points within a local area, which can serve as another way of distinguishing Poisson and Ginibre[1]. It also takes advantage of the different repulsion, though notably it would be an area measure rather than a length measure, which may be numerically more stable.

[1]I am grateful to P. Forrester for this suggestion.

Chapter 6

Concluding Remarks and Outlook

Random matrix theory provides insight into a number of physical and statistical systems through universality results. The topics under scrutiny are as diverse as quantum chromodynamics, solid state physics, quantum chaos, information theory, number theory, and biological or financial data. Especially the microscopic spectrum of Hamilton or Dirac operators is of interest. The eigenvalues here are of the order of the inverse system size and therefore hold information about large-scale properties. The modes exactly at the origin are of special importance here, as they are determined by the topology.

Further understanding of the local scale can found in the spacing between eigenvalues. In general, the spacing distribution is a feature that distinguishes correlated and uncorrelated variables, and in the context of quantum chaos, it shows the difference between integrable and chaotic systems. The spacing distribution known as the Wigner surmise has been observed in many different parts of nature, the separation between bus arrivals and between neutron resonances in heavy nuclei among them.

In this thesis I have presented a number of results within the application of random matrix theory in statistical physics. The focus of the first part was topological superconductors and how to model them. In Chapter 3 I introduced a matrix model that can transition between the chiral Gaussian orthogonal ensemble and the ensemble of antisymmetric Hermitian Gaussian matrices. This transition has been conjectured in conjunction with these systems, and the goal was to establish the k-point density correlation functions. This is done by showing that the ensemble builds a Pfaffian point process and calculating the corresponding skew-orthogonal polynomials using supersymmetry. The behaviour of the smallest eigenvalue was also studied through an expansion. I sketched the method needed to find the limit of large matrix size as well. At the time of writing this is still work in progress, but it is expected that the exact choice of distribution for the elements will be irrelevant. That is, the microscopic spectrum is expected to be universal.

The ensemble exhibits a preserved topological mode throughout the transition. It also allows for an analytical extension to a regime where a direct sum of two antisymmetric matrices is perturbed by off-diagonal generic ones. Zero modes arising from the two antisymmetric matrices are spread out by the perturbation, and this regime in particular is expected to be relevant for topological superconductors. It also ties in well with the framework established in Chapter 4, where I consider perturbed zero modes in a general setting. The results there hold for all ten Altland-Zirnbauer classes and the perturbative regime from Chapter 3 is therefore naturally a part of this.

Observed is a decoupling of the former zero modes from the bulk spectrum to leading order in perturbation theory. This becomes exact in the limit of large matrix size. Akin to a central limit theorem for matrices, the former zero modes spread out according to a finite size Gaussian ensemble.

The results rely on a sufficient mixing from the unitary matrices that change between the eigenbases of the unperturbed and perturbed system. In this work the full Haar measure was assumed for the unitary matrices, but a natural extension would be to see to which extend this assumption may be loosened while still obtaining the same results.

Taking a step back, there is also work to be done on understanding the full scope of the role RMT may play in making predictions for topological superconductors. As discussed in Section 2.6, it is possible to construct random matrix models that have the same symmetries as the solid state Hamiltonians, and as shown in Chapter 4, observables may also be calculated, but to my knowledge, a full analysis and comparison of the spectrum is still an open problem.

The second part of the thesis, Chapter 5 was dedicated to the study of spacing distributions for eigenvalues of non-Hermitian random matrices. As for Hermitian matrices, the spacing allows one to distinguish between correlated and uncorrelated variables as well as between integrable and chaotic systems. The biggest challenges when going from 1D to 2D are the lack of a Wigner surmise, which necessitates the simulation of the log-gasses rather than using the approximate analytic distribution, and a consistent unfolding procedure, which in general cannot be on a global scale. For $\beta = 0$ and $\beta = 2$ one may look at the full expression for the distribution at large matrix size, and the result for complex Ginibre in the bulk also holds for a number of ensembles, such as real and quaternion Ginibre. These have the same corresponding log-gas, which makes it obvious to conjecture that this is the distinguishing feature. Comparison of numerically generated log-gasses to data supports this idea. The unfolding procedure in 2D suffers from a well-known problem in differential geometry; it is not in general possible to flatten a manifold while preserving the local distances. I presented method that provides an unfolding on a local scale by weighting distances by the local density, which in turn is estimated by considering each point as Gaussian with a tuned width.

The spacing distributions were compared to simulations of a Liouville operator that shows a transitions between integrable and chaotic, and the simulated log-gasses seem to describe the cases between the two. Also the nests of buzzards in the local forest around Bielefeld seem to somewhat follow these distributions as well, though there are artefacts in the data that are not explained by the Coulomb gas alone. More data will of course help, but it is interesting that some similarities with random matrix ensembles already occurs, which shows the ubiquity of random matrix theory.

Appendix A

Technical Calculations for Chapter 3

A.1 Simplification of the Weight Functions $G_\nu(x,y)$ and $g_\nu(x)$

I first look at one-point weight function $g_\nu(x)$ from (3.40). Inserting from (3.33) it reads for $\nu = 0\ (1)$ with upper (lower) signs

$$\begin{aligned} g_{\nu=0,1}(x) &= \frac{1}{2}x^\nu e^{-\frac{2}{a^2}x^2}\int_0^\infty dt\, e^{-\frac{2}{a^2(1-a^2)}t^2}\left(e^{\frac{4}{a^2}xt} \pm e^{-\frac{4}{a^2}xt}\right) \\ &= \frac{1}{2}x^\nu e^{-\frac{2}{a^2}x^2+\frac{2(1-a^2)}{a^2}x^2}\left(\int_0^\infty dt\, e^{-\frac{2(t-x(1-a^2))^2}{a^2(1-a^2)}} \pm \int_0^\infty dt\, e^{-\frac{2(t+x(1-a^2))^2}{a^2(1-a^2)}}\right) \\ &= \frac{\sqrt{\pi}}{4}\sqrt{\frac{a^2(1-a^2)}{2}}\, x^\nu e^{-2x^2}\left(1+\mathrm{erf}\left[x\sqrt{\frac{2(1-a^2)}{a^2}}\right] \pm 1 \mp \mathrm{erf}\left[x\sqrt{\frac{2(1-a^2)}{a^2}}\right]\right)\ . \end{aligned} \tag{A.1}$$

The first equality is completion of the square. The last one comes from the definition of the complementary error function

$$\mathrm{erfc}(x) = \frac{2}{\sqrt{\pi}}\int_x^\infty dt\, e^{-t^2} = 1-\mathrm{erf}(x)\ , \tag{A.2}$$

and the parity of the error function, $\mathrm{erf}(-x) = -\mathrm{erf}(x)$. The last line of (A.1) is equivalent to (3.9) because $\nu = 0, 1$. Note that $g_\nu(x)$ is an even function in x for both values of $\nu = 0, 1$.

The simplification of the two-point weight function $G_\nu(z,u)$ is as follows, starting from (3.39). For $\nu = 0$ I use $\mathrm{sign}(y-x) = \mathrm{sign}(y^2-x^2)$, valid for $x, y > 0$, which means the integral can be extended to all of the real line

$$\begin{aligned} G_0(s,t) &= \frac{1}{4}e^{-\frac{2}{a^2}(s^2+t^2)}\int_{-\infty}^\infty dx\int_{-\infty}^\infty dy\ \mathrm{sign}(y^2-x^2)e^{-\frac{2}{a^2(1-a^2)}(x^2+y^2)}\cosh\left(\frac{4xs}{a^2}\right)\cosh\left(\frac{4yt}{a^2}\right) \\ &= \frac{1}{2}e^{-\frac{2}{a^2}(s^2+t^2)}\int_{-\infty}^\infty du\int_{-\infty}^\infty dv\ \mathrm{sign}(u)\mathrm{sign}(v)e^{-\frac{4}{a^2(1-a^2)}(u^2+v^2)} \\ &\quad\times\frac{1}{4}\left(e^{\frac{4}{a^2}(v-u)s}+e^{-\frac{4}{a^2}(v-u)s}\right)\left(e^{\frac{4}{a^2}(v+u)t}+e^{-\frac{4}{a^2}(v+u)t}\right) \\ &= \frac{\pi a^2(1-a^2)}{8}\, e^{-2(s^2+t^2)}\,\mathrm{erf}\left[(t-s)\sqrt{\frac{(1-a^2)}{a^2}}\right]\mathrm{erf}\left[(t+s)\sqrt{\frac{(1-a^2)}{a^2}}\right]\ . \end{aligned} \tag{A.3}$$

The integrals decouple after a change of variables $u = (y-x)/2$ and $v = (y+x)/2$ in the second line. The sign-functions may be evaluated in this way. Multiplying out and completing the square leads to (3.8) for $\nu = 0$.

For $\nu = 1$ the addition theorem $\sinh(x)\sinh(y) = \cosh(x)\cosh(y) - \cosh(x-y)$ is needed. This leads to

$$G_1(s,t) \;=\; stG_0(s,t) - \widetilde{G}_1(s,t), \qquad \text{for } a<1, \tag{A.4}$$

where $\widetilde{G}_1(s,t)$ still has to be calculated,

$$\begin{aligned}\widetilde{G}_1(s,t) &= ste^{-\frac{2}{a^2}(s^2+t^2)}\int_0^\infty dx\int_0^\infty dy\;\mathrm{sign}(y-x)e^{-\frac{2}{a^2(1-a^2)}(x^2+y^2)}\cosh\left(\frac{4(xs-yt)}{a^2}\right)\\ &= ste^{-\frac{2}{a^2}(s^2+t^2)}\int_0^\infty dx\int_0^x dy\;e^{-\frac{2}{a^2(1-a^2)}(x^2+y^2)}\frac{1}{2}\Big\{-e^{\frac{4}{a^2}xs}e^{-\frac{4}{a^2}yt}-e^{-\frac{4}{a^2}xs}e^{\frac{4}{a^2}yt}\\ &\quad + e^{\frac{4}{a^2}ys}e^{-\frac{4}{a^2}xt}+e^{-\frac{4}{a^2}ys}e^{\frac{4}{a^2}xt}\Big\}\;.\end{aligned} \tag{A.5}$$

Here the cosh has been written out and the sign-function have been evaluated. The term for the region $y>x$ was rewritten using $\int_0^\infty dx\int_x^\infty dy = \int_0^\infty dy\int_0^y dx$ and exchanged the labelling of the variables $x \leftrightarrow y$.

Now each term of (A.5) is calculated separately by completing the square

$$\begin{aligned}\widetilde{G}_1(s,t) &= -\frac{1}{2}ste^{-2(s^2+t^2)}\left\{\int_{-s(1-a^2)}^\infty dx\int_{t(1-a^2)}^{x+(s+t)(1-a^2)}dy+\int_{s(1-a^2)}^\infty dx\int_{-t(1-a^2)}^{x-(s+t)(1-a^2)}dy\right.\\ &\quad \left.-\int_{t(1-a^2)}^\infty dx\int_{-s(1-a^2)}^{x-(s+t)(1-a^2)}dy-\int_{-t(1-a^2)}^\infty dx\int_{s(1-a^2)}^{x+(s+t)(1-a^2)}dy\right\}e^{-\frac{2}{a^2(1-a^2)}(x^2+y^2)}\;.\end{aligned} \tag{A.6}$$

All the compact inner integrals over y can be computed with

$$\frac{2}{\sqrt{\pi}}\int_b^a dy e^{-y^2} \;=\; \mathrm{erf}(a)-\mathrm{erf}(b)\;. \tag{A.7}$$

Half of the integrals over x cancel. With the definition

$$A = s\sqrt{\frac{2(1-a^2)}{a^2}}\;,\; B = t\sqrt{\frac{2(1-a^2)}{a^2}}\;, \tag{A.8}$$

and the rescaling $u = x\sqrt{2/(a^2(1-a^2))}$, the remaining terms of (A.6) become

$$\begin{aligned}\widetilde{G}_1(s,t) &= -\frac{\sqrt{\pi}}{8}a^2(1-a^2)ste^{-2(s^2+t^2)}\left\{\int_{-A}^\infty du\;\mathrm{erf}[u+A+B]+\int_A^\infty du\;\mathrm{erf}[u-A-B]\right.\\ &\quad \left.-\int_B^\infty du\;\mathrm{erf}[u-A-B]-\int_{-B}^\infty du\;\mathrm{erf}[u+A+B]\right\}e^{-u^2}\\ &= -\frac{\sqrt{\pi}}{8}a^2(1-a^2)ste^{-2(s^2+t^2)}\left\{\int_A^B du\;\mathrm{erf}[u-A-B]+\int_{-A}^{-B}du\;\mathrm{erf}[u+A+B]\right\}e^{-u^2}\\ &= -\frac{\sqrt{\pi}}{4}a^2(1-a^2)ste^{-2(s^2+t^2)}\int_{s\sqrt{\frac{2(1-a^2)}{a^2}}}^{t\sqrt{\frac{2(1-a^2)}{a^2}}}du\;\mathrm{erf}\left[u-(s+t)\sqrt{\frac{2(1-a^2)}{a^2}}\right]e^{-u^2}\;.\end{aligned} \tag{A.9}$$

All parts of the integrals over $[0,\infty)$ cancel in the first step, and in the second step the parity of the error function has been used. The integration boundaries brings the antisymmetry. Inserting this result for $\widetilde{G}_1(s,t)$ in (A.4) gives (3.8) for $\nu = 1$.

The integrals over the weight functions are also needed for the modification of the scalar product for odd $n = 2m+1$, see (2.68). I start with

$$\bar{G}_\nu(t) \;=\; \int_0^\infty ds\, G_\nu(s,t) \tag{A.10}$$

and work from the definition (3.39). The integral over s is done by completing the square

$$\begin{aligned}
\bar{G}_\nu(t) &= \frac{1}{2}\int_{-\infty}^\infty ds(st)^\nu \int_0^\infty dx \int_0^\infty dy\, \mathrm{sign}(y-x) e^{-\frac{2}{a^2}(s^2+t^2)-\frac{2}{a^2(1-a^2)}(x^2+y^2)+\frac{4}{a^2}sx} f_\nu(ty) \\
&= \sqrt{\frac{\pi a^2}{2^3}}\int_0^\infty dx \int_0^\infty dy\, \mathrm{sign}(y-x)(xt)^\nu e^{-\frac{2}{a^2}t^2-\frac{2}{1-a^2}x^2-\frac{2}{a^2(1-a^2)}y^2} f_\nu(ty)\;.
\end{aligned} \tag{A.11}$$

For $\nu = 0$ I perform the integral over x and rescale $y = \sqrt{a^2(1-a^2)/2}u$

$$\begin{aligned}
\bar{G}_0(t) &= \sqrt{\frac{\pi a^2}{2^3}} e^{-\frac{2}{a^2}t^2}\int_0^\infty dx \int_0^\infty dy\, \mathrm{sign}(y-x) e^{-\frac{2}{1-a^2}x^2-\frac{2}{a^2(1-a^2)}y^2}\cosh\left[\frac{4}{a^2}ty\right] \\
&= \frac{\pi}{2^{7/2}}a^2(1-a^2)e^{-\frac{2}{a^2}t^2}\int_0^\infty du(2\,\mathrm{erf}(au)-1)e^{-u^2}\cosh\left[2\sqrt{\frac{2(1-a^2)}{a^2}}tu\right] \\
&= \frac{\pi}{2^{5/2}}a^2(1-a^2)e^{-\frac{2}{a^2}t^2}\int_0^\infty du\;\mathrm{erf}(au)e^{-u^2}\cosh\left[2\sqrt{\frac{2(1-a^2)}{a^2}}tu\right] \\
&\quad -\frac{\pi}{2^{9/2}}a^2(1-a^2)e^{-\frac{2}{a^2}t^2}\int_{-\infty}^\infty du\, e^{-u^2+2\sqrt{\frac{2(1-a^2)}{a^2}}tu} \\
&= \frac{\pi a^2(1-a^2)}{2^{7/2}}e^{-2t^2}\int_{-\infty}^\infty du\;\mathrm{erf}(a|u|)e^{-\left(u-\sqrt{\frac{2(1-a^2)}{a^2}}t\right)^2} - \frac{\pi^{3/2}a^2(1-a^2)}{2^{9/2}}e^{-2t^2}\;.
\end{aligned} \tag{A.12}$$

The second line comes from extending the integral over x to the whole real line and evaluating the sign-function. The terms can be simplified by writing out the cosh as exponentials and completing the square. The term without the error function can be evaluated directly.

For $\nu = 1$ all the integrals can be performed completely

$$\begin{aligned}
\bar{G}_1(t) &= \sqrt{\frac{\pi a^2}{2^3}}e^{-\frac{2}{a^2}t^2}\int_0^\infty dx\int_0^\infty dy\,\mathrm{sign}(y-x)xt\, e^{-\frac{2}{1-a^2}x^2-\frac{2}{a^2(1-a^2)}y^2}\sinh\left[\frac{4}{a^2}ty\right] \\
&= \frac{\sqrt{\pi}a(1-a^2)}{2^{7/2}}t\,e^{-\frac{2}{a^2}t^2}\int_0^\infty dy\left(e^{-\frac{2}{a^2(1-a^2)}y^2}-2e^{-\frac{2(1+a^2)}{a^2(1-a^2)}y^2}\right)\sinh\left[\frac{4}{a^2}ty\right] \\
&= \frac{\pi a^2(1-a^2)^{3/2}}{2^5}t\,e^{-2t^2}\,\mathrm{erf}\left[\sqrt{\frac{2(1-a^2)}{a^2}}t\right] - \frac{\pi a^2(1-a^2)^{3/2}}{2^4\sqrt{1+a^2}}t\,e^{-\frac{4}{1+a^2}t^2}\,\mathrm{erf}\left[\sqrt{\frac{2(1-a^2)}{a^2(1+a^2)}}t\right]\;.
\end{aligned} \tag{A.13}$$

The second line is obtained by evaluating the sign-function and using that the integrand for the x-integral has a known primitive.

The integral over the one-point weight function is g_ν can be done directly from (3.40)

$$\begin{aligned}\bar{g}_\nu &= \int_0^\infty ds\, g_\nu(s) = \int_0^\infty ds \int_0^\infty dx\, s^\nu e^{-\frac{2s^2}{a^2}-\frac{2x^2}{a^2(1-a^2)}} \frac{1}{2}\left(e^{\frac{4sx}{a^2}} + (-1)^\nu e^{-\frac{4sx}{a^2}}\right) \\ &= \frac{1}{2}\int_{-\infty}^\infty ds\, s^\nu e^{-\frac{2s^2}{a^2}} \int_0^\infty dx\, e^{-\frac{2x^2}{a^2(1-a^2)}} e^{\frac{4sx}{a^2}} = \frac{1}{2}\int_0^\infty dx\, e^{-\frac{2x^2}{(1-a^2)}} \int_{-\infty}^\infty ds\, s^\nu e^{-\frac{2}{a^2}(s-x)^2} \\ &= \sqrt{\frac{\pi a^2}{8}} \int_0^\infty dx\, x^\nu e^{-\frac{2x^2}{(1-a^2)}} = \frac{\pi\sqrt{a^2(1-a^2)}}{8}\left(\frac{1-a^2}{2\pi}\right)^{\frac{\nu}{2}} . \end{aligned} \tag{A.14}$$

The s-integral is extended to the whole real line and the square is completed. The shift $s \to s+x$ gives the term x^ν. The odd moments in s vanish.

A cross-check can be done by considering the normalisation of the jpdf (3.7) for $n = 1$, which

$$\bar{g}_\nu = C_{1,\nu}^{-1} = \frac{a(1-a^2)^{\frac{1}{2}(1+\nu)}}{2^{\frac{1}{2}(4+\nu)}}\Gamma\left(\frac{3}{2}\right)\Gamma\left(\frac{1+\nu}{2}\right) . \tag{A.15}$$

This agrees with (A.14).

A.2 Heine-Like Formulas for the Skew-Orthogonal Polynomials

For completeness I show how the skew-orthogonal polynomials of Chapter 3 may be obtained from the following representation

$$p_j^{(\nu)}(x) = x^{-\nu}\langle \det[x\mathbb{1}_{2j+\nu} - J]\rangle_{j,\nu} = \left\langle \prod_{k=1}^j (x^2-\lambda_k^2)\right\rangle_{j,\nu} , \tag{A.16}$$

$$\begin{aligned} q_j^{(\nu)}(x) &= x^{-\nu}\Big\langle \det[x\mathbb{1}_{2j+\nu} - J]\Big(x^2 + \tfrac{1}{2}\operatorname{Tr} J^2 + c_j^{(\nu)}(a)\Big)\Big\rangle_{j,\nu} \\ &= \left\langle \prod_{k=1}^j (x^2-\lambda_k^2)\left(x^2 + \sum_{p=1}^j \lambda_p^2 + c_j^{(\nu)}(a)\right)\right\rangle_{j,\nu} , \end{aligned} \tag{A.17}$$

for $N = 2j+\nu$ given. The averages $\langle \ldots\rangle_{j,\nu}$ are over a random matrix J of size $(2j+\nu)\times(2j+\nu)$ or over its singular values.

The constant $c_j^{(\nu)}(a)$ is arbitrary and reflects that the polynomials $q_j^{(\nu)}(x)$ are not uniquely defined. For this derivation I set them $c_j^{(\nu)}(a) = 0$, but they may be reintroduced by adding a multiple of $p_j^{(\nu)}(x)$.

The relations (A.16-A.17) are reminiscent of the form for general sOP in [44], where a general potential $\prod_{k=1}^j e^{-V(\lambda_k)}$ was considered. An important difference from [44] is that the polynomials in Chapter 3 are in the variables x^2. This leads to the term $\frac{1}{2}\operatorname{Tr} J^2$ in (A.17) rather than $\operatorname{Tr} J$ (J is traceless). This calculation follows [85] closely, see also [56].

The goal of this appendix is to show the skew-orthogonality relations (2.54) and (2.72) by showing that both $p_j^{(\nu)}(x)$ and $q_j^{(\nu)}(x)$ are skew-orthogonal to all polynomials of degree up to $j-1$. They are already skew-orthogonal to themselves because of antisymmetry. It also required that the product of $p_j^{(\nu)}(x)$ and $q_j^{(\nu)}(x)$ is non-zero.

That is, to be shown is that with $e_a(x) = x^{2a}$

$$\langle p_j^{(\nu)}|e_a\rangle_{e/o} = 0 \text{ for } a = 0,1,\ldots,j , \tag{A.18}$$

$$\langle q_j^{(\nu)}|e_a\rangle_{e/o} = 0 \text{ for } a = 0,1,\ldots,j-1 . \tag{A.19}$$

The subscripts "e/o" denotes even or odd j, corresponding to (2.54) and (2.72) respectively.

A.2.1 Even Dimension $j = 2m$

The representation (A.16) for $j = 2m$ even with $m = 0, 1, \ldots$ may be written as

$$\begin{aligned} p_{2m}^{(\nu)}(x) &= C_{2m,\nu} \int_0^\infty d\lambda_1 \ldots \int_0^\infty d\lambda_{2m} \prod_{l=1}^{2m} (x^2 - \lambda_l^2)\, \Delta_{2m}\left(\{\lambda^2\}\right) \mathrm{Pf}\left[G_\nu(\lambda_a, \lambda_b)\right]_{a,b=1}^{2m} \\ &= C_{2m,\nu} \frac{(2m)!}{2^m m!} \int_0^\infty d\lambda_1 \ldots \int_0^\infty d\lambda_{2m}\, \Delta_{2m+1}\left(\{\lambda^2\}, x^2\right) \prod_{l=1}^{m} G_\nu(\lambda_{2l-1}, \lambda_{2l}) \\ &= C_{2m,\nu} \frac{(2m)!}{2^m} \mathrm{Pf}\left[\begin{array}{cc} \langle e_{a-1}|e_{b-1}\rangle_e & e_{a-1}(x) \\ -e_{b-1}(x) & 0 \end{array} \right]_{a,b=1}^{2m+1} . \end{aligned} \tag{A.20}$$

The product $\prod_{l=1}^{2m}(x^2 - \lambda_l^2)$ has been combined with the Vandermonde determinant to yield a new Vandermonde determinant in both λ^2 and x^2. The Pfaffian has also been expanded. Each term gives the same contribution $\prod_{l=1}^{m} G_\nu(\lambda_{2l-1}, \lambda_{2l})$, and the sum therefore only gives a combinatorial factor. The last line is obtained with a generalisation of the de Bruijn integral identity [90, Appendix C.2]. The skew-orthogonal product (2.54)

$$\langle f_1|f_2\rangle_e = \int_0^\infty dx \int_0^\infty dy\, G_\nu(x,y) f_1(x) f_2(y) \tag{A.21}$$

for two functions f_1, f_2 for the final result (A.20) and the monomial $e_{c-1}(y)$ becomes

$$\begin{aligned} \langle p_j^{(\nu)}|e_{c-1}\rangle_e &= \int_0^\infty dx \int_0^\infty dy\, p_{2m}^{(\nu)}(x) G_\nu(x,y) e_{c-1}(y) \\ &= C_{2m,\nu} \frac{(2m)!}{2^m} \mathrm{Pf}\left[\begin{array}{cc} \langle e_{a-1}|e_{b-1}\rangle_e & \langle e_{a-1}|e_{c-1}\rangle_e \\ \langle e_{c-1}|e_{b-1}\rangle_e & 0 \end{array} \right]_{a,b=1}^{2m+1} = 0, \qquad \text{for } c = 1, \ldots, 2m+1 . \end{aligned} \tag{A.22}$$

The integrals are pulled into the Pfaffian. The right-hand side vanishes for equal rows and columns as claimed.

This may also be done for $q_j^{(\nu)}(x)$ in Equation (A.17)

$$\begin{aligned} q_{2m}^{(\nu)}(x) &= C_{2m,\nu} \int_0^\infty d\lambda_1 \ldots \int_0^\infty d\lambda_{2m} \prod_{l=1}^{2m} (x^2 - \lambda_l^2) \left(x^2 + \sum_{p=1}^{2m} \lambda_p^2 \right) \\ &\quad \times \Delta_{2m}\left(\{\lambda^2\}\right) \mathrm{Pf}\left[G_\nu(\lambda_a, \lambda_b)\right]_{a,b=1}^{2m} . \end{aligned} \tag{A.23}$$

The variable x is again pulled into the Vandermonde determinant $\Delta_{2m+1}\left(\{\lambda^2\}, x^2\right)$. The identity [85, Eq. (4.12)]

$$\sum_{a=1}^{j+1} \lambda_a^2\, \Delta_{j+1}(\{\lambda^2\}) = \det \begin{bmatrix} 1 & \lambda_1^2 & \cdots & \lambda_1^{2(j-1)} & \lambda_1^{2(j+1)} \\ \vdots & \vdots & & \vdots & \vdots \\ 1 & \lambda_{j+1}^2 & \cdots & \lambda_{j+1}^{2(j-1)} & \lambda_{j+1}^{2(j+1)} \end{bmatrix} \equiv \widetilde{\Delta}_{j+1}(\{\lambda^2\}) . \tag{A.24}$$

is used to deal with the sums. The rest of the procedure is the same as the previous case

$$\begin{aligned} q_{2m}^{(\nu)}(x) &= C_{2m,\nu}\frac{(2m)!}{2^m m!}\int_0^\infty d\lambda_1 \ldots \int_0^\infty d\lambda_{2m}\, \widetilde{\Delta}_{2m+1}\left(\{\lambda^2\}, x^2\right)\prod_{l=1}^{m} G_\nu(\lambda_{2l-1},\lambda_{2l}) \\ &= C_{2m,\nu}\frac{(2m)!}{2^m}\,\mathrm{Pf}\begin{bmatrix} \langle e_{a-1}|e_{b-1}\rangle_e & \langle e_{a-1}|e_{2m+1}\rangle_e & e_{a-1}(x) \\ \langle e_{2m+1}, e_{b-1}\rangle_e & 0 & e_{2m+1}(x) \\ -e_{b-1}(x) & -e_{2m+1}(x) & 0 \end{bmatrix}_{a,b=1}^{2m} . \end{aligned} \tag{A.25}$$

The Pfaffian has again been expanded and the generalised de Bruijn identity. The equal rows and columns again give

$$\begin{aligned} \langle q_{2m}^{(\nu)}|e_{c-1}\rangle_e &= \int_0^\infty dx \int_0^\infty dy\; q_{2m}^{(\nu)}(x) G_\nu(x,y) e_{c-1}(y) \\ &= C_{2m,\nu}\frac{(2m)!}{2^m}\,\mathrm{Pf}\begin{bmatrix} \langle e_{a-1}|e_{b-1}\rangle_e & \langle e_{a-1}|e_{2m+1}\rangle_e & \langle e_{a-1}|e_{c-1}\rangle_e \\ \langle e_{2m+1}|e_{b-1}\rangle_e & 0 & \langle e_{2m+1}|e_{c-1}\rangle_e \\ \langle e_{c-1}|e_{b-1}\rangle_e & \langle e_{c-1}|e_{2m+1}\rangle_e & 0 \end{bmatrix}_{a,b=1}^{2m} \\ &= 0 \text{ for } c = 1,\ldots,2m,2m+2\,. \end{aligned} \tag{A.26}$$

This concludes the proof for $j = 2m$. It is assumed that the product is non-degenerate and that the normalisation constants are non-zero $h_{2j}^{(\nu)} = \langle p_{2j}^{(\nu)}|q_{2j}^{(\nu)}\rangle_e \neq 0$. These are determined in Subsection 3.3.3.

A.2.2 Odd Dimension $j = 2m' + 1$

For odd dimension a rewriting of the jpdf is needed first. The skew-symmetric product has a different weight function (2.67)

$$\langle f_1|f_2\rangle_o = \int_0^\infty dx \int_0^\infty dy\; H_\nu(x,y) f_1(x) f_2(y)\,, \tag{A.27}$$

where f_1, f_2 are two suitably integrable functions and

$$H_\nu(x,y) = G_\nu(x,y) - \frac{g_\nu(x)}{\bar{g}_\nu}\int_0^\infty dx' G_\nu(x',y) - \frac{g_\nu(y)}{\bar{g}_\nu}\int_0^\infty dy' G_\nu(x,y')\,. \tag{A.28}$$

Because the Pfaffian is invariant under simultaneous addition of multiples of rows and columns, the jpdf for odd $j = 2m' + 1$, with $m' = 0, 1, \ldots$, can be written in terms of the new weight function

$$\begin{aligned} P_{2m'+1}^{(\nu)}(\lambda_1,\ldots,\lambda_n) &= C_{2m'+1,\nu}\Delta_{2m'+1}(\{\lambda^2\})\mathrm{Pf}\begin{bmatrix} G_\nu(\lambda_a,\lambda_b) & g_\nu(\lambda_a) \\ -g_\nu(\lambda_b) & 0 \end{bmatrix}_{a,b=1}^{2m'+1} \\ &= C_{2m'+1,\nu}\Delta_{2m'+1}(\{\lambda^2\})\mathrm{Pf}\begin{bmatrix} H_\nu(\lambda_a,\lambda_b) & g_\nu(\lambda_a) \\ -g_\nu(\lambda_b) & 0 \end{bmatrix}_{a,b=1}^{2m'+1} . \end{aligned} \tag{A.29}$$

Note that zeroth-order polynomials are automatically skew-orthogonal to all other polynomials

$$\begin{aligned}\langle 1|e_a\rangle_o &= \int_0^\infty dx \int_0^\infty dy\; H_\nu(x,y) y^{2a} \\ &= \int_0^\infty dx \int_0^\infty dy\; G_\nu(x,y) y^{2a} - \frac{\int_0^\infty dx g_\nu(x)}{\bar{g}_\nu} \int_0^\infty dy \int_0^\infty dx' G_\nu(x',y) y^{2a} \\ &\quad - \frac{\int_0^\infty dy g_\nu(y) y^{2a}}{\bar{g}_\nu} \int_0^\infty dx \int_0^\infty dy' G_\nu(x,y') \\ &= 0\,. \end{aligned} \tag{A.30}$$

The first two terms cancel, and the antisymmetry of $G_\nu(x,y)$ removes the last term. With this construction, the zeroth order polynomials are projected out for odd n. The rest of this appendix is dedicated to showing the skew-orthogonality of the remaining polynomials. The polynomial $p_j^{(\nu)}(x)$ of odd degree $j = 2m'+1$ reads, see (A.16),

$$p^{(\nu)}_{2m'+1}(x) = C_{2m'+1,\nu} \int_0^\infty d\lambda_1 \ldots \int_0^\infty d\lambda_{2m'+1} \Delta_{2m'+2}(\{\lambda^2\}, x^2) \mathrm{Pf} \begin{bmatrix} H_\nu(\lambda_a,\lambda_b) & g_\nu(\lambda_a) \\ -g_\nu(\lambda_b) & 0 \end{bmatrix}_{a,b=1}^{2m'+1} . \tag{A.31}$$

Here I have again combined the product $\prod_{k=1}^{2m'+1}(x^2-\lambda_k^2)$ with the Vandermonde determinant $\Delta_{2m'+1}(\{\lambda^2\})$. The generalised de Bruijn integration identity [31, Appendix A.1] yields

$$p^{(\nu)}_{2m'+1}(x) = (2m'+1)! C_{2m'+1,\nu} \mathrm{Pf} \left[\begin{array}{c|c|c|c} 0 & 0 & \bar{g}_\nu & 1 \\ \hline 0 & \langle e_a|e_b\rangle_o & \bar{g}_{a,\nu} & e_a(x) \\ \hline -\bar{g}_\nu & -\bar{g}_{b,\nu} & 0 & 0 \\ \hline -1 & -e_b(x) & 0 & 0 \end{array}\right]_{a,b=1}^{2m'+1} . \tag{A.32}$$

The entries involving the zeroth order monomial $e_0(x) = 1$ have been spelled out. I have also defined $\bar{g}_{a,\nu} = \int_0^\infty dz\; e_a(z) g_\nu(z)$ with $\bar{g}_{0,\nu} = \bar{g}_\nu$. It follows that

$$\begin{aligned}\langle p^{(\nu)}_{2m'+1}|e_k\rangle_o &= (2m'+1)! C_{2m'+1,\nu} \mathrm{Pf} \left[\begin{array}{c|c|c|c} 0 & 0 & \bar{g}_\nu & 0 \\ \hline 0 & \langle e_a|e_b\rangle_o & \bar{g}_{a,\nu} & \langle e_a|e_k\rangle_o \\ \hline -\bar{g}_\nu & -\bar{g}_{b,\nu} & 0 & 0 \\ \hline 0 & \langle e_k|e_b\rangle_o & 0 & 0 \end{array}\right]_{a,b=1}^{2m'+1} \\ &= (2m'+1)! C_{2m'+1,\nu} \mathrm{Pf} \left[\begin{array}{c|c|c|c} 0 & 0 & \bar{g}_\nu & 0 \\ \hline 0 & \langle e_a|e_b\rangle_o & 0 & \langle e_a|e_k\rangle_o \\ \hline -\bar{g}_\nu & 0 & 0 & 0 \\ \hline 0 & \langle e_k|e_b\rangle_o & 0 & 0 \end{array}\right]_{a,b=1}^{2m'+1} \\ &= 0, \qquad \text{for } k = 1,\ldots,2m'+1\,, \end{aligned} \tag{A.33}$$

which proves the skew-orthogonality for $p^{(\nu)}_{2m'+1}(x)$. The second line comes from simultaneously adding multiples of rows and columns. The identical rows and columns makes the Pfaffian vanish for the given indices.

The relation (2.72)

$$\int_0^\infty dx\, p_{2j-1}^{(\nu)}(x) g_\nu(x) \;=\; 0 \tag{A.34}$$

is also needed for the skew-orthogonality. This can be seen by pulling the integral into the last row and column in (A.32). The last two rows and columns are identical, and therefore the Pfaffian vanishes.

The relations for the polynomials $q_j^{(\nu)}(x)$ follow in a similar way. Note that these are now of even order $j+1 = 2m'+2$ in x^2. Writing out (A.17) yields

$$\begin{aligned} q_{2m'+1}^{(\nu)}(x) &= C_{2m'+1,\nu} \int_0^\infty d\lambda_1 \ldots \int_0^\infty d\lambda_{2m'+1} \widetilde{\Delta}_{2m'+2}(\{\lambda^2\}, x^2) \mathrm{Pf} \begin{bmatrix} H_\nu(\lambda_a,\lambda_b) & g_\nu(\lambda_a) \\ -g_\nu(\lambda_b) & 0 \end{bmatrix}_{a,b=1}^{2m'+1} \\ &= (2m'+1)! C_{2m'+1,\nu} \mathrm{Pf} \left[\begin{array}{c|c|c|c|c} 0 & 0 & 0 & \bar{g}_\nu & 1 \\ \hline 0 & \langle e_a|e_b\rangle_o & \langle e_a|e_{2m'+2}\rangle_o & \bar{g}_{a,\nu} & e_a(x) \\ \hline 0 & \langle e_{2m'+2}|e_b\rangle_o & 0 & \bar{g}_{2m'+2,\nu} & e_{2m'+2}(x) \\ \hline -\bar{g}_\nu & -\bar{g}_{b,\nu} & -\bar{g}_{2m'+2,\nu} & 0 & 0 \\ \hline -1 & -e_b(x) & -e_{2m'+2}(x) & 0 & 0 \end{array}\right]_{a,b=1}^{2m'} . \end{aligned} \tag{A.35}$$

The product has again been absorbed in the Vandermonde and the identity (A.24) has been used, following the same steps as above. The skew-symmetry also follows

$$\begin{aligned} \langle q_{2m'+1}^{(\nu)}|e_k\rangle_o &= (2m'+1)! C_{2m'+1,\nu} \mathrm{Pf} \left[\begin{array}{c|c|c|c|c} 0 & 0 & 0 & \bar{g}_\nu & 0 \\ \hline 0 & \langle e_a|e_b\rangle_o & \langle e_a|e_{2m'+2}\rangle_o & 0 & \langle e_a|e_k\rangle_o \\ \hline 0 & \langle e_{2m'+2}|e_b\rangle_o & 0 & 0 & \langle e_{2m'+2}|e_k\rangle_o \\ \hline -\bar{g}_\nu & 0 & 0 & 0 & 0 \\ \hline 0 & \langle e_k|e_b\rangle_o & \langle e_k|e_{2m'+2}\rangle_o & 0 & 0 \end{array}\right]_{a,b=1}^{2m'} \\ &= 0, \qquad \text{for } k = 1,\ldots,2m',2m'+2\,. \end{aligned} \tag{A.36}$$

Adding rows and columns in the Pfaffian has removed most of the second to last row and column containing the constants.

Finally, the relation (2.72),

$$\int_0^\infty dx\, q_{2j-1}^{(\nu)}(x) g_\nu(x) \;=\; 0 \tag{A.37}$$

follows from pulling the integral into the last row and column of (A.35). The last two rows and columns coincide, and the Pfaffian vanishes.

As for the even case, the norms must be non-zero $h_{2j-1}^{(\nu)} = \langle p_{2j-1}^{(\nu)}, q_{2j-1}^{(\nu)}\rangle_o \neq 0$, see Subsection 3.3.3.

A.3 Saddle Point Approximation

Given the integral

$$I \;=\; \int_a^b dx\; \exp\{nf(x)\}\, g(x) \tag{A.38}$$

for $n \gg 1$, Taylor expand around x_0, such that the first derivative vanishes $f^{(1)}(x_0) = 0$. Switch coordinates to $\tilde{x} = x_0 + \frac{\delta x}{\sqrt{n}}$

$$\begin{aligned}
I &= \frac{1}{\sqrt{n}} \int_{\sqrt{n}(a-x_0)}^{\sqrt{n}(b-x_0)} d(\delta x)\ \exp\left\{ nf\left(x_0 + \frac{\delta x}{\sqrt{n}}\right)\right\} g\left(x_0 + \frac{\delta x}{\sqrt{n}}\right) \\
&\overset{n\gg 1}{=} \frac{1}{\sqrt{n}} \int_{\sqrt{n}(a-x_0)}^{\sqrt{n}(b-x_0)} d(\delta x)\ \exp\left\{ nf(x_0) + \frac{f^{(2)}(x_0)}{2}(\delta x)^2 + \frac{f^{(3)}(x_0)}{6\sqrt{n}}(\delta x)^3 + \frac{f^{(4)}(x_0)}{24n}(\delta x)^4 \right\} \\
&\quad \times \left(g(x_0) + \frac{g^{(1)}(x_0)}{\sqrt{n}}\delta x + \frac{g^{(2)}(x_0)}{2n}(\delta x)^2 \right) \\
&\overset{n\gg 1}{=} \frac{1}{\sqrt{n}} \int_{\sqrt{n}(a-x_0)}^{\sqrt{n}(b-x_0)} d(\delta x)\ \exp\left\{ nf(x_0) + \frac{f^{(2)}(x_0)}{2}(\delta x)^2 \right\} \left(g(x_0) + \frac{g^{(1)}(x_0)}{\sqrt{n}}\delta x + \frac{g^{(2)}(x_0)}{2n}(\delta x)^2 \right) \\
&\quad \times \left(1 + \frac{f^{(3)}(x_0)}{6\sqrt{n}}(\delta x)^3 + \frac{f^{(4)}(x_0)}{24n}(\delta x)^4 + \frac{1}{2}\left(\frac{f^{(3)}(x_0)}{6\sqrt{n}}(\delta x)^3 + \frac{f^{(4)}(x_0)}{24n}(\delta x)^4 \right)^2 \right) . \qquad \text{(A.39)}
\end{aligned}$$

Terms smaller than $\frac{1}{n}$ are disregarded in the last parenthesis. Assume $\lim_{n\to\infty} \sqrt{n}(a - x_0) = -\infty$ and $\lim_{n\to\infty} \sqrt{n}(b - x_0) = \infty$. Otherwise the limits are at a or b and the antisymmetry cannot be used to remove the odd powers of δx.

$$\begin{aligned}
I &\overset{n\gg 1}{=} \frac{1}{\sqrt{n}} \int_{-\infty}^{+\infty} d(\delta x)\ \exp\left\{ nf(x_0) + \frac{f^{(2)}(x_0)}{2}(\delta x)^2 \right\} \left(g(x_0) + \frac{g^{(1)}(x_0)}{\sqrt{n}}\delta x + \frac{g^{(2)}(x_0)}{2n}(\delta x)^2 \right) \\
&\quad \times \left(1 + \frac{f^{(3)}(x_0)}{6\sqrt{n}}(\delta x)^3 + \frac{f^{(4)}(x_0)}{24n}(\delta x)^4 + \frac{1}{2}\frac{f^{(3)}(x_0)^2}{36n}(\delta x)^6 \right) . \qquad \text{(A.40)}
\end{aligned}$$

I expand the parentheses and again disregard lower orders. I also disregard the odd powers

$$\begin{aligned}
I &\overset{n\gg 1}{=} \frac{1}{\sqrt{n}} \int_{-\infty}^{+\infty} d(\delta x)\ \exp\left\{ nf(x_0) + \frac{f^{(2)}(x_0)}{2}(\delta x)^2 \right\} \Big[g(x_0) + \frac{1}{n}\Big(\frac{g^{(2)}(x_0)}{2}(\delta x)^2 \\
&\quad + \left(\frac{g^{(1)}(x_0) f^{(3)}(x_0)}{6} + \frac{g(x_0) f^{(4)}(x_0)}{24} \right)(\delta x)^4 + \frac{g(x_0) f^{(3)}(x_0)^2}{72}(\delta x)^6 \Big) \Big] . \qquad \text{(A.41)}
\end{aligned}$$

I finally perform the Gaussian integral

$$\begin{aligned}
I &\overset{n\gg 1}{=} \sqrt{\frac{2\pi}{nf^{(2)}(x_0)}} e^{nf(x_0)} \Big[g(x_0) + \frac{1}{n}\Big(\frac{g^{(2)}(x_0)}{2f^{(2)}(x_0)} + \frac{g^{(1)}(x_0) f^{(3)}(x_0)}{2f^{(2)}(x_0)^2} \qquad \text{(A.42)} \\
&\quad + \frac{g(x_0) f^{(4)}(x_0)}{8f^{(2)}(x_0)^2} + \frac{5g(x_0) f^{(3)}(x_0)^2}{24f^{(2)}(x_0)^3} \Big) \Big] .
\end{aligned}$$

This is the saddle point approximation with next-to-leading order included.

Bibliography

[1] J. Wishart, *The Generalised Product Moment Distribution in Samples from a Normal Multivariate Population,* Biometrika, **20A**, 32–52 (1928).

[2] E. P. Wigner, *On the statistical distribution of the widths and spacings of nuclear resonance levels,* Proc. Cambridge Phil. Soc. **47**, 790-798 (1951).

[3] M. V. Berry and M. Tabor, *Level clustering in the regular spectrum* Proc. Roy. Soc. A 356, 375 (1977).

[4] O. Bohigas, M. J. Giannoni, and C. Schmit, *Spectral Properties of the Laplacian and Random Matrix Theory* Phys. Rev.Lett. **52**, 1 (1984); Journal de Physique Lettres 45, 1015 (1984).

[5] Milan Krbálek and Petr Šeba, *The statistical properties of the city transport in Cuernavaca (Mexico) and random matrix ensembles,* J. Phys. A: Math. Gen. **33** (2000) [arXiv:nlin/0001015 [nlin.CD]].

[6] A. Holle, G. Wiebusch, J. Main, K. H. Welge, G. Zeller, G. Wunner, T. Ertl, and H. Ruder, *Hydrogenic Rydberg atoms in strong magnetic fields: Theoretical and experimental spectra in the transition region from regularity to irregularity,* Z. Phys D - Atoms, Molecules, and Clusters, **5**, 279 (1987); A. Holle, J. Main, G. Wiebusch, H. Rottke, and K. H. Welge, *Quasi-Landau Spectrum of the Chaotic Diamagnetic Hydrogen Atom,* Phys. Rev. Lett. **61**, 161 (1988); H. Friedrich and H. Wintgen, *The hydrogen atom in a uniform magnetic field — An example of chaos,* Physics Reports **183**, 2 (1989).

[7] H. Alt, C. Dembowski, H.-D. Gräf, R. Hofferbert, H. Rehfeld, A. Richter, R. Schuhmann, and T. Weiland *Wave Dynamical Chaos in a Superconducting Three-Dimensional Sinai Billiard,* Phys. Rev. Lett. **79**, 1026 (1997) [arXiv:chao-dyn/9706025].

[8] M. L. Mehta, *Random Matrices* (Third Edition, Elsevier, Amsterdam, 2004).

[9] G. Akemann, J. Baik, and P. Di Francesco (eds.), *The Oxford Handbook of Random Matrix Theory* (First Edition, Oxford University Press, 2011).

[10] G. Akemann, P. H. Damgaard, U. Magnea, and S. Nishigaki, *Universality of random matrices in the microscopic limit and the Dirac operator spectrum*, Nucl. Phys. B **487**, 721 (1997) [arXiv:hep-th/9609174].

[11] T. Banks and A. Casher, *Chiral Symmetry Breaking in Confining Theories,* Nucl. Phys. B **169**, 103 (1980).

[12] A. Altland and M. R. Zirnbauer, *Random Matrix Theory of a Chaotic Andreev Quantum Dot*, Phys. Rev. Lett. **76**, 3420 (1996) [arXiv:cond-mat/9508026]; *Novel Symmetry Classes in Mesoscopic Normal-Superconducting Hybrid Structures*, Phys. Rev. B **55**, 1142 (1997) [arXiv:cond-mat/9602137].

[13] M. F. Atiyah and I. M. Singer, *The index of elliptic operators on compact manifolds,* Bull. Amer. Math. Soc. **69**, 422-433 (1963).

[14] A. Pandey and M. L. Mehta, *Gaussian Ensembles Of Random Hermitian Matrices Intermediate Between Orthogonal and Unitary Ones*, Commun. Math. Phys. **87**, 449 (1983).

[15] M. L. Mehta and A. Pandey, *On Some Gaussian Ensembles of Hermitian Matrices*, J. Phys. A: Math. Gen. **16**, 2655 (1983).

[16] P. H. Damgaard, J. C. Osborn, D. Toublan and J. J. M. Verbaarschot, *The microscopic spectral density of the QCD Dirac operator*, Nucl. Phys. B **547**, 305 (1999) [arXiv:hep-th/9811212].

[17] J. Gasser and H. Leutwyler, *Thermodynamics of Chiral Symmetry*, Phys. Lett. B **188**, 477 (1987).

[18] J. Gasser and H. Leutwyler, *Spontaneously Broken Symmetries: Effective Lagrangians at Finite Volume*, Nucl. Phys. B **307**, 763 (1988).

[19] M. Tanabashi et al. (Particle Data Group), Phys. Rev. D 98, 030001 (2018) and 2019 update. Particle Data Group: `http://pdg.lbl.gov/`

[20] J. Gasser and H. Leutwyler, *Chiral perturbation theory to one loop,* Annals Phys. **158**, 142 (1984).

[21] A. Pich, *Effective Field Theory,* [arXiv:hep-ph/9806303].

[22] E. V. Shuryak and J. J. M. Verbaarschot, *Random matrix theory and Spectral Sum Rules for the Dirac Operator in QCD*, Nucl. Phys. A **560**, 306 (1993) [arXiv:hep-th/9212088].

[23] J. J. M. Verbaarschot and I. Zahed, *Spectral density of the QCD Dirac operator near zero virtuality,* Phys. Rev. Lett. **70**, 3852 (1993) [arXiv:hep-th/9303012].

[24] J. J. M. Verbaarschot, *The Spectrum of the QCD Dirac operator and chiral random matrix theory: The Threefold way*, Phys. Rev. Lett. **72**, 2531 (1994) [arXiv:hep-th/9401059].

[25] J. J. M. Verbaarschot, *The Spectrum of the Dirac operator near zero virtuality for $N_c = 2$ and chiral random matrix theory,* Nucl. Phys. B **426**, 559 (1994) [arXiv:hep-th/9401092].

[26] A. M. Halasz and J. J. M. Verbaarschot, *Effective Lagrangians and Chiral Random Matrix Theory*, Phys. Rev. D **52**, 2563 (1995) [arXiv:hep-th/9502096].

[27] K. Wilson, *Confinement of quarks*, Phys. Rev. D **10**, 2445 (1974) in *New Phenomena in subnuclear physics*, ed. A. Zichichi (Plenum, New York, 1977).

[28] P. H. Damgaard, K. Splittorff, and J. J. M. Verbaarschot, *Microscopic Spectrum of the Wilson Dirac Operator*, Phys. Rev. Lett. **105**, 162002 (2010) [arXiv:1001.2937 [hep-th]].

[29] G. Akemann, P. H. Damgaard, K. Splittorff, and J. J. M. Verbaarschot, *Spectrum of the Wilson Dirac Operator at Finite Lattice Spacings*, Phys. Rev. D **83**, 085014 (2010) [arXiv:1012.0752 [hep-lat]].

[30] G. Akemann and T. Nagao, *Random Matrix Theory for the Hermitian Wilson Dirac Operator and the chGUE-GUE Transition*, JHEP **10**, 060 (2011) [arXiv:1108.3035 [math-ph]].

[31] M. Kieburg, *Mixing of orthogonal and skew-orthogonal polynomials and its relation to Wilson RMT*, J. Phys. A: Math. Theor. **45**, 205203 (2012) [arXiv:1202.1768 [math-ph]].

[32] L. Del Debbio, L. Giusti, M. Luscher, R. Petronzio and N. Tantalo, *Stability of Lattice QCD Simulations and the Thermodynamic Limit*, JHEP **0602**, 011 (2006) [arXiv:hep-lat/0512021].

[33] V. I. Fal'ko and K. B. Efetov, *Statistics of prelocalized states in disordered conductors*, Phys. Rev. B **52**, 17413 (1995).

[34] C. W. J. Beenakker, *Random-matrix theory of Majorana fermions and topological superconductors*, Rev. Mod. Phys. **87**, 1037 (2015) [arXiv:1407.2131 [cond-mat.mes-hall]].

[35] A. Kitaev, *Periodic table for topological insulators and superconductors*, AIP Conf. Proc. **1134**, 22 (2009) [arXiv:0901.2686 [cond-mat.mes-hall]].

[36] J. Alicea, Y. Oreg, G. Refael, F. von Oppen, and M. P. Fisher, *Non-Abelian statistics and topological quantum information processing in 1D wire networks*, Nature Physics volume **7**, 412–417 (2011).

[37] P. Neven, D. Bagrets, and A. Altland, *Quasiclassical theory of disordered multi-channel Majorana quantum wires*, New J. Phys. **15**, 055019 (2013) [arXiv:1302.0747 [cond-mat.mes-hall]].

[38] S. R. Elliott and M. Franz, *Colloquium: Majorana fermions in nuclear, particle, and solid-state physics*, Rev. Mod. Phys. **87**, 137 (2015).

[39] E. Dumitrescu, B. Roberts, S. Tewari, J. D. Sau, and S. Das Sarma, *Majorana Fermions in Chiral Topological Ferromagnetic Nanowires*, Phys. Rev. B **91**, 094505 (2015) [arXiv:1410.5412 [cond-mat.supr-con]].

[40] Rebecca Werdehausen, *Eigenvalue Spacings of Random Matrices compared to Locations of Buzzard Nests*, Bachelor Thesis, Bielefeld University.

[41] G. Akemann and J. R. Ipsen, *Recent exact and asymptotic results for products of independent random matrices*, Acta Physica Polonica B **46**, 9, 1747-1784 (2015) [arXiv:1502.01667 [math-ph]].

[42] L. K. Hua, *Harmonic Analysis of Functions of Several Complex Variables in the Classical Domains* (American Mathematical Society, 1963).

[43] L. D'Alessio, Y. Kafri, A. Polkovnikov, amd M. Rigol, *From Quantum Chaos and Eigenstate Thermalization to Statistical Mechanics and Thermodynamics*, Adv. Phys. **65**, 239 (2016) [arXiv:1509.06411 [cond-mat.stat-mech]].

[44] B. Eynard, *Asymptotics of skew orthogonal polynomials*, J. Phys. A **34**, 7591–7605 (2001) [arXiv:cond-mat/0012046].

[45] G. Akemann, *Random Matrix Theory and Quantum Chromodynamics,* arXiv:1603.06011 [math-ph].

[46] E. Heine, *Handbuch der Kugelfunctionen* (Georg Reimer, 1861).

[47] G. Szegö, *Orthogonal Polynomials* (American Mathematical Society, 1939).

[48] Konstantin Efetov, *Supersymmetry in Disorder and Chaos* (Cambridge University Press, 1997).

[49] F. A. Berezin, *Introduction to Superanalysis*, (First Edition, D. Reidel Publishing Company, Dordrecht, 1987).

[50] H.-J. Sommers, *Superbosonization*, Acta Phys. Pol. B **38**, 4105—4110 (2007) [arXiv:0710.5375].

[51] P. Littelmann, H.-J. Sommers, and M. R. Zirnbauer, *Superbosonization of invariant random matrix ensembles*, Commun. Math. Phys. **283**, 343 (2008) [arXiv:0707.2929].

[52] M. Kieburg, H.-J. Sommers, and T. Guhr, *Comparison of the superbosonization formula and the generalized Hubbard–Stratonovich transformation*, J. Phys. A **42**, 275206 (2009) [arXiv:0905.3256].

[53] T. Nagao and P. Forrester, *Transitive Ensembles of Random Matrices Related to Orthogonal Polynomials*, Nucl. Phys. B **530**, 742–762 (1998).

[54] I. S. Gradshteyn and I. M. Ryzhik, *Table of Integrals, Series, and Products* (Academic Press, San Diego, 2000).

[55] P. J. Forrester and A. Mays, *A method to calculate correlation functions for $\beta = 1$ random matrices of odd size*, J. Stat. Phys. **134**, 443–462 (2009) [arXiv:0809.5116 [math-ph]].

[56] T. Kanazawa and M. Kieburg, *Symmetry Transition Preserving Chirality in QCD: A Versatile Random Matrix Model*, Phys. Rev. Lett. **120**, 242001 (2018) [arXiv:1803.04122]; *GUE-chGUE Transition preserving Chirality at finite Matrix Size*, J. Phys. A **51**, 345202 (2018) [arXiv:1804.03985 [math-ph]].

[57] M. R. Zirnbauer, *Riemannian Symmetric Superspaces and their Origin in Random Matrix Theory*, J. Math. Phys. **37**, 4986 (1996) [arXiv:math-ph/9808012].

[58] F. J. Dyson, *The Threefold Way. Algebraic Structure of Symmetry Groups and Ensembles in Quantum Mechanics*, J. Math. Phys. **3**, 1199 (1962).

[59] M. Caselle, *A New Classification Scheme for Random Matrix Theories* (1996) [arXiv:cond-mat/9610017 [cond-mat.stat-mech]].

[60] D. Bernard and A. LeClair, *A Classification of Non–Hermitian Random Matrices*, Contribution to the Proceedings of the NATO Advanced Research Workshop on Statistical Field Theories, Como 18-23 June 2001 [arXiv:cond-mat/0110649 [cond-mat.dis-nn]]; Ulrika Magnea, *Random matrices beyond the Cartan classification*, J. Phys. A: Math. Theor. **41**, 045203 (2008); Z. Gong, Y. Ashida, K. Kawabata, K. Takasan, S. Higashikawa, and M. Ueda, *Topological Phases of Non-Hermitian Systems*, Phys. Rev. X **8**, 031079 (2018).

[61] U. Magnea, *Random matrices beyond the Cartan classification*, J. Phys. A: Math. Theor. **41**, 045203 (2008) [arXiv:0707.0418 [math-ph]].

[62] A. Hüffmann, *Disordered Wires from a Geometric Viewpoint*, J. Phys. A **23**, 5733 (1990); M. Caselle, *A New Universality Class Describing the Insulating Regime of Disordered Wires with Strong Spin-Orbit Scattering*, Mod. Phys. Lett. B **10**, 681-688 (1996) [arXiv:cond-mat/9505068]; R. DeJonghe, K. Frey, and T. Imbo, *Bott Periodicity and Realizations of Chiral Symmetry in Arbitrary Dimensions*, Phys. Lett. B **718**, 603 (2012) [arXiv:1207.6547 [hep-th]]; M. Kieburg, J. J. M. Verbaarschot, and S. Zafeiropoulos, *A classification of 2-dim Lattice Theory*, PoS **LATTICE2013** 337 (2014) [arXiv:1310.6948]; *Dirac Spectra of 2-dimensional QCD-like theories*, Phys. Rev. D **90**, 085013 (2014) [arXiv:1405.0433 [hep-lat]].

[63] S. Ryu, A. P. Schnyder, A. Furusaki, and A. W. W. Ludwig, *Topological insulators and superconductors: Tenfold way and dimensional hierarchy*, New J. Phys. **12**, 065010 (2010).

[64] R. J. Slager, A. Mesaros, V. Juričić, C. L. Kane, and J. Zaanen, *Topological classification of crystalline insulators through band structure combinatorics*, Nature Physics **9**, 98 (2013) [arXiv:1209.2610 [cond-mat.mes-hall]].

[65] C. K. Chiu, J. C. Y. Teo, A. P. Schnyder, and S. Ryu, *Classification of topological quantum matter with symmetries*, Rev. Mod. Phys. **88**, 035005 (2016) [arXiv:1505.03535 [cond-mat.mes-hall]].

[66] J. Kruthoff, J. de Boer, J. van Wezel, C. L. Kane, and R. J. Slager, *Topological classification of crystalline insulators through band structure combinatorics*, Phys. Rev. X **7**, 041069 (2017) [arXiv:1612.02007 [cond-mat.mes-hall]]. [arXiv:0912.2157].

[67] M. Z. Hasan and C. L. Kane, *Topological Insulators*, Rev. Mod. Phys. **82**, 3045 (2010) [arXiv:1002.3895 [cond-mat.mes-hall]].

[68] M. Kieburg and T. R. Würfel, *Shift of symmetries of naive and staggered fermions in QCD-like lattice theories*, Phys. Rev. D **96**, 034502 (2017) [arXiv:1703.08083 [hep-lat]].

[69] H. Leutwyler and A. V. Smilga, *Spectrum of Dirac operator and role of winding number in QCD,* Phys. Rev. D **46**, 5607 (1992).

[70] M. Srednicki, *Quantum field theory*, (Cambridge University Press, Cambridge, 2007).

[71] Shun-Qing Shen: *Topological Insulators,* (Springer Berlin Heidelberg, 2012).

[72] M. Koshino, T. Morimoto, and M. Sato, *Topological Zero Modes and Dirac Points Protected by Spatial Symmetry and Chiral Symmetry,* Phys. Rev. B **90**, 115207 (2014) [arXiv:1406.3094 [cond-mat.mes-hall]].

[73] P. J. Forrester, T. Nagao, and G. Honner, *Correlations for the Orthogonal-Unitary and Symplectic-Unitary Transitions at the Hard and Soft Edges*, Nucl. Phys. B **553**, 601 (1999) [arXiv:cond-mat/9811142].

[74] T. Nagao and P. J. Forrester, *Quaternion determinant expressions for multilevel dynamical correlation functions of parametric random matrices*, Nuclear Physics B **563**, 547–572 (1999).

[75] M. Katori, H. Tanemura, T. Nagao, and N. Komatsuda, *Vicious walk with a wall, noncolliding meanders, and chiral and Bogoliubov-deGennes random matrices*, Phys. Rev. E **68**, 021112 (2003) [arXiv:cond-mat/0303573 [cond-mat.stat-mech]].

[76] M. Katori and H. Tanemura, *Infinite systems of non-colliding generalized meanders and Riemann-Liouville differintegrals,* Probab. Th. Rel. Fields **138**, 113 (2007) [arXiv:math/0506187].

[77] G. Akemann and A. C. Ipsen, *Individual Eigenvalue Distributions for the Wilson Dirac Operator*, JHEP **1204**, 102 (2012) [arXiv:1202.1241 [hep-lat]].

[78] S. M. Nishigaki, *Universality crossover between chiral random matrix ensembles and twisted SU(2) lattice Dirac spectra*, Phys. Rev. D **86**, 114505 (2012) [arXiv:1208.3452 [hep-lat]]; T. Yamamoto and S. M. Nishigaki, *Individual eigenvalue distributions of crossover chiral random matrices and low-energy constants of $SU(2) \times U(1)$ lattice gauge theory*, Prog. Theor. Exp. Phys. **2018**, 023B01 (2018) [arXiv:1711.03388 [hep-lat]].

[79] D. Bagrets and A. Altland, *Class D Spectral Peak in Majorana Quantum Wires*, Phys. Rev. Lett. **109**, 227005 (2012) [arXiv:1206.0434 [cond-mat.mes-hall]].

[80] A. Edelman and N. R. Rao, *Random matrix theory*, Acta Numerica **14**, 233 (2005).

[81] Harish-Chandra, *Differential operators on a semisimple Lie algebra*, Amer. J. Math. **79**, 87–120 (1957).

[82] A. Prats Ferrer, B. Eynard, P. Di Francesco, and J.-B. Zuber, *Correlation Functions of Harish-Chandra Integrals over the Orthogonal and the Symplectic Groups*, J. Stat. Phys. **129**, 885–935 (2009) [arXiv:math-ph/0610049].

[83] M. Kieburg and T. Guhr, *A new approach to derive Pfaffian structures for random matrix ensembles*, J. Phys. A **43**, 135204 (2010) [arXiv:0912.0658].

[84] N. G. de Bruijn, *On some multiple integrals involving determinants*, J. Indian Math. Soc. **19**, 133 (1955).

[85] G. Akemann, M. Kieburg, and M. J. Phillips, *Skew-orthogonal Laguerre polynomials for chiral real asymmetric random matrices*, J. Phys. A **43**, 375207 (2010) [arXiv:1005.2983 [math-ph]].

[86] F. W. L Olver et al. (eds.), *NIST Handbook of Mathematical Functions* (Cambridge University Press, Cambridge 2010).

[87] M. Kieburg, *Surprising Pfaffian factorizations in Random Matrix Theory with Dyson index $\beta = 2$*, J. Phys. A **45**, 095205 (2012) [arXiv:1109.5109 [math-ph]]. [arXiv:math-ph/0604041].

[88] I. Schur, *Über die Darstellung der symmetrischen und der alternierenden Gruppe durch gebrochene lineare Substitutionen*, J. Reine Angew. Math. **139**, 155–250 (1911).

[89] S. Schechter, *On the Inversion of Certain Matrices*, Mathematical Tables and Other Aids to Computation **13**, 73–77 (1959).

[90] M. Kieburg and T. Guhr, *Derivation of determinantal structures for random matrix ensembles in a new way*, J. Phys. A **43**, 075201 (2010) [arXiv:0912.0654].

[91] G. Akemann and P. H. Damgaard, *Distributions of Dirac operator eigenvalues*, Phys. Lett. B **583**, 199 (2004) [arXiv:hep-th/0311171].

[92] A. Edelman, *The Distribution and Moments of the Smallest Eigenvalue of a Random Matrix of Wishart Type*, Lin. Alg. Appl. **159**, 55-80 (1991).

[93] P. H. Damgaard and S. M. Nishigaki, *Distribution of the k-th smallest Dirac operator eigenvalue*, Phys. Rev. D **63**, 045012 (2001) [arXiv:hep-th/0006111].

[94] G. Akemann, T. Guhr, M. Kieburg, R. Wegner, and T. Wirtz, *Completing the picture for the smallest eigenvalue of real Wishart matrices*, Phys. Rev. Lett. **113**, 250201 (2014) [arXiv:1409.0360 [math-ph]]; *The smallest eigenvalue distribution in the real Wishart–Laguerre ensemble with even topology*, J. Phys. A **48**, 245202 (2015) [arXiv:1502.03685 [math-ph]].

[95] M. Kieburg, J. J. M. Verbaarschot, and S. Zafeiropoulos, *Spectral Properties of the Wilson Dirac Operator and random matrix theory*, Phys. Rev. D **88**, 094502 (2013) [arXiv:1307.7251 [hep-lat]]; *The Effect of the Low Energy Constants on the Spectral Properties of the Wilson Dirac Operator*, PoS **LATTICE2013**, 117 (2014) [arXiv:1310.7009 [hep-lat]].

[96] M. Kieburg, J. J. M. Verbaarschot, and S. Zafeiropoulos, *Dirac Spectrum of the Wilson Dirac Operator for QCD with Two Colors*, Phys. Rev. D **92**, 045026 (2015) [arXiv:1505.01784 [hep-lat]].

[97] A. Mielke and K. Splittorff, *Universal Distribution of Would-be Topological Zero Modes in Coupled Chiral Systems*, Phys. Rev. D **95**, 074516 (2017) [arXiv:1609.04252 [hep-lat]].

[98] A. Deuzeman, U. Wenger, and J. Wuilloud, *Spectral properties of the Wilson Dirac operator in the ε-regime*, JHEP **1112**, 109 (2011) [arXiv:1110.4002 [hep-lat]]; *Topology, Random Matrix Theory and the spectrum of the Wilson Dirac operator*, PoS **LATTICE2011**, 241 (2011) [arXiv:1112.5160 [hep-lat]].

[99] P. H. Damgaard, U. M. Heller, and K. Splittorff, *Finite-Volume Scaling of the Wilson-Dirac Operator Spectrum*, Phys. Rev. D **85**, 014505 (2012) [arXiv:1110.2851]; *New Ways to Determine Low-Energy Constants with Wilson Fermions*, Phys. Rev. D **86**, 094502 (2012) [arXiv:1206.4786 [hep-lat]]; *Wilson chiral perturbation theory, Wilson-Dirac operator eigenvalues and clover improvement*, PoS **ConfinementX**, 077 (2012) [arXiv:1301.3099 [hep-lat]].

[100] K. Cichy and S. Zafeiropoulos, *Wilson chiral perturbation theory for dynamical twisted mass fermions vs lattice data—A case study*, Comput. Phys. Commun. **237**, 143 (2019) [arXiv:1612.01289 [hep-lat]]; K. Cichy, E. Garcia-Ramos, K. Splittorff, and S. Zafeiropoulos, *The microscopic Twisted Mass Dirac spectrum and the spectral determination of the LECs of Wilson χ-PT*, PoS **LATTICE2015**, 058 (2016) [arXiv:1510.09169 [hep-lat]].

[101] M. Capitaine and C. Donati-Martin, *Spectrum of deformed random matrices and free probability Advanced Topics in Random Matrices, Florent Benaych-Georges, Charles Bordenave,* Mireille Capitaine, Catherine Donati-Martin, and Antti Knowles (edited by F. Benaych-Georges, D. Chafaï, S. Péché, B. de Tilière) *Panoramas & Synthèses* **53** (2018) [arXiv:1607.05560 [math.PR]].

[102] D. Bagrets and A. Altland, *Class D Spectral Peak in Majorana Quantum Wires*, Phys. Rev. Lett. **109**, 227005 (2012) [arXiv:1206.0434 [cond-mat.mes-hall]].

[103] T. Guhr and B. Kälber, *A new method to estimate the noise in financial correlation matrices*, J. Phys. A: Math. Gen. **36**, 3009 (2003) [arXiv:1609.04252 [hep-lat]]; M. Vyas, T. Guhr and T. H. Seligman, *Multivariate analysis of short time series in terms of ensembles of correlation matrices*, Sci. Rep. **8**, no. 1, 14620 (2018) [arXiv:1801.07790 [physics.data-an]].

[104] M. Sieber and K. Richter, *Physica Scripta Correlations between periodic orbits and their rôle in spectral statistics* Physica Scripta **T90**, 128 (2001); S. Müller, S. Heusler, A. Altland, P. Braun, and F. Haake, *Periodic-orbit theory of universal level correlations in quantum chaos* New J. Phys. **11**, 103025 (2009).

[105] R. Grobe, F. Haake, and H.-J. Sommers, *Quantum Distinction of Regular and Chaotic Dissipative Motion*, Phys. Rev. Lett. **61**, 1899 (1988).

[106] T. A. Brody, *A statistical measure for the repulsion of energy levels*, Lett. Nuovo Cimento **7**, 482 (1973).

[107] T. Guhr, A. Mueller-Groeling, and H. A. Weidenmueller, *Random Matrix Theories in Quantum Physics: Common Concepts*, Phys. Rept. **299**, 189-425 (1998) [arXiv:cond-mat/9707301].

[108] C. Andréief, *Note sur une relation les intégrales définies des produits des fonctions,* Mem. de la Soc. Sci. de Bordeaux **2**, 1 (1883).

[109] J. Ginibre, *Statistical Ensembles of Complex, Quaternion, and Real Matrices* , J. Math. Phys. **6**, 440 (1965).

[110] H.-J. Sommers and W. Wieczorek, *General eigenvalue correlations for the real Ginibre ensemble*, J. Phys. A Math. Theor **41**, 405003 (2008).

[111] A. Borodin and C. D. Sinclair, *The Ginibre Ensemble of Real Random Matrices and its Scaling Limits*, C.D. Commun. Math. Phys. **291**, 177 (2009) [arXiv:0805.2986 [math-ph]].

[112] P. J. Forrester, *Log-Gases and Random Matrices* (Princeton University Press 2010).

[113] S. Serfaty, *Microscopic description of Log and Coulomb gases,* (2017) [arXiv:1709.04089 [math-ph]].

[114] D. Chafaï, G. Ferré, *Simulating Coulomb gases and log-gases with hybrid Monte Carlo algorithms*, J. Stat. Phys. **174**, 3, 692-714 (2019) [arXiv:1806.05985].

[115] F. Haake, *Quantum Signatures of Chaos* (Springer 1991).

[116] H. Markum, R. Pullirsch, and T. Wettig, *Non-Hermitian Random Matrix Theory and Lattice QCD with Chemical Potential*, Phys. Rev. Lett. **83**, 484 (1999) [arXiv:hep-lat/9906020].

[117] Z. Burda, R. A. Janik, and B. Waclaw, *Spectrum of the Product of Independent Random Gaussian Matrices,* Phys. Rev. E **81**, 041132 (2010) [arXiv:0912.3422 [cond-mat.stat-mech]]; F. Götze and A. Tikhomirov, *On the Asymptotic Spectrum of Products of Independent Random Matrices,* [arXiv:1012.2710 [math.PR]]; Z. Burda, A. Jarosz, G. Livan, M. A. Nowak, and A. Swiech, , Phys. Rev. E **82**, 061114 (2010) [arXiv:1007.3594 [cond-mat.stat-mech]]; Acta Phys. Polon. **B42** 939-985 (2011) [arXiv:1103.3964 [cond-mat.stat-mech]].

[118] G. Akemann and Z. Burda, *Universal microscopic correlation functions for products of independent Ginibre matrices*, J. Phys. A: Math. Theor. **45**, 465201 (2012) [arXiv:1208.0187 [math-ph]].

[119] R. J. Barlow, *Statistics* (Wiley 1993)

[120] A. Clauset, C. R. Shalizi, and M. E. J. Newman, *Power-Law Distributions in Empirical Data*, SIAM Rev., **51**, 4, 661–703 (2009) [arXiv:0706.1062 [physics.data-an]].

[121] T. Prosen, *Exact nonequilibrium steady state of a strongly driven open XXZ chain*, Phys. Rev. Lett. **107**, 137201 (2011) [arXiv:1106.2978 [quant-ph]].

[122] B. Buča and T. Prosen, *A note on symmetry reductions of the Lindblad equation: transport in constrained open spin chains*, New J. Phys. **14**, 073007 (2012) [arXiv:1203.0943 [quant-ph]].

[123] M. V. Medvedyeva, F. H. L. Essler, and T. Prosen, *Exact Bethe ansatz spectrum of a tight-binding chain with dephasing noise*, Phys. Rev. Lett. **117**, 137202 (2016) [arXiv:1606.09122 [quant-ph]].